Systems analysis of early endosome motility through identification of molecular motors

A dissertation submitted to the

Technical University of Dresden

For the degree of
Doctor rerum naturalium
In Biology

by
Akhila Chandrashaker

Max-Planck Institute of Molecular Cell Biology and Genetics

1st reviewer: Prof. Dr. Marino Zerial
2nd reviewer: Prof. Dr. Bernard Hoflack

Submitted on: 1st April 2010
Defended on: 6th September 2010

Erklärung entsprechend §5.5 der Promotionsordnung

Hiermit versichere ich, dass ich die vorliegende Arbeit ohne unzulässige Hilfe Dritter und ohne Benutzung anderer als der angegebenen Hilfsmittel angefertigt habe; die aus fremden Quellen direkt oder indirekt übernommenen Gedanken sind als solche kenntlich gemacht. Die Arbeit wurde bisher weder im Inland noch im Ausland in gleicher oder ähnlicher Form einer anderen Prüfungsbehörde vorgelegt.

Die Dissertation wurde von Prof. Dr. Marino Zerial Max Planck Institute of Molecular Cell Biology and Genetics, Dresden betreut und im Zeitraum vom 1st May 2006 bis 30th April 2010 verfasst.

Meine Akhila Chandrashaker betreffend erkläre ich hiermit, dass keine früheren erfolglosen Promotionsverfahren stattgefunden haben.

Ich erkenne die Promotionsordnung der Fakultät für Mathematik und Naturwissen - schaften, Technische Universität Dresden an.

29/04/2010, Akhila Chandrashaker

Declaration

I herewith declare that I have produced this paper without the prohibited assistance of third parties and without making use of aids other than those specified; notions taken over directly or indirectly from other sources have been identified as such. This paper has not previously been presented in identical or similar form to any other German or foreign examination board.

The thesis work was conducted from 1st May 2006 to 30th April 2010 under the supervision of Prof. Dr. Marino Zerial at the Max Planck Institute of Molecular Cell Biology and Genetics, Dresden.

I declare that I have not undertaken any previous unsuccessful doctorate proceedings.

I declare that I recognize the doctorate regulations of the *Fakultät für Mathematik und Naturwissenschaften* of the *Technische Universität Dresden*.

29/04/2010, Akhila Chandrashaker

Acknowledgements

I would like to thank Marino at the outset for hosting me in the lab, guiding me through this thesis work and supporting me financially during my stay here.

I would also like to thank Jochen Rink for this project that is now my thesis and Yannis Kalaidzidis for his mentoring during the course of this work. A big thanks to Jochen, Yannis, Inna Kalaidzidis and Sasha Kalaidzidis for helping me find my footing during my initial days in Dresden and thereafter.

I would like to express my gratitude to my Thesis Advisory Committee, Profs. Marino Zerial, Bernard Hoflack, Stefan Diez and Yannis Kalaidzidis for their time in supervising my work, and to my thesis reviewers Profs. Marino Zerial and Bernard Hoflack for reviewing my work.

My heart felt gratitude to Marisa McShane and Angelika Giner for supporting me through thick and thin of my memorable stay in DD, Greg O'Sullivan, Rashi Tiwari, Varadharajan Sundaramurthy and Thierry Galvez for their incessant entertainment - you guys made burning the midnight oil very lively and spirited.

Special thanks to Eugenio Fava, Marc Bickle and Claudia Moebius for helping me with TDS-related experiments, Mirko Theis for the esiRNA library and Yury Bodrov for his expert analytical skills with Motion Tracking. Thank you Charles Bradshaw, Alba Diz-Muñoz and Thomas Widmann for being on hold for all my SOS calls. I would like to express my gratitude to the Zerial lab, both past and present members for their contributions toward my work and for providing a pleasant working atmosphere.

An astronomical thanks to Ma, Pa and Anand for their unconditional support and encouragement all through my stay in Deutschland - I don't think I would have made it without you. Last, but not least, thanks to Bala for injecting in me a new found zest for life. You have been an incredible source of inspiration, distraction and motivation! Thanks you all for egging me on to completion!

Table of Contents

Synopsis

Endocytosis is an evolutionary conserved process of internalization of cargo from the extracellular environment, be they ligands, nutritional and signaling or pathogens into cells. Following their entry, cargo is received into vesiculo-tubular network of early endosomal compartments from where they are sorted and routed to appropriate cellular destinations through transport along the endocytic network. Recycling cargo is sorted away from other cargo resident in early endosomes through tubulation resulting in fission of recycling vesicles, while those to be degraded are progressively concentrated in early endosomes to be degraded in lysosomes.

Early endosomes are dynamic organelles that have been shown to move centripetally following the internalization of cargo into at the cell periphery. Their motility from the cell periphery to the juxtanuclear location of the cell involves convoluted trajectories that include directed motility, bi-directional switches, saltatory behavior and stalls. This complex motility presumably contributes toward the cargo sorting, duration of cargo residence and spatio-temporal signaling by early endosomes. How the different regimes of motility, and nature and number of molecular motors involved in early endosome motility contribute toward endosome function is not understood.

The aim of this study was to probe into the regulation of endosome motility and understand how transport organizes early endosome network. Towards this end, live cell time-lapse movies of Rab5 endosomes were analyzed to derive motility properties contributing to organization of early endosomes. Consistent and significant bias toward the cell centre (minus end motility) in kinetic parameters such as speed, displacement and duration of motility contribute to centripetal flux of Rab5 early endosomes.

A phenomenological property of early endosome motility is its saltatory behavior that produces saturation curves in Mean Square Displacement (MSD) plots. This phase of motility is descriptive, with no understanding of its mechanism or function. Live cell candidate RNAi screen and cytoskeletal perturbation analysis were performed to identify molecules regulating saltatory motility. To this end, cellular microtubule perturbation and RNAi knock down of several Kinesin motor candidates showed a loss in saturation behavior. Potential candidates identified have to be tested for their effect on endosome function through cargo sorting and kinetic assays to gain insights into the role of saltatory motility in endosome function.

Molecular motors mediate Rab5 motility. Therefore, understanding regulation of motility requires identifying number and nature of molecular motors involved in their transport. Towards this end, a functional cargo (LDL) degradation RNAi screen targeting molecular motors was performed. The Ambion Select technology was used with 3 siRNAs targeting every gene in the library. Analysis of screen produced by lack of phenotype consistency between the multiple siRNAs targeting the same gene. Hence, a search for technology with better target specificity was initiated. Technologies tested were Ambion Select, Ambion Silencer Select, Dharmacon ON-TARGET Plus, esiRNA and Invitrogen Stealth. Invitrogen Stealth technology was found to produce the least off-targets and was most specific in terms of consistency of phenotypes produced by multiple siRNAs silencing the same target gene. Assay conditions were also found to influence the silencing specificities to a significant extent. Hence, a systematic assay optimization exercise was performed in terms of the concentration of siRNA used for transfection and time window of assay to maximize specificity of siRNA silencing. Insights obtained from methodologies developed herein not only provide invaluable guidelines in choosing RNAi commercial libraries for screens, but also underscore the importance of establishing optimal assay conditions to minimize off-targets and improve specificity of silencing target genes.

The motor screen was repeated with RNAi library from Invitrogen Stealth. Several potentially interesting candidates have been identified. Also, correlation analyses of phenotypes produced in the screen have indicated toward potential regulatory motor complexes, all of which await biochemical validation.

1 Introduction

1.1 Cellular Organization - Theories expounding organelle positioning

A distinctive property of life is self-organization of cellular constituents. Cell geometry, size and distribution of organelles dictate function. Organelle distribution, which is the non-random organization of cellular components, plays a pivotal role in maintenance and adaptation of a wide spectrum of cellular activities. Origin and maintenance of organelle distribution have been a matter of intense speculation and investigation for well over half a century. Some of the outstanding questions and theories expounding organelle positioning and distribution are -

Where is positional information for organelle distribution stored?

How are positional codes for spatial localization of organelle transduced and transmitted in cells?

What is the purpose of organelle distribution and its contribution to cellular homeostasis?

Several theories that have been put forth to explain the organelle's positional codes in the cell –

1. Genetic code - spatial codes for organelle positioning are hardwired in cell's genome and are thus transmitted through generations until environment rewires the genetic imprint (Albrecht-Buehler, 1977). This genetic theory is valid only in the absence of trans-differentiation.
2. Somatic inheritance theory – which proposes organization of organelle distribution by protein or lipidic component driven by cell physiology (Locke, 1990).
3. Cellular cytoskeleton and molecular motors - attributes organelle distribution to density of microtubules or of microfilaments, co-coordinated with activity of molecular motors (Pangarkar et al., 2005).

In Eukaryotes, intracellular positioning of organelles and communication between them necessitates active transport mechanisms and logistics of positioning therefore becomes relevant to the functioning of cellular process. Transport can be achieved through diffusion, however, it would neither suffice in achieving motility over distances beyond several nanometers nor sustain kinetically optimal transport rates in the cell. Polarized cells exemplify organelle distribution, which is less apparent, but nevertheless extant in non-polarized cells.

In the following sections, a general overview of intracellular transport in eukaryotic cells is presented.

1.2 Intracellular transport and transport machinery

Eukaryotic cells are distinguished by their complex network of intracellular membrane bound compartments where in cellular functions are segregated in spatially distinct organelles. Intracellular transport is mediated by membranous vesicles probably to increase efficiency of transport owing to high protein to lipid ratio (Takamori et al., 2006). Intracellular transport is the fundamental means of communication and transport of molecules between these compartments, crucial for cellular function, survival and morphogenesis. It is also required for the maintenance of compartment identity by inhibiting promiscuous delivery of cargo, and for organelle homeostasis in terms of its size. The central tenet of intracellular transport lies in its directionality where vesicle bud from donor compartments and fuse with acceptor compartments. Vesicular transport involves the following steps –

Formation of vesicles by coated vesicle assembly at the donor compartment involving recognition and sequestration of cargo by adaptor proteins and assembly of coat proteins.

Vesicular budding by deformation of membrane and vesicle scission

Vesicle transport to destination

Fusion of vesicle to the acceptor membrane

An overview of the process of intracellular transport is presented in Fig1. Each of the above mentioned events are described below. Given this complex multistep process, several classes of molecules are required to coordinate to execute and sustain this complex means of transport.

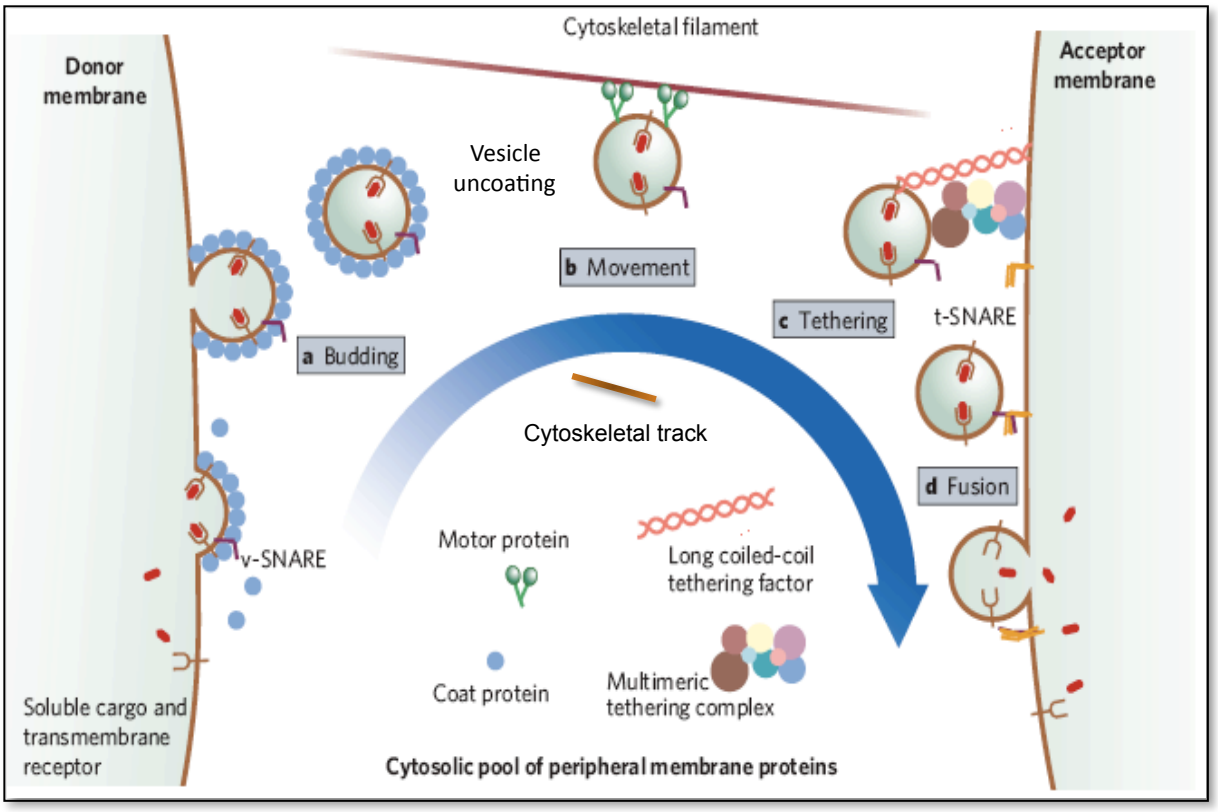

Fig1: Steps involved in intracellular vesicle transport. a. Molecular sorting and sequestration of cargo to be transported by adaptor and coat proteins, invagination of membrane, formation of vesicles and vesicle scission, b. Uncoating of vesicles and transport of vesicle to cellular destination by molecular motors along cytoskeletal tracks. c. Tethering of vesicle to target compartment by tethering factors d. Fusion of vesicle with acceptor compartment to release luminal contents. Targeting of transport vesicles to their destination and fusion is mediated by SNARE proteins (SNARE – Soluble NSF Attachment protein Receptor, v-SNARE – Vesicle SNARE, t-SNARE – target SNARE) – see text below for description of events (Behnia and Munro, 2005)

1.2.1 Coated vesicle assembly

Coated vesicles are forms of transport containers within the exocytic and endocytic pathways. A discernible feature of these vesicles is the presence of coat proteins. Transport from the plasma membrane, endosomes and trans-golgi network use clathrin coats, while that from the Golgi and endoplasmic reticulum use COPI (Coatomer Protein) and COPII respectively (Schmid, 1997).

Coated vesicle formation occurs in three steps –

1. Sequestration and sorting of cargo,
2. Acquisition of membrane curvature and

3. Vesicle scission,

all of which are temporally regulated. The efficiency of vesicle transport depends on ability of cargo sorting and rate of maturation and scission of the vesicle from the donor compartment (Pucadyil and Schmid, 2009).

1.2.1.1 Sequestration and sorting of cargo

Molecular sequestration of cargo is through adaptor proteins that recognize sorting motifs in the cytoplasmic tail of transmembrane receptor molecules. Adaptor proteins can be multimers such as the tetrameric AP (Adapter Proteins-AP1-AP4), or monomeric such as Dab2, ARH, Epsin, β-arrestin, Eps15 and AP180/CALM (Ungewickell and Hinrichsen, 2007). Sorting motifs are primarily of 4 types - tyrosine based, diLeucine acidic, NPXY and polyubiquitination motifs, recognized by different adaptor proteins. Tyrosine based motifs are recognized by the μ2 subunit of AP2 complex (Ohno et al., 1995) while the NPXY motifs are recognized by Dab2 (Maurer, 2006) and ubiquitination motifs are recognized by the Epsin and Eps15 (Hawryluk et al., 2006). With the exception of Eps15/Eps15R, all adaptors harbor phosphoinositol binding motifs that preferentially bind plasma membrane phospholipid, PtdIns $4,5P_2$ and transmembrane cargo reinforcing interaction through coincident detection (Carlton and Cullen, 2005). Adaptor proteins are important in selecting and sequestering cargo and linking them clathrin scaffolds.

Clathrin coats are tesselated mechanical triskelia scaffolds on vesicular structures. Each triskelion is composed of three heavy and 3 light chains. Purified clathrin can be assembled into clathrin coats in the absence of APs at low pH (Keen et al., 1979). However, APs are absolutely required under physiological conditions for assembly of coats. Adaptor and accessory proteins coordinate clathrin nucleation at sites of the plasma membrane that is to be internalized (Schmid et al., 2006). Nucleation promotes the polymerization of clathrin into curved lattices, and consequently stabilizes the deformation of the attached membrane.

1.2.1.2 Acquisition of membrane curvature

Membrane deformation and bending can be induced by several factors that include enrichment of cone-shaped lipids in the cytoplasmic leaflet of the membrane, insertion of protein into the cytoplasmic leaflet, binding of coat proteins with intrinsic curvature, and force exerted by the

cytoskeleton (McMahon and Gallop, 2005). Although clathrin is essential for the invagination of coated structures (Hinrichsen, 2006), proteins of the ENTH, BAR and EFC/F-BAR protein families are required to induce, sense and stabilize membrane curvature (Ungewickell and Hinrichsen, 2007).

1.2.1.3 Vesicle scission

Once the membrane has been deformed into a bud, the coated vesicle needs to be released into the cytoplasm through its scission mediated by the recruitment of the large GTPase dynamin in conjunction with the actin polymerization machinery. Dynamin is a multidomain tetramer (Fig2A) whose GTPase activity is stimulated over 100 fold by its self-assembly into helical collars on lipid templates (Stowell et al., 1999). There are two models to explain the scission activity of dynamin. They are the mechanochemical model and regulatory model. The mechanochemical model posits GTP hydrolysis by pre-assembled dynamin in driving a conformational change in the molecule that generates tension resulting in vesicle fission. The regulatory model requires dynamin-GTP to recruit effectors that mediate fission. However, a third reconciliatory model that involves both models has been put forth, where in, early, rate-limiting steps of endocytosis are monitored by unassembled dynamin, at coated pits to ensure coat assembly, cargo capture and membrane curvature formation. At late stages of CCV formation, dynamin self assembles into a short, transient collar around the neck of deeply invaginated, fully mature coated pits and catalyses membrane fission (Fig2B) (Mettlen et al., 2009).

The actin polymerization machinery is also important for vesicle scission and functions in conjunction with dynamin. Formation of actin plumes at the constricted neck of the budding vesicle provides the necessary force for pushing the bud deeper into the cytoplasm and increases strain on the stalk until it severs (Ungewickell and Hinrichsen, 2007). Motor proteins such as Myosin VI (Spudich et al., 2007) and Myo1E (Krendel, 2007) also produce traction such that the plus-end motor myosin 1E pulls the dynamin ring toward the plasma membrane while the minus-end motor myosin VI pulls the vesicle into the cytoplasm resulting in strain that severs the constricted stalk beneath the dynamin ring.

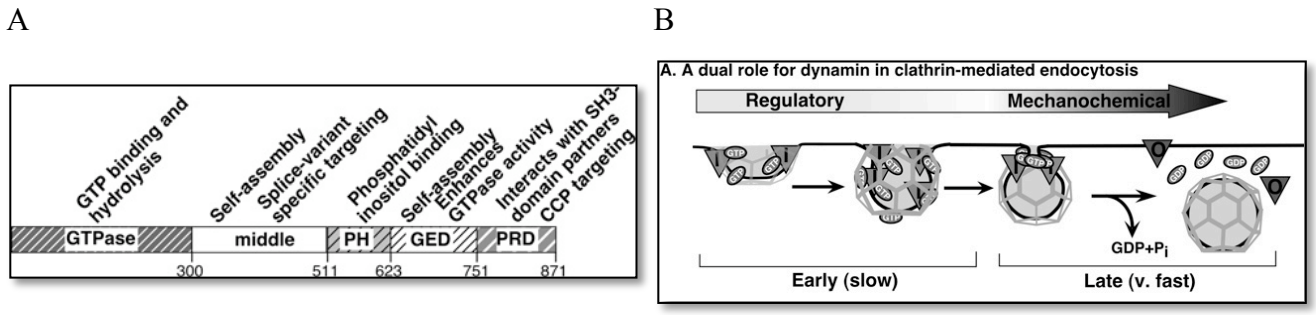

Fig2: Dynamin protein topology and function. A: Protein domain topology of dynamin. B: Dual role for Dynamin in coated vesicle formation. Dynamin functions in early, rate-limiting stages of clathrin coated pit maturation as a regulatory GTPase that receives input from SH3 domain-binding partners that monitor coat assembly, cargo concentration and curvature generation. Subsequently, dynamin functions as an assembly-stimulated GTPase collar that catalyses membrane fission. Adapted from (Mettlen et al., 2009).

1.2.2 Vesicle uncoating

Before fusion of vesicles with their destination compartment, coats and adapters are released to be recycled for a fresh round of coated vesicle formation. The clathrin basket is released from the vesicle by Hsc70, an ATPase and its co-chaperone GAK (cyclin G associated protein kinase)/auxilin (Massol, 2006). The naked vesicle undergoes further trafficking within the cell before appropriate delivery of its cargo through fusion with a destination intracellular compartment. Trafficking is discussed in section 1.5. Upon being trafficked to its destination, vesicles fuse with target compartments releasing their luminal contents.

1.2.3 Vesicle tethering

Vesicle tethering is the initial interaction between a vesicle and its target membrane that precedes the fusion event mediated by association of transmembrane SNAREs (soluble N-ethylmaleimide-sensitive factor attachment protein receptor) on apposing membranes. Tethers act as molecular bridges that "capture" vesicles thus imparting specificity between fusing compartments. Membrane fusion by SNAREs pairing was shown to drive specificity of vesicle targeting (Söllner et al., 1993), however, several lines of evidence indicate that this is not the case. First, interactions between SNAREs are promiscuous (Tsui and Banfield, 2000). Second, disruption of SNARE complex formation does not block vesicle tethering (Broadie et al., 1995). These observations indicate that SNAREs do not mediate the first point of contact between a vesicle

and its target. Instead, tethers, which act upstream of the SNAREs, appear to perform this function. The restricted subcellular localization of tethers and their ability to interact with Rab proteins and SNAREs suggests that tethers participate in determining the specificity of membrane fusion (Cai et al., 2007). Tethers are of two types - proteins with long coiled-coil and multisubunit complexes, both, tethering vesicles at distances beyond 200nm (Sztul and Lupashin, 2006). Several tethering factors, both coiled-coil as well as multiprotein complexes have been identified along the secretory pathway, such as the p115, Giantin, GM130 and TRAPP (Transport Protein Particle) complexes at the Golgi, to name a few. EEA1, an effector of Rab5 is a tethering factor for early endosomes that tethers Rab5 endosomes before the SNARE-dependent fusion event occurs (Christoforidis et al., 1999a).

1.2.4 Vesicle Fusion

Vesicle fusion occurs in two steps, first docking and then fusion. The SNARE complex constitutes the core fusion machinery. SNARE proteins harbor SNARE motifs that are heptad repeats that are required to form the 4-helix bundle. SNARE motifs are structurally distinguished into 4 classes - R, Qa, Qb and Qc (Kloepper et al., 2007). R-SNAREs are vesicle SNAREs present on donor membranes, while the Q-SNAREs are target SNAREs on the acceptor vesicles. Distribution of SNARES renders specificity for fusion between donor and acceptor compartments. SNARE complex formed are extremely stable. The energy of formation of the complex can be harvested to overcome the energy barrier for fusion (Fasshauer et al., 2002). The v- and t-SNAREs consumed during the fusion reaction are reused/recycled for repetitive rounds of transport by molecular machinery that dissociates the extremely stable cis v-/t-SNARE complexes. SNAPs and NSF are cytosolic proteins that target cis-SNARE (Block et al., 1988). SNAP (Soluble NSF Attachment Protein) proteins bind SNARES and recruit NSF (N-ethylmaleimide-sensitive factor, which are hexameric ATPase. ATP-hydrolysis by NSF segregates v- and t-SNAREs for the next round of fusion Fig3. Vesicle fusion reactions mediated by core SNARE machinery is slow and requires accessory factors such as proteins of the Rab machinery to drive kinetically relevant *in vivo* fusion rates as was shown through *in vitro* reconstitution experiments (Ohya et al., 2009).

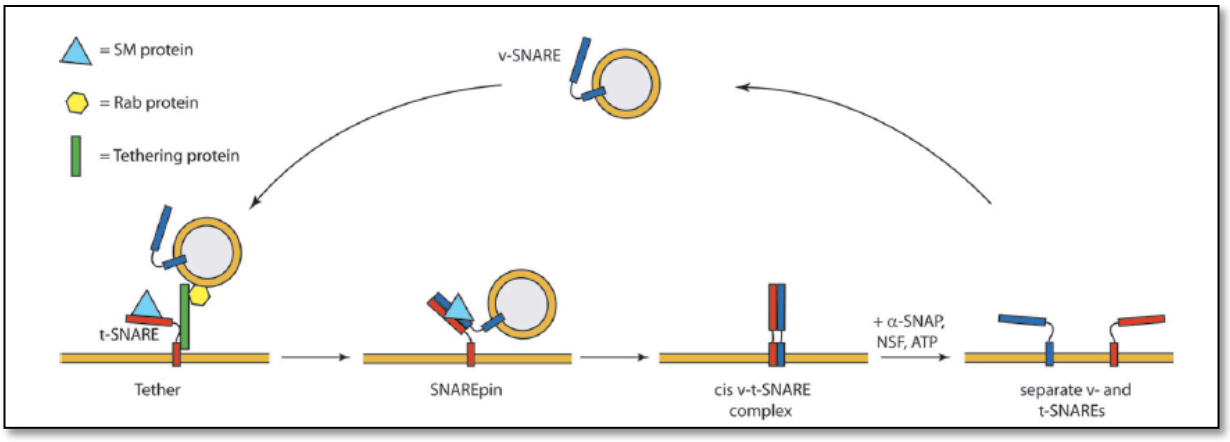

Fig3: Basic machinery controlling membrane fusion and SNARE recycling. The initial interaction of a vesicle with its target membrane is mediated by tethering proteins and a small Rab GTPase. Subsequently, v- and t-SNARE proteins form SNARE pins. These events involve SM proteins and finally culminate in membrane fusion, which results in cis v-/t-SNARE complexes. In the presence of SNAPs, ATP-hydrolysis by NSF segregates v- and t-SNAREs for another round of fusion (Malsam et al., 2008).

Fundamental to intracellular vesicular trafficking is motility Trafficking and targeting to intracellular compartment destinations is regulated through molecules essential for identity of organelles, namely Rab proteins.

1.3 Organelle Identity

Rab proteins, the largest of the Ras superfamily of small GTPases are molecular determinants of organelle identity (Zerial and McBride, 2001). They show distinct subcellular organelle localization (Chavrier et al., 1990) through their ability to associate reversibly with target membranes. Rab GTPases are essential for fidelity of organelle trafficking and organize protein scaffolds. They forge links with cargo adaptors, coat proteins, molecular motors and SNARES to mediate targeted membrane flux between intracellular compartments. Rab GTPases recruit effectors, and their combinations define the identity of organelles. The combinatorial usage of effectors molecules is used to alter subtle properties of organelles and function.

Salient properties of Rab proteins that make them determinants of organelle identity are the following. Several of these features are due to their ability to organize “domains”, distinct

biochemical scaffolds on morphologically contiguous membrane bilayers (Sönnichsen et al., 2000).

1. Reversible assembly/disassembly on membranes – Rab proteins are cytosolic and are capable of reversible recruitment onto membranes depending on the nucleotide bound. Hence, their membrane recruitment is amenable for modulation through the activities of several proteins (see Fig3), unlike integral membrane proteins such as SNARES that cannot be removed from membrane once incorporated.

2. Effector multivalency – Rab proteins can recruit several effectors (Christoforidis and Zerial, 2000) leading to the formation of protein scaffolds on target membrane.

3. Combinatorial use of effectors to define distinct biochemical environments - that contribute to specific functionality such as distinct subpopulations of Rab5 endosomes marked by EEA1 or APPL in the early endocytic network. EEA1-Rab5 endosomes are canonical early endosomes, while APPL1 endosomes support signal transduction (Miaczynska et al., 2004), (Schenck et al., 2008).

4. Ability to organize functional domains on membranes - being cytosolic and multivalent, they are capable of organizing functional domains on membranes important for transport of cargo along membrane networks such as the Rab5, Rab4, Rab11 along the recycling pathway (de Renzis et al., 2002), or Rab5, Rab7 along the degradative pathway (Rink et al., 2005).

5. Ability to reinforce organelle identity through recruitment of effectors – Rab proteins such as Rab5 recruit and activate Phosphoinositol 3 kinases, that generate a local pool of phosphatidylinsositol-3-phosphate (PtdIns(3)P) on early endosomes (Christoforidis et al., 1999b). Rab5 in conjunction with PtdIns(3)P function in defining Rab5 compartments and recruiting effectors.

Several proteins coordinate the Rab-GTP cycle and their recruitment to membranes as depicted in Fig4.

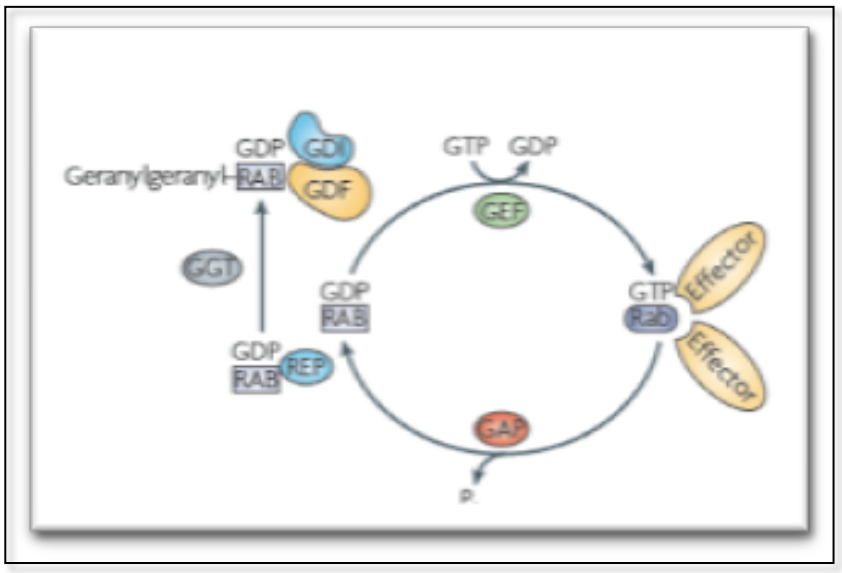

Fig 4: Rab GTPase cycle – Rab-GTPases cycle between their active membrane bound GTP-form and inactive cytosolic GDP-form. Rab-GTP binds effectors and coordinates membrane trafficking. Hydrolysis of GTP by Rab-GAPs to Rab-GDP inactivates and returns Rab-GDP to the cytosol. GDP is prevented from dissociation from Rab-GDP by Rab-GDI. Rab-GDI also regulate targeting of Rab-GDP to membranes by associating with GDFs. Rab-GEF catalyze the exchange of GDF for GTP, activating allowing for their recruitment to the target membrane. REP chaperone Rab-GDP akin to GDIs, only, the former associates with *de novo* synthesized Rab GTPases and presents it to GGTs for geranlygernylation that allows membrane recruitment of Rab proteins. Rab-Ras Associate protein from rat Brain, GAP-GTPase Activating Protein, GEF-Guanidine nucleotide Exchange Factor, GDI-GDP Dissociation Inhibitor, GDF-GDI Displacement Factor, REP-Rab Escort Protein, GGT-GeranylGeranyl Trannnsferase. Adapted from (Stenmark, 2009).

The following sections focus on endocytosis, the biological process that I have worked on for my thesis, with a general introduction to the process followed by a description of the endosomal populations. Since my work focuses on early endosome motility, later sections describe intracellular motility starting with an introduction to molecular motors, their classification, regulation, targeting to intracellular compartments and finally ending with a speculative note on why early endosome need to move in the cell.

1.4 Endocytosis

Adaptive response to external stimuli is a hallmark of organismal systems, continual iterative sampling of the environment being obligatory for survival. Eukaryotes have evolved endocytosis as a means of perceiving signals impinging on the cell's receptive field. By the canonical definition, endocytosis is a process of molecular ingestion, recycling and/or degradation; however, the cell seems to have diversified the functions for this process in using endosomes as platforms for spatio-temporal fine-tuning of signaling cascades.

The predominant mode of endocytosis is clathrin mediated. The efficiency of clathrin dependent endocytosis is so much so that in an hour, as much as the whole cells volume can be endocytosed in fibroblasts (Bretscher, 1982). Nevertheless, internalization of various cargoes is largely unaffected in the absence or perturbation of clathrin mediated endocytosis, indicating the existence of clathrin independent routes of endocytosis. Cargo molecules internalized by non-clathrin mediated pathways are more sensitive to membrane cholesterol than are CME cargoes. Table1 summarizes various modes of internalization of cargoes based on their morphology and molecular requirements.

Endocytic mechanisms	Morphology	Implicated cargoes[b]	Small G-protein dependence	Dynamin implicated?	Other proteins implicated
Clathrin mediated	Vesicular	RTKs, GPCRs, transferrin receptor, anthrax toxin	Rab5, Arf6 implicated	Well established	Clathrin, AP2, epsin, SNX9, synaptojanin, actin amphiphysin, plus many others
Caveolae-/ caveolin1-dependent	Vesicular/ tubulovesicular	CTxB, SV40, GPI-linked proteins	Unclear (cavelolins may regulate cdc42 activity)	Some evidence	Caveolins, PTRF, src, PKC, actin (many signaling proteins localize to these sites)
CLIC/GEEC	Tubular/ring like	Fluid phase markers, CTxB, GPI-linked proteins	Cdc42, Arf1	Not as yet	ARHGAP10, actin, GRAF1, other GRAFs
IL2Rβ pathway	Vesicular?	IL2Rβ, FCεRI, Kir3.4, γc-cytokine receptor	RhoA, Rac1	Implicated	PAK1, PAK2
Arf6 dependent	Vesicular/tubular	MHC class I proteins, CD59, carboxypeptidase E	Arf6	Not as yet	Unclear as yet
Flotillin dependent	Vesicular	CTxB, CD59, proteoglycans	Unclear	Implicated but unclear	Flotillin 1 and 2
Phagocytosis	Cargo shaped	Pathogens, apoptotic remnants	Arf6/cdc42/rac1/rhoA (depending on type)	Implicated	Actin, IQGAP1, amphiphysin1, Rho kinase, adhesion proteins
Macropinocytosis	Highly ruffled	Fluid phase markers, RTKs	Rac1	Not as yet (CtBP1/BARS implicated in scission)	Actin, PAK1, PI3K, Ras, Src, HDAC6
Circular dorsal ruffles	Highly ruffled	Fluid phase markers, RTKs	Unclear	Implicated	Cortactin, actin
Entosis	Cell shaped	Matrix-deligated cells	RhoA	Not as yet	Adherens junctions

Table1: Modes of internalization into the cell (Doherty and McMahon, 2009).

Ligands internalized in cells are all received into early Rab5 endosomes, the cell's sorting stations from where cargo is sorted and routed to their intracellular destinations.

1.4.1 Early endosomes

Early endosomes are organelles that receive incoming cargo from vesicles that have been generated by clathrin dependent and independent endocytosis. They are a network of pleiomorphic tubular-vesicular structures with a vesicular body of ~0.5μm in diameter and

tubules of ~50nm emanating from the vesicular body (Gruenberg, 2001). Early endosomes are the major sorting stations of internalized cargo. Cargo in early endosomes is sorted to the plasma membrane, late endosomes or recycling endosomes. Molecular sorting begins with the dissociation of ligand-receptor complex owing to mild acidic pH (~6.3) conditions of the endocytic lumen (Casey et al., 2010). Sorting of cargo for recycling from early endosomes is based largely on geometrical of molecules. Membrane with cargo to be recycled is removed by pinching off of narrow-diameter tubules (Dunn et al., 1989). Since the surface area-to-volume ratio of the tubules is greater than that of the vesicular portion of the sorting endosome, iterative pinching tubulation preferentially sorts recycled membrane from the soluble molecules even in the absence of specific targeting information. Hence, recycling occurs mainly through bulk flow of membrane tubules back to the plasma membrane (Mayor et al., 1993) as opposed to degradative cargo that are actively sorted through sorting motifs.

The small GTPase Rab5 recruits a plethora of effectors (Christoforidis and Zerial, 2000) that allows for functioning of early endosomes in not only cargo sorting, but also in modulating signaling and gene transcription events that contribute to higher order functions such as cell survival, apoptosis, differentiation, migration and interferon response to name a few (Schenck et al., 2008), (Scita and Di Fiore, 2010), (Sorkin and Von Zastrow, 2009).

1.4.2 Recycling endosomes

Recycling endosomes function in returning membrane and molecules that have been internalized during endocytosis. This process replenishes lipids and proteins lost during internalization thus maintaining mass and composition of plasma membrane. Based on the kinetics of recycling, two routes have been identified - the fast recycling route mediated by Rab4 proteins where molecules are returned from Rab5 sorting (early) endosomes to the plasma membrane with a $t_{1/2}$ of ~2mins, and a slower Rab11 recycling route where cargo reach the perinuclear Endocytic Recycling Compartment (ERC, also called perinuclear recycling compartment) (Ullrich et al., 1996) and return the cell surface with $t_{1/2}$ of ~12mins (Maxfield and McGraw, 2004). Whether recycling endosomes are independent entities is ambiguous, since morphologically Rab4 and Rab5 are resident on the same vesicular structure, however they are segregated into distinct domains (Sönnichsen et al., 2000). Recycling endosomes are involved in functions other than returning membrane and cargo back to the plasma membrane such as in abscission of cleavage furrow

during cytokinesis (requires Rab11 endosomes) and in focal adhesion dynamics during cell migration that is mediated through Wnt signaling by Rab4 endosomes (Gould and Lippincott-Schwartz, 2009).

Several molecular motors have been identified for both the rapid and slow recycling routes - MyoV was shown to be required for rapid transferrin recycling; functional ablation of MyoV resulted in transferrin accumulation in ERCs (Yan et al., 2005). MyoVI, the minus end myosin was shown to be important for tubulation of recycling endosomes. RNAi knock down of MyoVI resulted in swollen, tubulation deficient endosomes with inhibited delivery of transferrin to ERCs (Chibalina et al., 2007) while MyoVb functions as dynamic tethers in localizing transferrin loaded vesicles at the cell periphery retarding their transport to ERCs (Provance et al., 2008). Transport of cargo (transferrin) from the ECR was shown to be dependent on Kinesin motors that specifically associate with stable glutamated, detyrosynylated microtubules (Lin et al., 2002). Transferrin recycling, especially fast transport was shown to be independent of Dynein (Valetti et al., 1999). Molecular motors hence are involved in multiple functions along the recycling pathway that include motility of recycling endosomes, tethering and membrane tubulation.

1.4.3 Late endosomes and Lysosomes

Late endosomes and lysosomes are organelles of the degradative endocytic pathway. They are devoid of recycling cargo. Late endosomes are prelysosomal organelles that localize to the MTOC. They are characterized by low intra-luminal pH of ~5-6, are multivesicluar in morphology and enriched in Mannose 6-Phosphate Receptors (MPR). The lipid composition of late endosomes differs from that of earlier endocytic compartments, in that, they are enriched in triglycerides, cholesterol esters and phospholipids, predominantly Lysobisphosphatidic Acid (LBPA) (Kobayashi et al., 1998).

Degradative cargo in the early sorting endosomes have been shown to be transported to late endosomes by intermediate carrier vesicles termed Endosomal Carrier Vesicles (ECV) that are ~0.5μm in diameter. Transport by ECVs is dependent on microtubules (Gruenberg et al., 1989).

Lysosomes are the terminal hydrolytic compartment along the degradative arm in the endocytic pathway (Kornfeld and Mellman, 1989). They are distinguished from late endosomes by the absence of Mannose Phosphate Receptors (MPR), and presence of hydrolytic enzymes with

acidic pH optima. There are two main models that explain transport of cargo from late endosomes to lysosomes namely, fusion and kiss and run (kiss and linger). Transport from late endosome to lysosome occurs through direct fusion forming hybrid organelles as shown by EM and density centrifugation experiments (Mullock et al., 1998) and through kiss an run where, cargo is delivered through repeated transient fusion events (Bright et al., 2005).

Lysosomes are clustered at the MTOC of cells by the Dynein motor. Disruption of Dynein distributes lysosomes throughout the cell, underscoring the importance of molecular motors as potential anchors (Harada et al., 1998). Lysosomes are dynamic organelles that respond to Growth factors and cellular stress by reorganizing distribution. Decrease in cellular pH or serum starvation redistributes lysosomes throughout the cell, while simulation with growth factors or alkalinization of cytosol clusters them to the MTOC (Heuser, 1989). Dispersion of lysosomes has been shown to be dependent on Kif5B in mouse fibroblast (Nakata and Hirokawa, 1995).

1.5 Cellular Cytoskeleton and Molecular motors – a prelude

Intracellular motility it is a dynamic process in which distribution of organelles is constantly remodeled as a consequence of response to stimuli. Several forces that include molecular motors, cellular cytoskeleton and regulatory proteins need to be co-coordinated to achieve transport kinetics conducive for optimal kinetics of transport. Motors provide spatial and vectorial context to organelle trafficking. Endosome localization under steady state is achieved through the complex interplay between molecular motors of opposing polarity and regulatory mechanisms that control motor activity and microtubule dynamics.

1.5.1 Cellular Cytoskeleton

Actin and microtubules are the principle cytoskeletal components used in intracellular transport and organelle localization in cells. Both structural elements are polymers of actin and tubulin heterodimers respectively. Unlike yeasts that use actin and myosin driven intracellular transport, animal cells use microtubule system for their intracellular trafficking events. Organelle motility in giant squid axons suggested the use of microtubules for long-range movement, while actin mediates short-range motility. This is due in part to the length of the polymers, with MT extending to >25um, and actin extending upto 1um (Langford, 1995). This might explain the

evolutionary transition from a predominantly actin based transport system to one dominated by microtubule cytoskeletal system from yeast to man with concomitant increase in cell size.

Actin has been shown to be important for initial stages of internalization in mammalian cells. The first evidence for involvement of actin in clathrin-mediated endocytosis in higher eukaryotic cells was in 1980s (Salisbury et al., 1980). Actin is involved in lateral movement of coated patches, vesicle fission and the movement of the vesicle away from the plasma membrane (Merrifield et al., 2005), (Merrifield et al., 2002), (Yarar et al., 2005) However, invagination of coated structures appears not to be effected by inhibiting actin dynamics as accumulation of deeply invaginated coated pits was observed in cells exposed to Latrunculin A (Merrifield et al., 2002). Actin has also been implicated in delivering degradative cargo from early to late endosomes along the degradative pathway in mammalian cells (Durrbach et al., 1996).

Microtubules are polarized polymers that radiate from the perinuclear region and provide a vectorial framework for intracellular transport of organelles. Depolymerization of the microtubules through pharmacological drugs results in gross mislocalization of organelle components, albeit affecting rates of transport that too only moderately. Hence, transport is not an all or none process. Microtubules in cells can be dynamic, undergoing phases of growth and shrinkage during dynamic instability. Dynamic instability allows microtubules to explore three-dimensional space for rapid remodeling of the cytoskeleton during processes such as spindle assembly and cell migration (Schulze and Kirschner, 1986). They can acquire Post Translational Modifications (PTMs), bind Microtubule Associated Proteins (MAPs) and/or Plus end tracking proteins (TIPs) and thus be stabilized (Westermann and Weber, 2003). PTMs of microtubules include detyrosinylation, glutamation, acetylation, phosphorylation, glycation and palmitoylation. All of these other than acetylation occur at the c-ter region or one or both of the tubulins (Verhey and Gaertig, 2007) and can alter stability of microtubules, motor binding and activity and modulate various processes such as development of polarity.

1.5.2 Molecular Motors

All motors have a force generative element that hydrolyzes ATP to generate energy for their motion. This motive force allows them to progressively translocate along the cytoskeletal substrate. The mechanochemical cycle of Dynein and myosin family of motors are evolutionarily related, while that of Kinesin is divergent (Romberg and Vale, 1993) despite similarity in protein

topology and organization of the motor domain between kinesins and Myosins (Kull et al., 1998). Why is there an expansion of the genetic complement of molecular motors from yeast to man? A naïve explanation would be to diversify functions allowing for functional specialization that is concomitant with increased cellular complexity thereby allocating motors to discrete membranous components in the cell. Expansion of motors paralogues in genomes as a consequence of gene duplication and domain fusion have increased the repertoire of molecular motors represented in the cell. The human genome encodes 14, 18 and 2 families of Kinesins, Myosins and dyneins respectively based on the phylogenetic analysis of their motor domains (Verhey and Hammond, 2009), (Berg et al., 2001), (Pfister et al., 2006).

Single-molecule *in vitro* studies have been used to characterized several motors. Kinesin-1, cytoplasmic dynein, and myosin V are all processive, meaning that they go through several ATPase cycles without releasing from their filament. Thus, in principle, a single motor is sufficient to move a cargo some distance in the cell before detaching from the cytoskeletal track. *In vitro*, kinesin's processivity is approximately between 800 and 1200 nm (Thorn et al., 2000) (Schnitzer et al., 2000) and that of myosin V is between 700 and 2100 nm (Sakamoto et al., 2003). Most other unconventional myosins are however non-processive. Dynein has a processivity of approximately 1000 nm, however, association with Dynactin (King and Schroer, 2000) enhances processivity. Speed of Kinesins and Dyneins are on an average 500-700nm/sec (Kojima et al., 1997), (King and Schroer, 2000), while of unconventional mysoins is 0.015–0.4 μm/sec (O'Connell et al., 2007), making them less suited for intracellular transport. Each of the class of molecular motors is described below.

1.5.2.1 Kinesins

Kinesins are microtubule based molecular motors that were first identified in Squid giant axons as molecules necessary for translocation of microtubules on glass surfaces and beads on microtubules (Vale et al., 1985). Ever since, several Kinesins have been cloned and characterized. They are classified ino14 classes based on their domain phylogeny as depicted in Fig5. Most Kinesins translocate cargo toward the plus end of microtubules, but some do so toward the minus end as well.

Activity of Kinesins can be regulated though several means that include post translational modifications (phosphorylation), association with accessory components and intramolecular clamping (Hirokawa et al., 2009), (Verhey and Hammond, 2009).

Protein phosphorylation can modulate association and dissociation of motors with their cargos or binding of kinesins to microtubules. Protein kinase A (PKA) dependent phosphorylation of KIF5–KLC complexes inhibits the association of this motor with synaptic vesicles (Sato-Yoshitake et al., 1992). Glycogen synthase kinase 3 phosphorylates KLC and inhibits association of KIF5–KLC complexes with membrane organelles (Morfini et al., 2002). JNK phosphorylates KIF5 motors (Stagi et al., 2006) leading to decreased affinity of motors to microtubules.

Autoinhibition of Kinesin heavy chains is yet another mechanism to prevent futile intracellular translocation of motors in the absence of cargo and congestion of cytoskeletal tracks. Several Kinesins such as Kif5 and Kif1A transit between active extended and inactive folded conformations in the absence of cargo (Coy et al., 1999; Hammond et al., 2009). Cargo binding relieves autoinhibition, engaging active transport by motors (Coy et al., 1999). Associated Kinesin light chains also maintain heavy chains in inactive basal state by inducing interaction between the tail and motor head domain of heavy chains (Verhey et al., 1998). Hence regulation of Kinesin activity is achieved by several means in the cell.

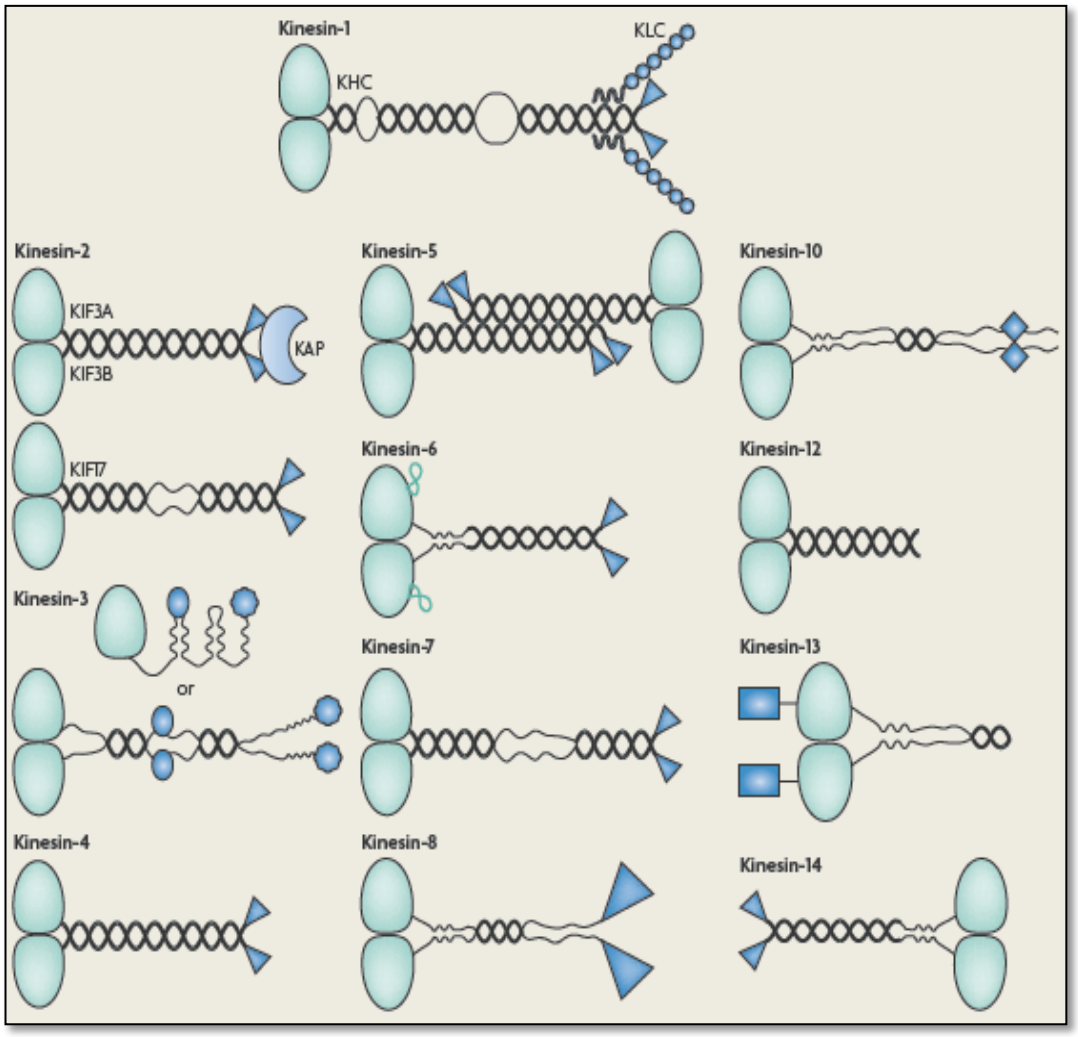

Fig 5: Organization of Kinesins families. Green-motor domain, blue-MT binding or protein associating domain. Most Kinesins are homodimers, except Kinesin3, which can homodimerize or function as monomers. Some of the Kinesins associate with accessory components known as Kinesin Related Proteins (KRPs). Adapted from (Verhey and Hammond, 2009).

1.5.2.2 Kinesin Related Proteins (KRPs)

Kinesin motor chains often associate with accessory components called Kinesin Related Proteins or KRPs. These proteins include Kinesin Light Chains (KLCs) and Kinesin Associated Protein (KAP). KLCs represented by 4 genes in the human genome have been shown to interact with the conventional homdimeric Kinesin 1 as homodimers forming a heterotetrameric holo motor complex (Johnson et al., 1990). KLCs associate with the heavy chain through heptad coiled-coli region at the N-terminus, while tetratricopeptide repeats at the C-terminus interacts with cargo.

KLCs have been shown to be important for motor localization (Rahman et al., 1999) and cargo specificity (Woźniak and Allan, 2006) and motor activity (Verhey et al., 1998).
KAPs associate with Kinesin 2 (Kif3A/3B) and probably regulate motor properties. However, it has also been shown through *in vitro* experiments that each of the motor heavy chains are active in the absence of KAP3 (Yamazaki et al., 1995).

1.5.2.3 Myosins

The myosin superfamily of mechanoenzymes comprises 18 classes (Berg et al., 2001). The human genome encodes about 40 myosin genes (Fig6), among which about 25 are unconventional and come from at least 11 classes. Myosin II form the conventional class, while all other myosins are unconventional, in that the former are involved in muscle contraction, while the latter are involved in transport and regulatory functions (Woolner and Bement, 2009). Myosins have undergone extensive divergent evolution through domain fusion events. Hence these multidomain proteins are capable not only of coupling their actin-based motor activities to membrane dynamics, but of directly and indirectly affecting actin assembly and disassembly.
Myosin heavy chains contain a head (catalytic, motor domain), generally N-terminal, followed by a neck domain to which the light chains bind and a C-terminal tail domain, which, in some myosins, dimerizes with an identical heavy chain by forming coiled-coil helical regions and through which some myosin dimers polymerize into filaments (muscle-myosinII). The tail domain of other myosin heavy chains is thought to associate with cargoes that the myosin molecules transport along actin filaments. Light chains in the case of Myosins are regulatory in function (Korn, 2000).
Most unconventional myosins so far characterized are relatively slow motors when assayed for their ability to transport F-actin *in vitro*, having transport rates typically between 0.015–0.4 μm/sec. Some myosins such as myo-11 have rates an order of magnitude faster, i.e ~4.5 μm/s. The latter rates are similar to those of organelle transport on microtubules in animal cells, implying that unconventional myosins are unlikely to be serving transport functions (O'Connell et al., 2007) in higher eukaryotes. They have been proposed to serve as tethers for organelles instead as was shown for MyoVb. These motors were shown to be dynamic tethers for transferrin vesicles in HeLa cells (Provance et al., 2008). Mysoins together with actin are important for regulatory functions. For example, Myosin motors (MyoVa) have been shown to be required

along with Kinesins to specify localization of dendritic cargo and actin is important in establishing polarity in neurons (Lewis et al., 2009).

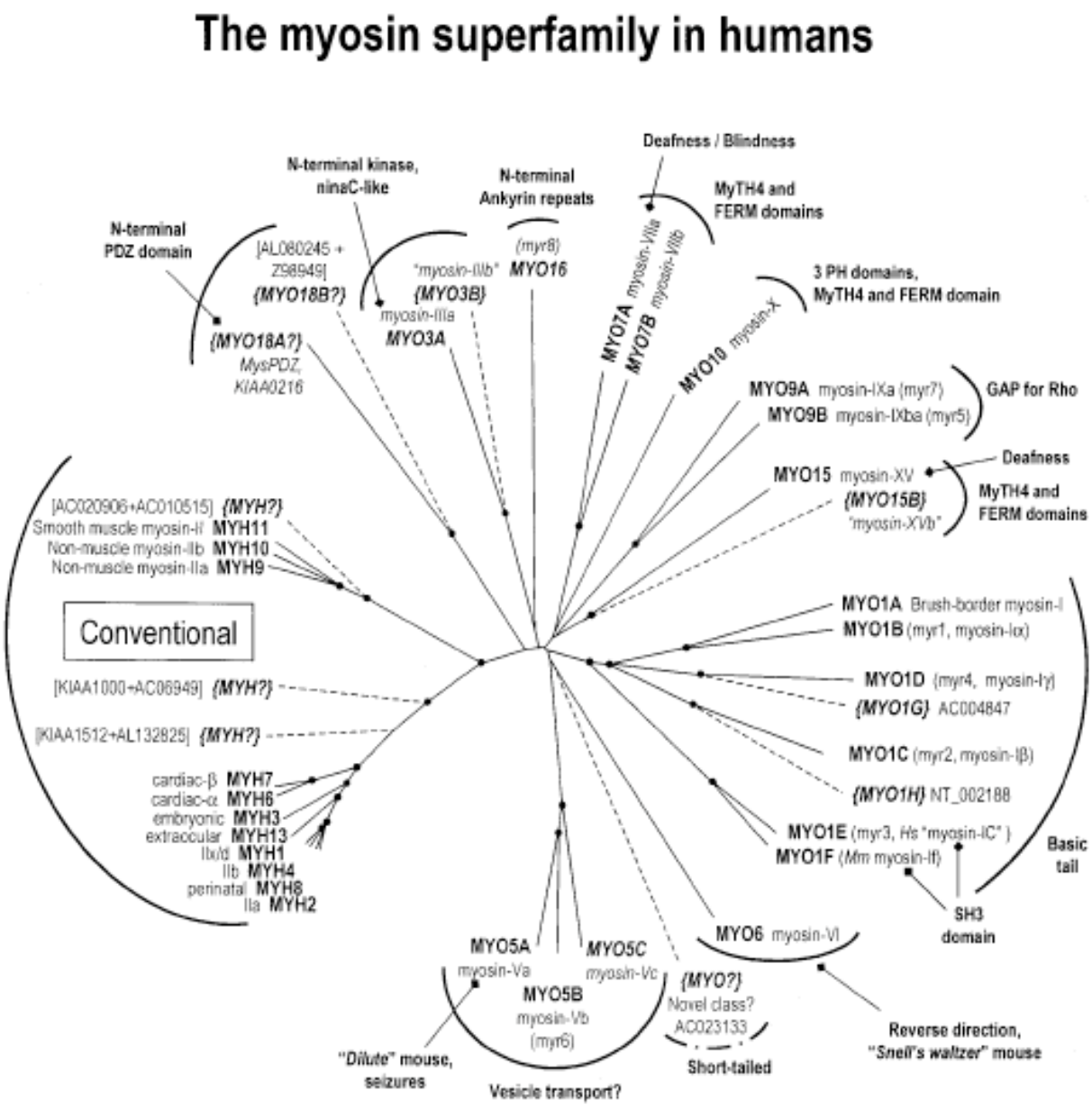

Fig6: Phylogenetic tree of the myosin superfamily in humans. Solid lines indicate myosins known from cDNA sequences and dashed lines indicate putative myosins predicted from genomic sequence. Black dots represent validated nodes. Official HUGO human gene names are indicated in bold, and synonymous names from human or related organisms such as rat (Myr) are indicated in plain type. Recently discovered or newly predicted myosin genes are italicized, and potential gene names suggested for myosins predicted from genomic sequence are indicated in brackets. Sequences assembled from overlapping genomic clones or cDNAs are indicated in square brackets. Phylogenetic tree was generated from myosin head domain

amino acid sequences. PH, pleckstrin homology; MyTH4, myosin tail homology 4; FERM, band four point one/ezrin/radixin/moesin. Adapted from (Berg et al., 2001).

1.5.2.4 Dyneins

Dyneins are a family of minus end directed microtubule dependent molecular motors whose structure, topology of the motor domain is evolutionarily divergent from that of Kinesins and Myosins. Dynein motor is a complex of at least six polypeptides, consisting of the Dynein (DYNCH) motor protein that associates with accessory components that include Intermediate chains (DYNCI), Light Intermediate chains (DYNLCI) and the Light chains (DYNCL) to form the holo-motor.

Based on the evolutionary phylogeny, Dynein heavy chains cloned/annotated in silico thus far, are categorized into cytoplasmic or axonemal. Dynein motor proteins are ~4,600 amino acid residues long, have 3 recognizable structures by EM– a hexameric AAA ATPase ring at the C-ter, a 15nm protrusive stalk capped by a globular head that emanates from between the fourth and fifth AAA ATPase domain (Vallee et al., 2004) (Fig7A). The first 4 ATPase domains can potentially bind ATP since they have the conserved the P-Loop or the Walker motif, but it is only the first and third that can hydrolyze ATP to produce motive force. The Stem has a homo-oligomerization domain, along with sites for interaction with the dimeric DYNICs and DYNLICs.

The most abundant cytoplasmic dynein complex, cytoplasmic dynein 1, is involved in functions as diverse as spindle-pole organization and nuclear migration during mitosis, the positioning and functioning of the endoplasmic reticulum, the Golgi apparatus, and the nucleus, and also the minus-end-directed transport of vesicles, including endosomes and lysosomes, along microtubules and retrograde axonal transport in neurons. Axonemal Dyneins are responsible for movement of cilia and flagella. Cytoplasmic Dynein heavy chain knock out mice are embryonic lethal (Harada et al., 1998) underscoring the importance of functional Dynein in the cell.

Dynein light chains bind intermediate chains. Dynein light chains were thought to bind cargo however, recent crystallographic studies have shown that binding of dimeric DYNICs sterically occludes DYNLCs. Light chains are thought to stabilize the intrinsically disordered intermediate chains. Cargo specificity was instead shown to be dependent on DYNLICs in the Dynein complex.

Functional cytoplasmic Dyneins have been shown to bind all of the accessory components, i.e

DYNIC, DYNLIC and DYNLC, while axonemal Dyneins have been shown only light intermediate chains (Pfister et al., 2006)(Fig7B).

Accessory components of the cytoplasmic Dynein have a particularly expanded genetic inventory in animals, allowing for combinatorial assembly of complexes. This, added to splicing variants and posttranslational modifications of components produce a large regulatory repertoire of functional Dynein complexes. Higher plants on the other hand lack Dyneins and instead have an expanded inventory of minus end Kinesisn genes (Murray and Wolkoff, 2003). With Kinesins and Myosins, the motor chain diversity increases the functional heterogeneity, while with Dyneins, the accessory components do the same.

The combinatorial assembly of complex provides target specificity as well as specificity in regulation. It is however not known if axonemal components can be assembled with cytoplasmic components to from holo-complexes in cells. This would expand permutation window and increase the cellular gamut of Dyneins in the cell.

A

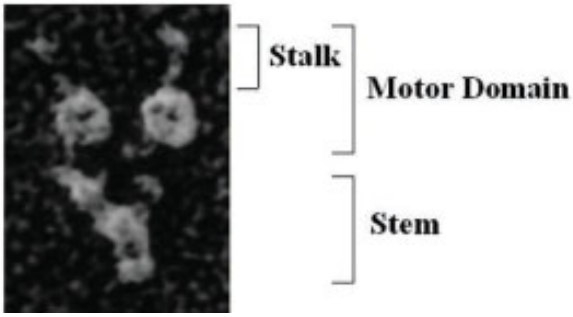

(Vallee et al., 2004)

B

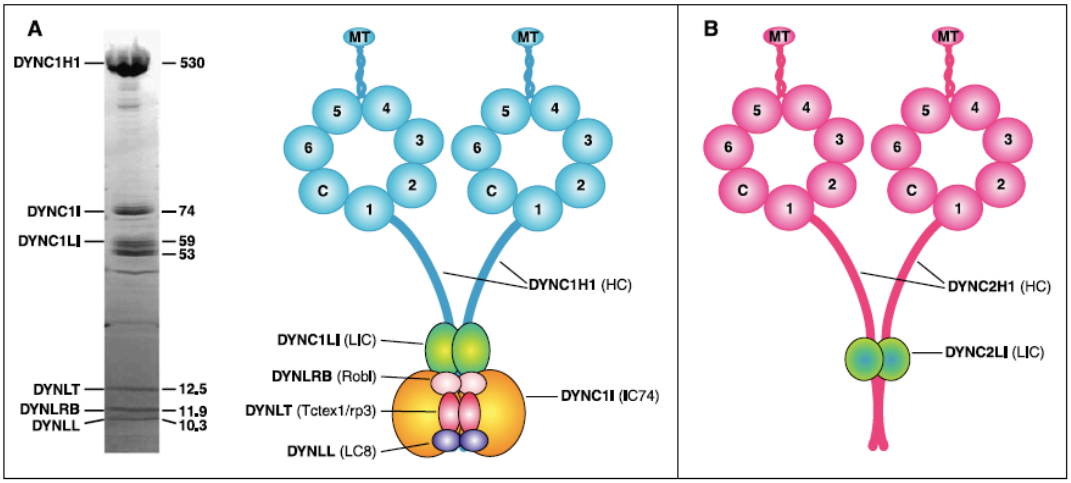

(Pfister et al., 2006)

Fig7: Organization of Dynein complex. A: Electron micrograph represents rotary shadowed image of single cytoplasmic dynein particle, with motor domain, microtubule-binding stalk and cargo-binding stem. B: Subunit composition of cytoplasmic and axonemal Dyneins.

1.5.2.5 Dynactin

Dynactin is a multi-protein complex that was initially isolated as an activator of Dynein motility of vesicles in vitro (Schroer and Sheetz, 1991). It is composed of 11 polypeptides (Gill et al., 1991), each in one or more copy numbers in the holo complex, adding up to a molecular mass of ~1.2MDa. In electron microscopy images, purified Dynactin consists of 2 structural elements - a 25-50nm rod that forms the base and 10 × 40nm side arm that projects from the rod (Schafer et al., 1994) (Fig8A). The composition and their location in the structure are summarized in Table2.

Dynactin subunit composition			
Component	**Alternate name**	**Stoichiometry**	**Incorporated in**
DCTN1	P150Glued	2	Side arm
DCTN2	P50-dynamitin	4	Side arm
DCTN3	P24	2	Side arm
DCTN4	P62	1	Pointed end complex
DCTN5	P25	1	Pointed end complex
DCTN6	P27	1	Pointed end complex
Arp11	ACTR10	10 to 11	Pointed end complex
Arp1	ACTR1A	7	Rod
CapZ-α		1	Rod
CapZ-β		1	Rod
Actin		1	Rod

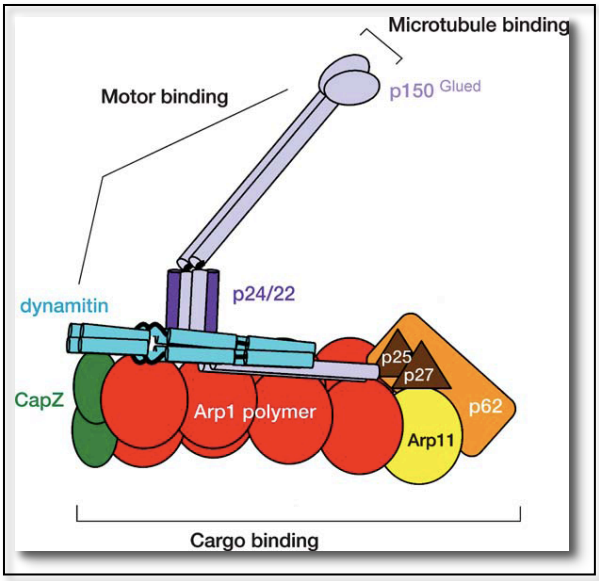

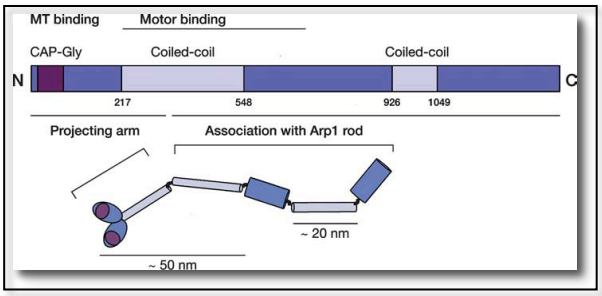

The Dynactin complex. Table2: Composition of Dynactin complex.
Fig8 A: Schematic of subunit composition of Dynactin complex. B: Protein topology of Dynactin1

DCTN1 (p150*Glued*) is the business end of the Dynactin complex (Fig8B). It is the most conserved and probably the best studied subunit of the complex. It has a N-ter CAP-Gly (Cytoskeletal Associated Protein - Glycine rich) domain, followed by 2 coiled-coil motifs. In EM images of Dynactin complex, DCTN1 is the side arm with its N-ter microtubule-binding domain splayed out. This region is also subject to alternative splicing which alters affinity for microtubules (Zhapparova et al., 2009). Amino acids 600-800 of DCTN1 interacts with the intermediate chain of the Dynein complex (Vaughan and Vallee, 1995). The same region also interacts with Kinesin II (Deacon et al., 2003), while amino acids 410-811 interacts with Eg5, a

mitotic Kinesin (Blangy et al., 1997). Hence Dynactin can interact and recruit multiple partners such as Dynein or KinesinII and Eg5 through the DCTN1 subunit.

The side arm is also constituted by DCTN2 (dynamitin) and DCTN3. DCTN2 interacts with both DCTN1 and DCTN3 and links DCTN1 to the Arp1 located in the rod. Over-expression of DCTN2 disassembles the side arm from the rod, disrupting the function of Dynein both *in vivo* (Echeverri et al., 1996) and *in vitro* (Melkonian et al., 2007). The function of DCTN3 is not clear other than the fact that it interacts with DCTN1. Overexpression of DCTN3 does not have any effect on the structure or function of the Dynactin complex (Karki et al., 1998).

The rod is composed mainly of a homoheptamer of Arp1 proteins that is organized as minifilaments resembling polymerized actin and contains a monomer of β-actin. It is capped on one end by the heterodimerize Cap-α and Cap-β(Cap-Z) and on the other by a point end complex, a tetramer of DCTN4, DCTN5, DCTN6 and Arp11 (Schroer, 2004). The point end complex is organized into a triangular disc. Arp1 can interact with βIII spectrin present on Golgi vesicles and hence recruit Dynein for retrograde transport of Golgi vesicles (Holleran et al., 2001). Arp11 probably functions as an actin cap on the minus end of the rod. The functions of DCTN4, DCTN5 and DCTN6 are also not known, although they are thought to bind cargo. These genes are not present in yeast and so might not be obligatory for the assembly and/or function of Dynactin.

Dynactin performs several functions in the cell –It is a processive factor for Dynein (King and Schroer, 2000) increasing run lengths of Dynein and Kinesin2 (Berezuk and Schroer, 2007). It functions as an adaptor in recruiting Dynein to membranous structures, such as the Golgi via its association with Arp1 (Holleran et al., 2001). It is a microtubule plus end Tip Interacting Protein (+TIP) as DCTN1 interacts with several plus TIPs such as EB1 to suppress dynamic instability altering microtubule dynamics (Manna et al., 2008). DCTN1 of Dynactin also interacts with CLIP170, a +TIP present on endosomes and recruits Dynein at the plus end of microtubules thus loading Dynein with cargo for retrograde transport (Valetti et al., 1999).

Dynactin can potentially function as a tether through the CAP-GCY domain of DCTN1 that can bind microtubules since this domain is not necessary for the processivity function of Dynactin (Kardon et al., 2009).

1.6 Targeting motors to compartments

How motors engage cargo is not very well understood. Several motor receptors identified have been through two-hybrid screens, where the interaction between motors and cargo is mediated through protein-protein interactions. In some cases however, motor specific receptors are domains fused with the motor head as with the PX domain in Kif16B that binds PI3P enriched endosomal membrane (Hoepfner et al., 2005) and Unc104/KIF1A kinesin. The latter in worms (*Caenorhabditis elegans*) and mice, is involved in the anterograde transport of synaptic precursors in neurons through the binding of its PH (Pleckstrin Homology) to PtdIns(4,5)P_2 on synaptic vesicles (Klopfenstein et al., 2002). With conventional Kinesins however, cargo binding and specificity have been shown to be mediated by light chains they associate with. The tricopeptide repeats in light chains are though to be important in specifying cargo as was shown for KLC1B and KLC1D with specificities for Gogli and rough endoplasmic reticulum respectively (Woźniak and Allan, 2006). In some cases such as RabKinesin6 (Kif20A), the motor binds to the GTP form of Rab6 GTPase (Echard et al., 1998). Rab6 in its active GTP form has also been shown to bind p150Glued subunit of Dynactin and recruit Dynein (Short et al., 2002).

Dynein has also been shown to bind via Arp1 of Dynactin binding to βIII spectrin on Golgi membranes (Holleran et al., 2001). Binding specificity is thought to be reinforced by the PH domain of βIII spectrin binding to acidic phospholipids such as PtdIns(4,5)P2 or phosphatidic acid (Muresan, 2001).

Motors can be recruited to organelles through effectors such as Rab7 Interacting Lysosomal Protein (RILP), a Rab7 effector that binds Dynein (Jordens et al., 2001) or can be targeted to membranes by coincident detection such as with Myo6 recruitment to clathrin coated vesicles through its binding to both Dab2 and PtdIns(4,5)P_2 (Spudich et al., 2007).

In the case of early endosomes, with the exception of Kif16B, how other motors are recruited is not known.

1.7 Bi-directional motility of organelles

Several organelles display bidirectional motility such as mitochondria, endosomes, mRNA and chromosomes, however the reason for this mode of motility and its function in the cell is not

understood. For some organelles, such as endosomes, mitochondria and mRNA, it is thought to allow for the steady state distribution in the cell. Other hypotheses are for navigating around roadblocks imposed by MAPs and /or other cargoes along microtubules and track switching from microtubules to microfilaments and *vice versa*. Other hypotheses for bi-directional motility of early endosomes are - exploring cytoplasmic environment in space and time, especially in the context of signaling. Endosomes transporting signaling cargo can potentially modulate the residence with the endosomes by indulging in increased bi-directional regimes. Bi-directional motility has been shown to be important in cargo sorting through and vesicle scission through opposing forces exerted through tug of war mode of bi-directional motility (Soppina et al., 2009), (Nath et al., 2007).

Bi-directional motility of organelles can be achieved by several mechanisms (Fig9), although controversial, widely accepted is that of coordinated transport. It has been shown with several systems that ablation of motor of one polarity also disrupts motility in the other direction. Injection of Kinesin function blocking antibody in Squid axoplasm resulted in disruption of both anterograde as well as retrograde movements (Brady et al., 1990). Similarly, in S2 *Drosophila melanogastor* cells, Kinesin1 and Dynein mediate peroxisome transport. Functional disruption of any of the two motors resulted in loss of motility in both directions, while reconstitution with unrelated motor bearing peroxisome localization signal rescued bi-directional motility (Ally et al., 2009). The same was shown in neurons, where functional ablation of either the plus end motor Kif1A or minus end motor Dynein led to disruption in bidirectional motility showing a tight coordination of bi-directional motility (Uchida et al., 2009). Bi-directional motility has been proposed to serve in functions other than transport such as in vesicle fission where traction forces exerted by motors of opposite polarity results in fission (Soppina et al., 2009).

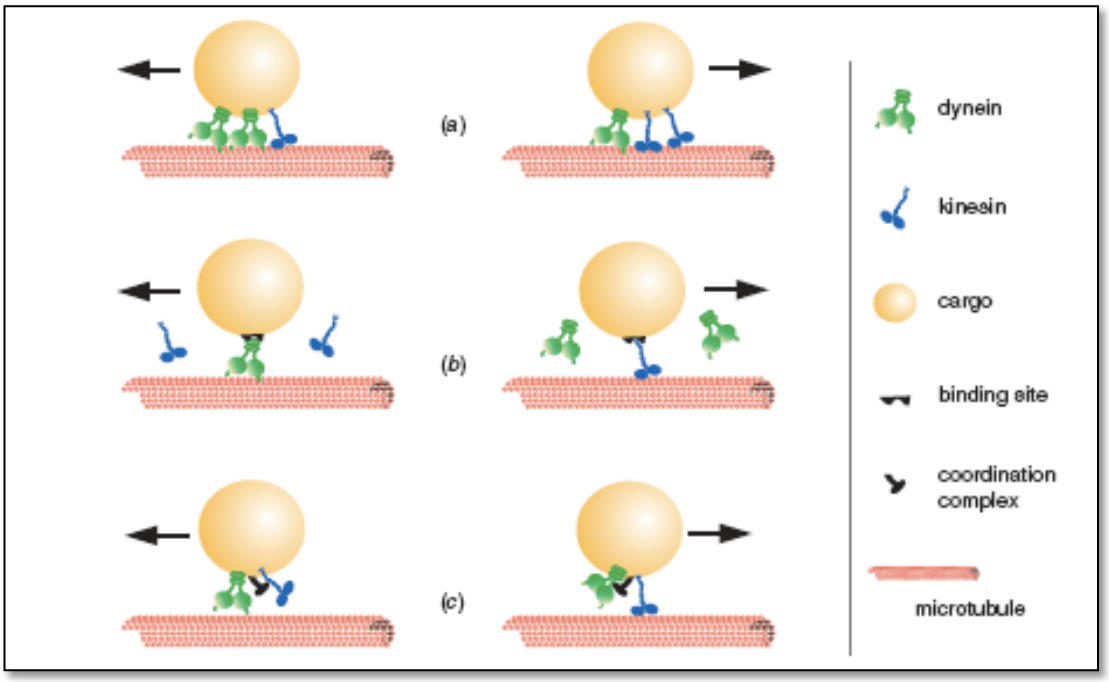

Fig9: Mechanisms of bi-directional motility. (a) Tug of war model - motors of both polarities are present and are active on cargo simultaneously. The direction of movement depends on the instantaneous velocity of the "stronger" team of motors. (b) Exclusivity model - cargo engages only one species of motor at any given point, the direction of motion of cargo being that the motor engaged. (c) Co-ordination model - motors of both polarities attach to cargo, however their activities are coordinated such that only a single type of motor is active at any point in time. Adapted from (Gross, 2004)

1.8 Regulation of organelle motility

Regulation of intracellular transport of organelles is achieved through the functional co-ordination of transport machinery, cellular cytoskeleton and other regulatory proteins together with molecular motors. Such co-ordination allows for coupling between organelle motility and function together with feedback regulation between the two processes.

Rab proteins recruit molecular motors. Rab6 in its GTP form recruits RabKinesin6 to Gogli vesicles (Echard et al., 1998). Rab GTPases also recruit motors through effectors. Examples of the later include Rab5 endosomes recruiting Kif16B through Rab5 effector, PI3P (Hoepfner et al., 2005) and Rab3 GEF, DENN physically interacting and recruiting Kif1β and Kif1A (Niwa et al., 2008). RILP, a Rab7 effector recruits Dynein. It was shown that overexpresion of RILP led

to increase in minus end motility and clustering of Rab7 vesicles at the MTOC along with stabilization of Rab7-GTP on membranes (Jordens et al., 2001). Motors bound by effectors and Rab GTPases ensure regulation by stoichiometry and valency. Motor copy number has no impact on speed of cargo (Howard et al., 1989) but affects processivity, in that, it enhances processivity non-linearly with increase in motors recruited. It also suppresses of non-productive states as in the case of multiple dyneins (Mallik et al., 2005).

Cellular cytoskeleton, its post translational modifications (PTMs) and organization regulate molecular transport. PTMs influence recruitment of microtubule effectors such as MAPs, TIPs and motors, which in turn contribute to microtubule-based functions.

Activities of motors along microtubules are modulated by presence of MAPs that bind statically along the length of microtubules and are thought to contribute to its stability and organization. Motor activity and affinity to microtubules are also regulated through MAPs. Kineisns are much more sensitive than Dynein to MAPs such as Tau in terms of both inhibition of its activity and binding to microtubules (Dixit et al., 2008) providing local spatial regulation of motor activities along microtubules. PTMs on microtubules have been shown to regulate binding of effectors. *In vitro*, Tau, MAP1B, and MAP2 bind preferentially to tubulins with moderate levels of polyglutamylation (~3 glutamyl units) whereas MAP1A shows optimal affinity for highly modified tubulins (~6 glutamyl units) (Bonnet et al., 2001). In neurons and fibroblasts isolated from tubulin tyrosine ligase (adds Glutamates on α and β-tubulin) null mice, increased levels of detyrosination results in mislocalization of +TIPs such as CLIP-170 and p150Glued (Peris et al., 2006). Motors exhibit preferential affinity for microtubules with PTMs. Kinesin-1 has been shown to move preferentially on acetylated microtubules tracks (Reed et al., 2006), while Kinesin-2 (Kif17) and Kinesin-3 (Kif1A) show no such preference (Cai et al., 2009). Recycling of transferrin from perinuclear recycling compartments depend on presence of Glutamated micotubules and Kinesins in CHO cells (Lin et al., 2002). Also Kif5c was shown to translocate tyrosynylated microtubules with lower velocities than detyrosynylated ones indicating selective bias for microtubules tracks with PTMs (Dunn et al., 2008). Stimulation of Hela cells with EGF results in qualitative microtubule remodeling (Kharchenko et al., 2007), presumably through its stabilization by acetylation. Stable acetylated microtubules was shown o promote transport of EGF for degradation (Lissanu Deribe et al., 2009). Neurons have morphological and functionally

distinct processes that are important in conduction of action potentials in the neuronal circuitry. Neuronal polarization demonstrates segregation of cellular components and functions. PTMs on microtubules have been shown to be important in establishing and maintenance of neuronal polarity. Axons are populated by polarized MT arrays with the minus end being proximal to the soma and plus end being distal, while the somatodendrites have MT of mixed polarity. MTs of the somatodendritic region are also tyrosynylated, which allows the differential usage of molecular motors. Conventional kinesin Kif5 is an axonal kinesin, which is well segregated from the dendritic arm due to the tyrosynylation of MT in the dendrite (Konishi and Setou, 2009). All of these studies indicate intricate regulatory mechanisms that ensure fidelity in intracellular trafficking.

Another important mode of regulation of organelle trafficking is through cross talk between microtubule (MT) and microfilament (MF) networks. The arrangement of the axonal cytoskeleton led Atkinson (Atkinson et al., 1992) to propose that microtubules might be responsible for the long-range transport of organelles, whereas actin might be used for local delivery. Several systems such as fish melanophores respond to extracellular cues and redistribute melanososmes using both microtubules and microfilaments. MTs are involved in the initial fast motion towards the cell periphery, and actin filaments are required for the even dispersal of granules throughout the cytoplasm (Rodionov et al., 1998). In mammalian systems, association of mysoins with microtubules has been shown: myosin-5 has been reported to bind to kinesin (Huang et al., 1999) myosin-6 binds to CLIP-190 (Lantz and Miller, 1998). RhoD, a regulator of actin dynamics localizes and regulates early endosome motility. Over-expression of RhoD or its effector Diaphranous2C results in increased localization of endosomes with actin and decrease in endosome motility (Gasman et al., 2003). Also, Htt-associated protein 40 (HAP40), a Rab5 effector recruits Huntingtin (Htt) to regulate motility of early endosomes. Overexpression of HAP40 or polyQ expansion of Htt that occur in Huntingtin's disease lead to increased association of early endosomes with MF and consequently decreased motility (Pal et al., 2006). Hence it is evidently clear that cross talk between the two cytoskeletal systems regulates intracellular motility of organelles.

1.9 Motors in early endosome transport

Several molecular motors have been shown to be involved in early endosome motility. Among Kinesins identified, Kif16B (Hoepfner et al., 2005) has been shown to move early endosomes *in vivo*. Kinesin-1, Dynein and Kinesin-2 have been shown to move early endosomes in *in vitro* cell-free assays (Loubéry et al., 2008), although lacking *in vivo* functional demonstration. Kinesin-3 (Kif1A) has been shown to be involved in early endosome motility in *Ustilago maydis* (Lenz et al., 2006), however, if mammalian cells also the same motor is not known. KifC2 has been identified as a motor for Rab4 early endosomes that are devoid of Rab5 and EEA1, canonical early endosomal markers (Bananis et al., 2003).

There is no direct demonstration of Dynein being involved in early endosome transport, although, function ablation disrupts early endosome localization (Valetti et al., 1999) and leads to cargo sorting defects (Driskell et al., 2007). Dynein and Dynactin components have been immuno-localized to early endosomes through EM in only macrophages (Habermann et al., 2001). However, localization of the motor complex does not necessarily imply transport function. Dynein function blocking antibodies failed to inhibit minus end motility of early endosomes in *in vitro* motility assays (Nielsen et al., 1999) leaving the transport function of Dynein-Dynactin complex in early endosomes and open question.

No myosins have been implicated in intracellular transport of early endosomes, however, MyoVI (Aschenbrenner et al., 2004) and Myo1E (Krendel et al., 2007) have been sown to be important for transport of uncoated vesicles through the cortical actin mesh and internalization of cargo respectively.

Hence the number of molecular motors that have been shown to be involved in early endosome motility *in vivo* are few and far in between.

1.10 Why do Rab5 endosomes have to move?

Centripetal motility of early endosomes after internalization of cargo has been observed as early as 1980s (Herman and Albertini, 1984), however, the purpose is not clear. Several viruses require centripetal transport and acidification for virulence and exit from endosomal compartment (Gruenberg, 2009). Cargo (LDL) degradation was shown to be impaired when cellular microtubules are depolymerized, thus preventing centripetal movement of internalized

LDL (Rink et al., 2005). Hence, the rate of centripetal transport probably determines degradation kinetics.

Given that early endosomes hubs for signaling circuits in the cell, kinetics of centripetal transport could potentially determine duration of residence of signal ligand and therefore signaling output.

Rab5-Rab7 conversion events were shown to occur at the MTOC region of the cell (Rink et al., 2005). This region of the cell could presumably harbor high local densities of activators that catalyze conversion, or favor high endosomal fusion events due to increased local density of endosomes, necessitating centripetal transport of Rab5 endosomes.

A considerable body of experiments performed in this thesis involved RNAi knock down of target genes and analysis of phenotypes produced thereof. The following sections therefore deal with an introduction to RNAi biology and the current challenges in interpreting phenotypes produced by RNAi silencing.

1.11 Introduction to RNAi biology

Non-coding RNAs perform several essential regulatory functions in development, gene expression, cellular metabolism, growth and differentiation, cell cycle, apoptosis, defense against viruses and genome surveillance against mobile genetic elements in the cell (Bartel, 2004). Given the multiplicity of functions, it is not surprising that deregulation of these non-coding RNAs are associated with several cancers (Garzon et al., 2009).

Non-coding RNAs includes siRNA (Short Interfering RNA), miRNA (Micro RNA) and piRNA (PIWI interacting RNA). siRNA and miRNA have received increasing interest since their discovery in plants (Ecker and Davis, 1986) in being able to silence genes through post-transcriptional antisense mechanisms. Over the last decade, however, the gene-silencing prowess of siRNAs has been harnessed as a tool in reverse genetics. The ability to introduce exogenous double stranded RNA to silence genes in animals (Fire et al., 1998) and in culture cells (Elbashir et al., 2001) has widened the scope of RNAi as a tool in functional genomics and its ramifications in probing biology of pathways, cellular systems and in therapeutics.

The mechanism of siRNA processing in post-transcriptional gene silencing (PTGS) is summarized in the schematic in Fig10.

siRNAs can be used to specifically silence target genes provided their sequence are known, exploiting the cell's anti-sense silencing mechanism. For sequenced genomes therefore, this technique provides unparalleled opportunities in understanding and exploring biological functions through reverse genetics. The ease of both synthesis of RNAi probes and its delivery has made possible several RNAi based screens in model systems from flies, worms to mammalian cell culture lines to address various cellular processes (Perrimon and Mathey-Prevot, 2007). The advantage of RNAi mediated gene knock down as opposed to knock out strategies is that the former recapitulates hypomorphic conditions and therefore allows for viable phenotypes even for essential genes.

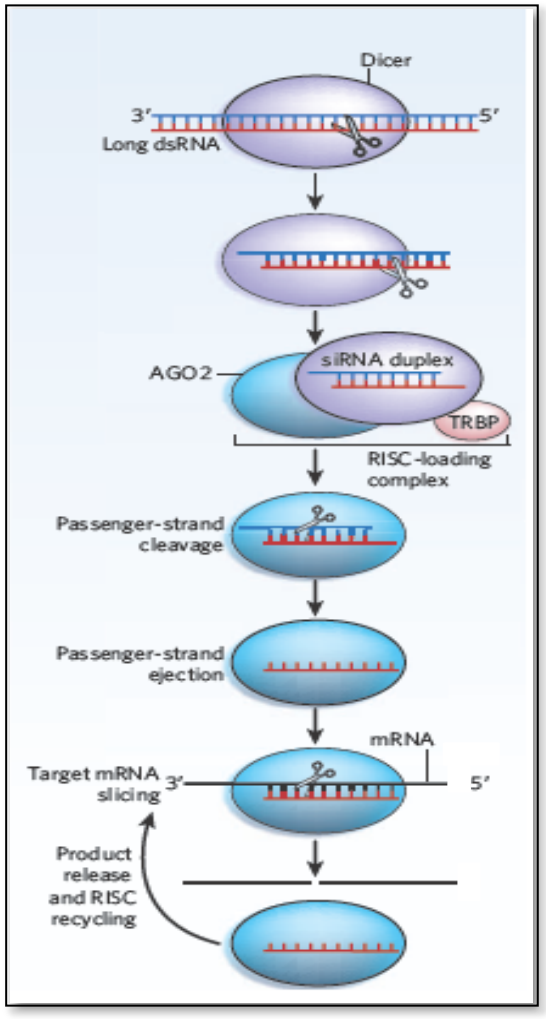

Fig 10: Mechanism of RNAi mediated gene silencing - Exogenous dsRNA (viral or siRNA probe) with a monophosphate at the 5' end and a 2 nucleotide overhang at the 3' end are recognized by the cellular endonuclease Dicer and cleaved into 21-25mers. One of the strands of the duplex, the antisense strand or guide strand is loaded into the RNA Induced Silencing Complex (RISC), a ternary complex consisting of Argonaute, Dicer and TRBP. The other strand of the duplex, the sense or passenger strand is cleaved by Argonaute and excluded from RISC. Argonaute uses the guide strand to recognize and incorporate complementary cellular mRNA transcript and catalyzes the cleavage of the transcript, silencing the gene at the transcriptional level. The degraded mRNA products are released, and the RISC complex is recycled for the next round of catalytic degradation reaction. Adapted from (Jinek and Doudna, 2009).

Gene silencing by siRNA was thought to be specific to its target (Fire et al., 1998), until microarray analysis revealed rampant cross silencing of genes that were unintended targets (Jackson et al., 2003) producing epi-phenotypes collectively known as off-target effects. Although the general mechanism of siRNA mediated gene silencing is fairly well understood, the field is still in its infancy in grappling with specificity issues involved in silencing unintended target transcripts. Off-targets and gene cross silencing have been attributed to one or several of the following –

Induction of interferon response

The cell mounts interferon response toward dsRNAs as a defense mechanism against RNA viruses infecting the cell as defense mechanism (Alexopoulou et al., 2001). However, exogenously introduced dsRNA sequences also do the same. The response was thought to be dependent on the length of the introduced dsRNA with oligonucleotides greater than 30nts evoking a response. Therefore, 19-21mers considered short enough to eschew immuno stimulation, were used for RNAi gene silencing, however, they can also be potent immunological triggers (Hornung et al., 2005) making it a concern in the RNAi field.

Saturation of RNAi machinery and deregulation of cellular homeostasis

It has been shown that physiologically irrelevant siRNAs such as GFP induce considerable cross silencing at high concentrations. This is attributed to possible saturation of cellular RNAi machinery so much so that housekeeping homeostasis functions are also perturbed leading to transcriptional alterations of transcriptional profiles (Tschuch et al., 2008) (Persengiev et al., 2004). RNAi administered at high concentration have also been shown to be lethal in mice (Grimm et al., 2006).

Sequence design of probe

Probe design is an important criterion defining specificity of silencing of target transcripts since the sequence of the guide strand dictates the target transcript incorporated in the RISC complex and subsequently degraded. The sequence of the 5' region of the guide strand called the "seed" is especially important in defining silencing target. The seed specified by nucleotides 2-8 of the guide strand should posses identical complementary to the indented target (Birmingham et al., 2006) akin to that in miRNA (Lewis et al., 2003). Thermodynamic stability of the siRNA duplex also biases its incorporation into the RISC. The strand of the duplex with lower thermodynamic stability at its 5' end is preferentially loaded in the RISC. The guide strands should therefore possess lower internal stability or higher flexibility at its 5' end for directional unwinding of the duplex and incorporation in the RISC (Khvorova et al., 2003).

Reagents used to deliver RNAi across the cellular membrane

Although thought to be neutral to cells in the absence of silencing siRNA, can alter transcriptional profile to a large extent owing to its non-neutralized cationic property (Fedorov et al., 2005).

Given the multitude of factors that contribute to off-target silencing, it is imperative to develop methodologies that allow for reliable identification and assessment of off-target phenotypes while evaluating results from screening exercises.

2 Motivation for study and Aims

The aim of this study was to probe into the regulation of the complex motility behavior exhibited by early endosomes and its implications on early endosome function at the mechanistic level. This problem is multifaceted, involving the functional integration of molecular motors, cellular cytoskeleton and other regulatory proteins. Since motility is a dynamic process, most of the work performed toward understanding motility has been addressed by live cell imaging of Rab5 early endosomes in A431 cells stably expressing GFP-Rab5 and RNAi screening approach. A431 GFP-Rab5 cell line has been characterized before (Sönnichsen et al., 2000), in that, the expression levels of GFP-Rab5 is between 2-5 fold higher than endogenous Rab5, with unaltered transport kinetics as shown with transferrin recycling. Therefore A431 GFP-Rab5 was used extensively to follow kinetic properties of Rab5 endosomes under conditions of perturbation of various molecules to gain insights into the mechanism of endosome motility. Following were the aims –

1. Evaluating contribution of kinetic properties of Rab5 endosomes toward organization of the Rab5 endosome network by live cell time lapse microscopy in A431 GFP-Rab5 cells.

2. Search for molecular regulators of saltatory motility of early endosomes by live cell time-lapse microscopy using A431 GFP-Rab5 cells.

3. Identification of molecular motors of early endosomes through functional LDL degradation RNAi screen.

4. Transcriptional profiling of molecular motors in A431 cells.

Each of the above is discussed as follows -

1. Evaluating contribution of kinetic properties of Rab5 endosomes toward organization of the Rab5 endosome sink network by live cell time lapse microscopy in A431 GFP-Rab5 cells - Previous works in fixed cells have demonstrated general design principles underlying organization of early endosomes known as the sink model, in that, endosome size, number, surface Rab5 density and spatial localization in the cell are all correlated. Nascent endosomes formed after cargo internalization are small, proximal to the plasma membrane and several in number with low Rab5 vesicular density. Cargo processing by sorting entails an increase in Rab5 density with increase in size of endosomes due to homotypic fusion events and concomitant

translocation to the centre of the cell (Rink et al., 2005), (Collinet et al., 2010). Whether motility contributes toward the sink organization of endosomes is an open question. Addressing this issue necessitated quantitative analysis of kinetic properties from live cell time lapse movies and standardizing conditions for extracting kinetic parameters of endosome motility.

2. Search for molecular regulators of saltatory motility of early endosomes by live cell time-lapse microscopy in A431 GFP-Rab5 cells - saltatory motility by an operative definition is the residence of endosomes within "spatial confines" or "territories" before "escaping" into modes of coherent direction motion. Mean Square Displacement (MSD) plots of early endosome motility show saturation with time and the size of the spatial confine is unique to early endosome. Several mechanistically speculative hypotheses involving cellular cytoskeleton, molecular motors and regulatory proteins have been proposed to explain saltatory behavior and its potential contribution in early endosome function. Hence, these molecular candidates were tested by pharmacological drug perturbation and RNAi loss of function knock-down approaches to evaluate perturbation of saltatory motility.

3. Identification of molecular motors of early endosomes through functional LDL degradation RNAi screen - the aim of the screen was to gain insights into of the nature and number of molecular motors that contribute to endosome motility, regulation of bi-directional motility and the effect of perturbation of motility on cargo degradation capacity of the endocytic system.

An important motivation for the screen was the observation that the Rab5 machinery could potentiate minus end motility in *in vitro* motility assays that could not be inhibited with function blocking anti-Dynein antibodies, but were effectively inhibited with anti-Kinesin antibodies suggesting the function of minus end Kinesins, none of which have been identified as motors for early endosomes (Nielsen et al., 1999). Also, motors for early endosomes identified and characterized *in vivo* are few are far in between. Hence the aim of the screen was to identify exhaustively all motor involved in early endosome motility.

The motor screen resulted in an interesting ramification –

Analysis of the maiden RNAi motor screen presented unexpected complications in terms of the high incedence of cross-silencing and off-target phenotypes that made interpretation of the

screen difficult. This warrented development of methdologies for detection of off-targets and an exercise in technology triage of various commercial RNAi technologies available at the time of screening.

4. Transcriptional profiling of molecular motors in A431 cells - the aim being to assess transcriptional and by extension, proteomic complexity of molecular motors in A431 cells. This exercise was performed to complement results from the RNAi screen in terms of validating candidate hits identified by the screen.

3 Results

Following is an overview of the results section. Studies from this work have been dealt with in 4 sections –

Section 3.1: Connecting early endosome transport to Rab5 machinery and function

Wherein a systems analysis of early endosome motility from kinetic properties extracted from a large collection of live-cell time lapse movies were analyzed to extract correlative properties underlying sink organization of Rab5 endosomes. This section is discussed under the following topics -

A. Method for computing endosome speed.

B. General principles of early endosome motility.

C. Correlation analysis between Rab5 endosome motility and Rab5 machinery.

Section 3.2: Analysis of Rab5 endosome saltatory dynamics

This section deals with defining saltatory motility, along with a search for molecular candidates regulating saltatory motility through candidate RNAi screen and cytoskeletal perturbation experiments. Following are the topics presented –

A. Analysis of saltatory motility under cytoskeletal perturbations.

B. Identifying regulators of saltatory motility through candidate gene approach and Kinesin motor screen.

Section 3.3: Functional siRNA screen to identify molecular motors of early endosomes

Is segregated and dealt with as follows

A. LDL degradation kinetics in A431 cells – standardization of motor screen assay

B. Functional LDL degradation RNAi screen to identify molecular motors involved in early endosome motility.

C. RNAi off-target detection and technology triage of commercial RNAi technologies

i. Methodology to estimate specificity of siRNA library using Quantitative Multi-Parametric Image Analysis (QMPIA) using LDL degradation assay on a motor pilot screen

ii. Technology triage of commercial RNAi libraries

iii. Optimization of siRNA motor pilot screen assay to improve RNAi specificity

D. Analysis of motor candidates that score in the motor screen

i. Kinesins and potential complexes

ii. Dynein-Dynactin complex

iii. Novel endosomal Myosins

iv. Potential molecular complexes

v. Differential utilization of Dynein functions by sub-populations of early endosomes

Section 3.4: Expression profiling of molecular motors in A431 cell line

Semi-quantitative RT-PCR was performed to assess the number of molecular motors expressed by A431 cell line.

.

3.1 Connecting early endosome transport to Rab5 machinery and function

The aim was to understand how the "sink" topology within the early endosomal network is established and maintained under steady state conditions, the hypothesis being motility and vectorial translocation bias are important in driving centripetal translocation of endosomes. Toward this end, GFP-Rab5 endosomes were imaged in A431 GFP-Rab5 cell line and their kinetic parameters calculated. Conditions for imaging, calculations of parameters are described below.

3.1.1 Method for computing endosome speed

Movies wherein cells showed minimum photo-toxicity as judged by lack of cell expansion/contraction and movement out of imaging field were considered for analysis. Also, those where beaching of fluorophore (GFP) was greater than 15% were rejected for analysis. Tracking of endosomes were performed as described in (Rink et al., 2005). Tracks shorter than 5secs (50 frames) were rejected since they were contributed by endosomes transiently jumping into focus and fading out. Tracking error estimated manually for at least 10 endosomes from 10 randomly chosen cells was less than 0.5%.

Time-lapse movies were processed by identifying Rab5 vesicles, tracking their trajectory, and computing morphometric and kinetic parameters using the QMPIA as described in Materials and Methods. Kinetic parameters were calculated as plus or minus end with respect to directional polarity of microtubules. The Microtubule Organizing Centre (MTOC) of cells marked the minus end, while the cell periphery was considered the plus end. This assumption may not be valid for few individual endosomes since microtubules in the cells could be aligned with anti-parallel polarity or may be bent, however, on a gross level, most microtubules emanate from the MTOC and radiate towards the periphery. Hence assigning plus and minus polarity to kinetic parameters is a valid assumption for endosome populations. Also, measurement of early endosome flux (as described in (Rink et al., 2005)) in time-lapse movies indicates centripetal flux validating the above assumption.

Movies were acquired at high frame rates (10.4frames/sec) to decrease tracking errors and maximize tracking resolution, however, calculation of endosome speeds at tandem step intervals or consecutive frame rate (0.096sec) resulted in high-speed values of upto 10um/sec for

endosomes, which is spurious. It was necessary to therefore assign stable time interval over which speeds of endosomes could be estimated. A plot of speed vs. speed step (time integrated over sequential frames) gives an exponential decrease in speed with decreasing speed step initially and stabilizes by speed step 5. At speed step 1, noise in measurement predominates over calculated speed. Hence speed step 5, meaning speed averaged over 5 frames was used to estimate endosome speed. Also, trajectories of endosomes tracked were averaged with a floating mean of 2 and the corrected trajectory was used to estimate all kinetic parameters owing to the inaccuracy of estimating the position of a given endosomal structure (Fig11).

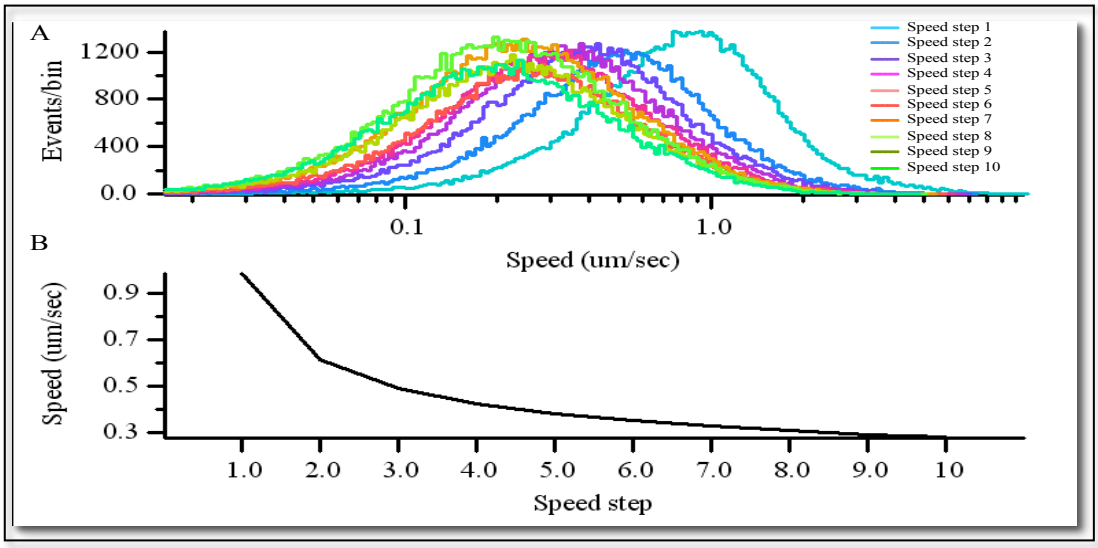

Fig 11: A - Binned distribution of Rab5 endosome speeds with increasing step size. B - Mean speed at respective step size computed from (A) as a function of speed step.

3.1.2 General principles of early endosome motility

Kinetic parameters from wild type A431-GFPRab5 cells were computed as mean values for cumulative distribution of respective parameter. Endosome displacement and directed movement were all calculated using a track threshold of 4, meaning that the values are for track segments where endosomes are tracked for a minimum of 4 frames with deviation in trajectory of less than 30°. These values are arbitrary and set to measure endosomes transport along a single microtubule track (estimated qualitatively). All kinetic parameters were

calculated as mean of distributions. Shown in Fig 12 are binned distributions to depict differences in distributions their tails.

For all calculated parameters, endosomes exhibit a small but consistent minus end bias despite bi-directional motility (Table2). Biases in kinetic parameters toward minus end may be a contributing factor for observed net centripetal flux of early endosomes. Observed bias may be attributed either engagement of molecular motors with differences in their kinetic properties, and/or regulation by Rab5 machinery.

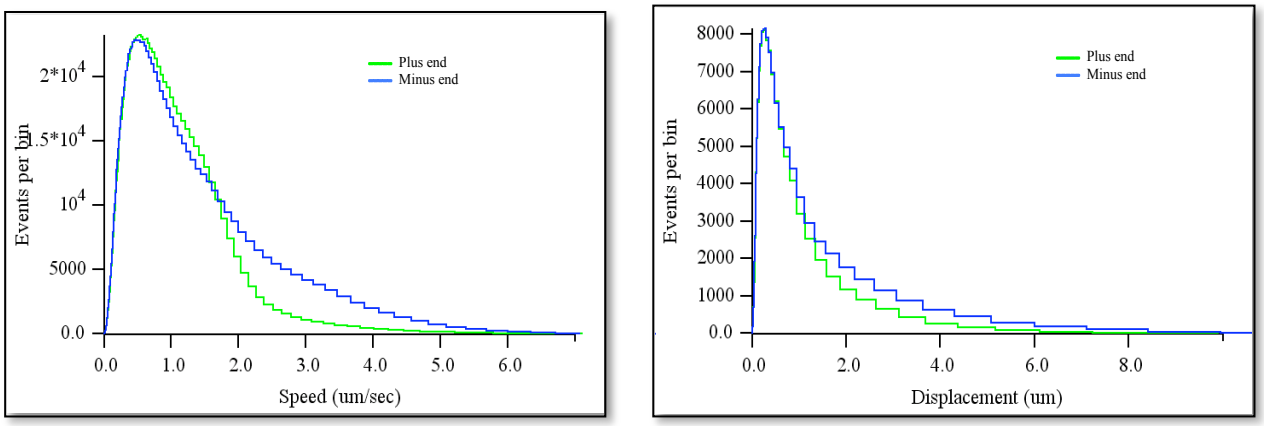

Fig 12: Binned distributions for plus and minus end kinetic parameters of Rab5 endosome speed and displacement.

Parameter	Plus end directed	Minus end directed
Mean Speed	0.65±0.0005	0.74±0.0007
Mean Displacement	0.43±0.001	0.51±0.002
Mean Processive Movement	0.86±0.002	0.96±0.002

Table 2: Plus and minus end kinetic parameters from distributions. Minus end values are significant with p values much below 0.005.

3.1.3 Correlation analysis between Rab5 endosome motility and Rab5 machinery

Live cell time-lapse movies of ~80 individual A413 GFP-Rab5 cells was performed. Each movie acquisition was 1200 frames (~2mins), sampled at 10.4frames/sec. This was the minimum time required to establish centripetal endosome flux stably and reliably. Endosomes were tracked, kinetic and morphometric parameters were calculated and a correlation matrix was constructed. From the analysis, two main conclusions could be drawn –

Correlation between endosome speed and Rab5 density (Fig13A) – Endosome speed and Rab5

density show a strong negative correlation, meaning that higher the Rab5 density, slower are the speeds of endosomes in both plus and minus end directions. Conversely, it could also mean that when speeds of endosomes are low, Rab5 density increases (perhaps due to increased fusion events). However, the negative correlation is stronger for minus end directed motility (Fig13B), implying that endosomes that move centripetally are inhibited to a greater extent than those moving to the cell periphery.

Correlation between endosome speed and size – Plus end directed speed and size of early endosomes are not correlated, however, there is a negative correlation between minus end directed speed and size (Fig13C), meaning that the more endosomes grow in size, the slower is their motility. However, the correlation here is not as strong as that between Rab5 density and speed. Rab5 size and content are correlated positively, implying that larger endosomes have higher Rab5 density. Hence the inverse dependence between size and Rab5 density could in part be due to increase in Rab5 density.

All of the above correlations could possibly be a part of a regulatory mechanism, which manifests in the sink model, allowing for endosomes to mature along the degradative pathway by slowing down speeds thereby increasing frequency of encounter and fusion between peers. This possibly results in a feed forward loop, until the endosomes have accumulated sufficient density of Rab5 for conversion concomitant with their perinuclear localization.

A

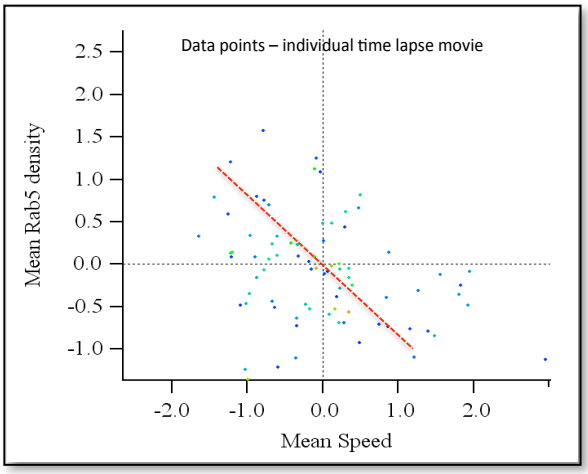

B

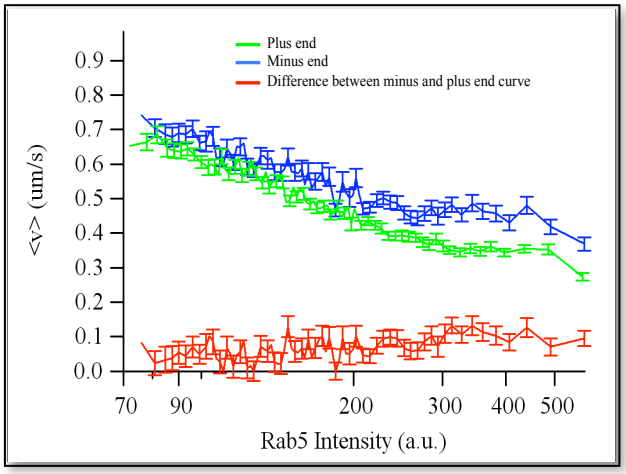

C

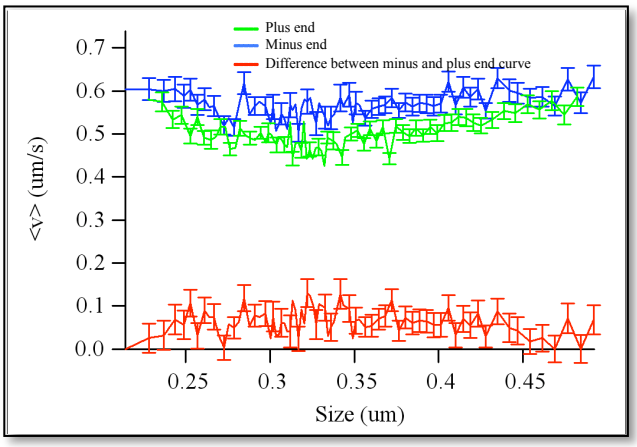

Fig13: Correlation between early endosome speed and mean Rab5 intensity. A: Negative correlation between Rab5 endosome density and cumulative speed (both plus and minus directions). Each data point represents a single time-lapse movie. B: Plot of mean speed vs. mean Rab5 intensity for ~70 endosomes. Red track shows a significance difference between minus and plus end directed trends. C: Plot of mean speed vs. size of early endosomes, for ~70 endosomes. Red track shows a significance difference between minus and plus end directed trends.

3.2 Rab5 endosome saltatory dynamics

Rab5 endosomes execute complex motility trajectories (Fig14A). Dissection of each track qualitatively defines phases of short-range movement, long-range movement, stalls and saltatory dynamics or "territories". Saltatory dynamics is defined as phenomenological confines that are predominated short-range movements and stalls. Saltatory regimes are not phases of Brownian motion of endosomes, but of active motor driven transport. However, this phase of motility is devoid of long-range transport.

Since early endosomes for most part of their motion are this mode of motility, a plot of Mean Square Displacement (MSD) vs. time interval (MSD plot) for all endosomes in a time-lapse movie shows saturates with time (Fig14B). Point of inflection of the MSD curve is a measure of spatial dimension of saltatory motility. It varies from ~1.4-1.6μm. The saltation shown by early endosomes is different from that shown by other organelles such as late endosomes (data not shown).

A

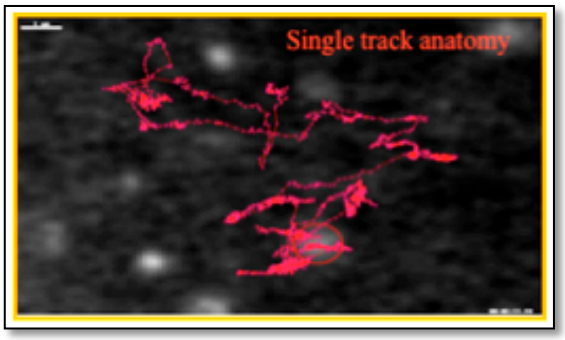

B

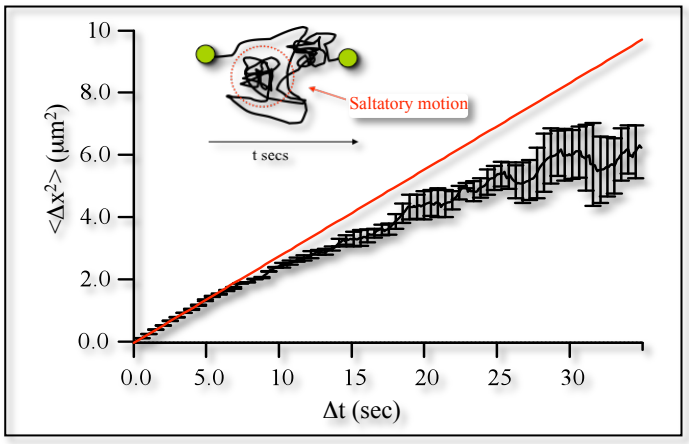

Fig14: Endosome saltatory regime of motility. A- Representative trajectory of Rab5 endosome. B - Average MSD plot for all endosomes from 10 time-lapse movies tracked in a wild type A431 GFP-Rab5 cell. Schematic in B is a cartoon representation of an endosome track depicting saltatory motility.

The molecular mechanism and function of saltatory motion are unknown and speculative; one of the potential mechanisms mediating saltatory motility is cytoskeletal tethered to perhaps cytoskeletal associated proteins (MAPs). To gain mechanistic insights, perturbation analyses were performed under conditions of disrupting cytoskeletal elements using pharmacological drugs and candidate gene RNAi screen under conditions of live cell microscopy.

3.2.1 Analysis of saltatory motility under cytoskeletal perturbations

MSD plots for Rab5 motility were analyzed under conditions of depolymerization of microtubules and microfilaments using nocodazole, latrunculin A and cytochalasin D respectively. Depolymerization of actin by latrunculin A or cytochalasin D did not alter MSD behavior of early endosomes, however, nocodazole abolished endosome saltation, in that, MSD plot did not saturate, but showed a linear dependence of MSD with time interval. This effect could be attributed to either a loss in MSD saturation behavior, or due to Brownian motion since endosomes cease to move over long distances under conditions of microtubule depolymerization. Hence, a dose of nocodozole from sub-nanomolar (1nM) concentrations of the drug to that where

microtubules were completely depolymerized (3.3μM) were tested for their effect on saltation behavior. Nocodazole concentrations of 1-10nM of the drug abolished saturation of MSD plots, while higher concentration (200-500nM) recapitulated saturation MSD plots (Fig15B). Microtubule distribution and density were not qualitatively altered at sub-nanomolar nocodazole concentrations, however, dynamic instability is known to be inhibited at these low nocodazole concentrations (Vasquez et al., 1997). In order to test if microtubule stabilization was responsible for loss of saturation MSD behavior, cells were treated with taxol or Trichosatin A (TSA, an inhibitor of HDAC, promotes acetylation and stabilization of microtubules). Neither treatment altered MSD plots relative to their respective controls (Fig15A, C). Hence, stabilization of microtubules may not directly be responsible for saturation MSD kinetics, however, dynamics of microtubules might regulate MSD behavior of early endosomes.

A

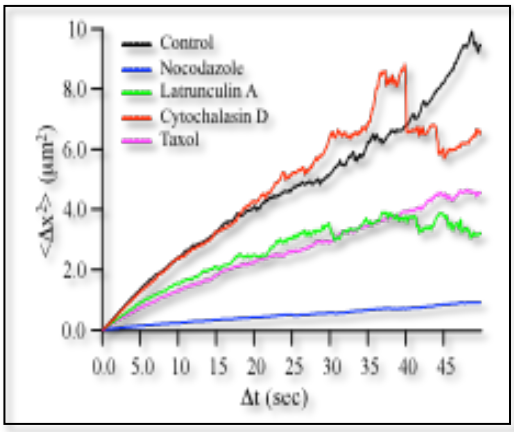

B

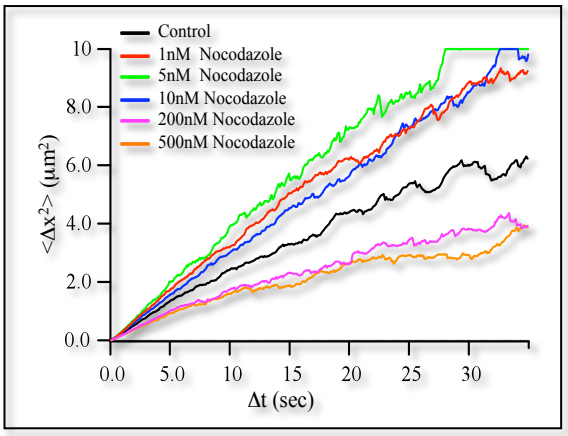

C

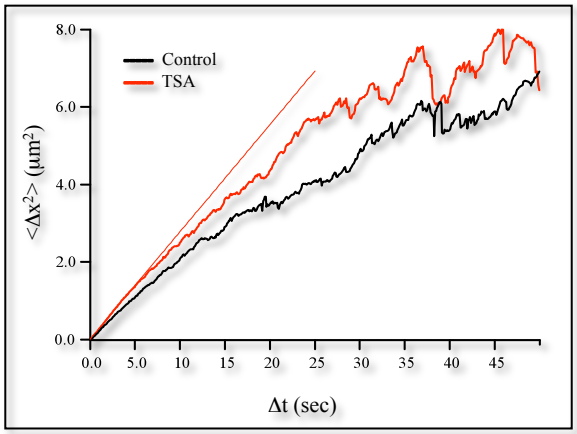

Fig15: MSD analysis of Rab5 endosomes under A - cytoskeletal perturbation with pharmacological drugs, B – Nocodazole dose analysis, C – TSA treatment (acetylation of tubulin).

3.2.2 Identifying regulators of saltatory motility through candidate gene approach and Kinesin motor screen

A RNAi candidate screen was performed to test several candidate genes for their perturbation of saltatory behavior of early endosomes. Genes tested (Table3) were those reported for their role in altering cargo trafficking (EHD family proteins), early endosome motility (RhoD), interaction with cytoskeleton (HOOKs) or ability to induce actin tubulation on early endosomes (annexin2), in line with proposed speculative hypothesis of saltatory motility (see discussion). In addition to mentioned genes, all annotated Kinesins in the human genome were also tested for their regulation of saltatory motility of early endosomes. RNAi knock down was performed in A431-GFP Rab5 cell line with 4 siRNA oligos per gene by live cell time lapse movies of 1200frs sampled a 10.4fps. 5 cells were imaged per condition. MSD plots were plotted for individual movie and averaged for all siRNA oligos of every gene.

Effectors Characterized	Function	Proteins on Rab5 affinity column
EHD family proteins (EHD1-4)	involved in early endosome transport and recycling	EHD1
Hook family proteins (Hooks1-3)	Microtubule Associated Proteins	Hook1 and Hook3
Annexin2	forms actin patches and nucleates cables on endosomes	
RhoB	Overexpression aligns endosomes along actin, decreases EE motility	
RhoD	Overexpression aligns endosomes along actin, decreases EE motility	

Table3: Candidate genes screened for potential regulation of MSD behavior of early endosomes

Form the MSD analysis, none of the tested gene candidates perturbed MSD behavior, however, knock down of several Kinesins show a loss of saturation behavior (Table4). Some of these

Kinesins also scored as candidates in the motor screen such as STARD9 (Fig16), Kif22 and KifC2 (see section on motor screen). This could imply that Kinesins that are early endosome motors directly regulate endosome motility, or that they do so indirectly through perhaps remodeling microtubule dynamics.

Kinesins with loss of MSD phenotype
Kif22
KifC2
STARD9
Kif16B
Kif20A
Kif21A
kif21B
kif23

Table4: Kinesin motors whose knock down result in loss of saturation behavior of Rab5 endosomes. Green – candidates hits in motor screen

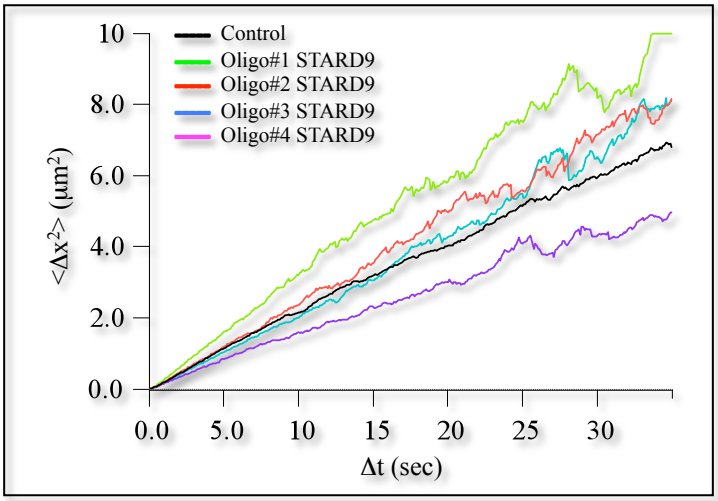

Fig16: MSD plots for Rab5 endosomes under STARD9 knock down conditions. Each curve is an average of 5 movies. 3 siRNAs out of 4 do not show saturation in MSD curve.

Given the multitude of Kinesins involved in saltatory dynamics, it was of interest to identify motors of early endosomes, both in terms of nature and number in order to understand the regulation of motility between different motors, not only in saltatory dynamics but in other

phases of motility as well. Toward this end, a functional siRNA screen was performed to identify endosomal motors. It was also of interest to assess the number of motors expressed in A431 cells. Hence, a transcriptional profiling exercise was performed through semi-quantitative RT-PCR. The following sections deal with the RNAi motor screen and transcriptional profiling of molecular motors in A431 cell line.

3.3 Functional siRNA screen to identify early endosome motors

Given the long-standing aim in understanding the regulation of endosome motility, a functional RNAi screen was performed to identify the ensemble of molecular motors involved in early endosome motility. The RNAi screen used a functional degradative assay to assess the contribution of motility by individual motors to the efficiency of degradation of internalized cargo (LDL). Given that overexpression of plus end motors delay degradation kinetics of internalized cargo as was shown with Kif16B (Hoepfner et al., 2005), or that knock down of Dynein impaired cargo sorting (Driskell et al., 2007), the functional cargo degradation RNAi screen was designed to identify molecular motors of early endosomes that result in perturbed cargo degradation kinetics.

3.3.1 LDL degradation kinetics in A431 cells - standardization of motor screen assay

A functional image based cargo degradation assay was established for the motor screen with the canonical degradative cargo LDL. The assay was based on pulse and chase protocol with fluorescently labeled LDL to monitor degradation of cargo internalized (Fig17A). For efficient detection and optimal signal to noise of internalized cargo, a minimum of 10mins of pulse time was required for both LDL conjugated to Alexa488 (DL-Alexa488) and LDL conjugated to DiD (LDL-DiD) cargoes (data not shown). To establish the chase time interval, serum starved A431 cells were co-pulsed with LDL-Alexa488 and LDL-DiD for 10mins, and chased for the time intervals indicated in the schematic below. Cells were fixed, imaged, fluorescence signal associated with LDL-Alexa488 and LDL-DiD, and their exit and entry from and to the early and late endocytic compartments respectively (colocalization with the early endosome marker EEA1 and late endosome Lamp1) were quantified using Motion Tracking as in Materials and Methods. The total content of LDL-Alexa488 decreased with chase time, with a $t_{1/2}$ of ~50 minutes (Fig17B). This decay in fluorescence is potentially due to the metabolism of LDL and clearance

of Alexa488-tyrosine from cells, and is inhibited upon treatment with ammonium chloride, an inhibitor of lysosomal acidification. The fluorescence intensity associated with LDL-DiD did not saturate with chase time as expected. This is possibly due to a de-quenching effect (see discussion). Both the fluorophore conjugated LDLs however showed similar exit and entry kinetics from and to the EEA1 and Lamp1 compartments indicating that the differential fluorophore conjugation and fluorophore chemistry did not affect the trafficking properties of LDL (Fig17C, D).

LDL-conjugated flourophores were internalized through receptor mediated endocytosis by binding to LDL receptor (LDLR), as knock down of LDLR resulted in ~70-80% decrease in intracellular LDL. Hence LDLs were internalized through receptor mediated endocytosis and not fluid phase endocytosis (Fig18A, B, C).

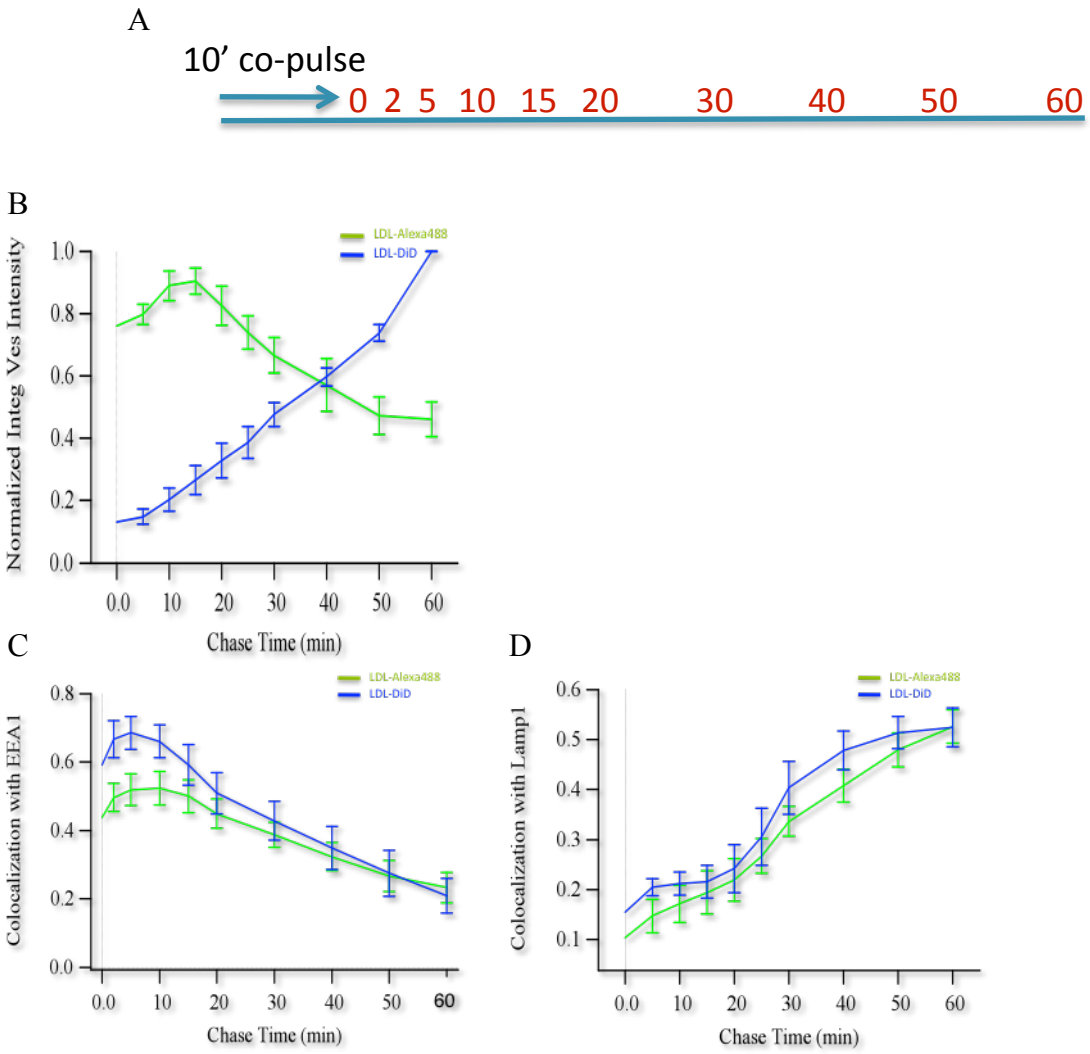

Fig17: LDL transport kinetics. A: Assay of LDL kinetics assay, B: Kinetics of cargo clearance with time, C: Kinetics of cargo exit from early endosomes, D: Kinetics of cargo entry into late endosomes,

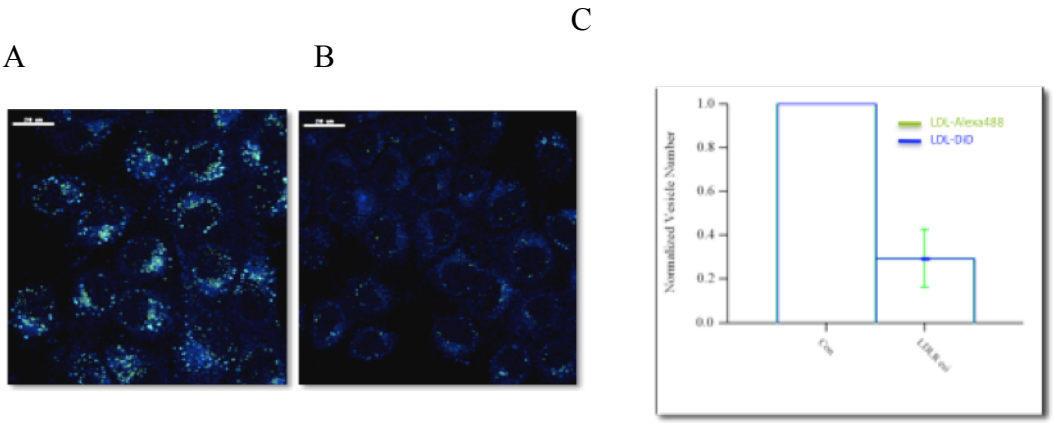

Fig18: Representative images of LDL-Alexa488 and LDL-DiD co-pulse for 10mins of A: Mock treated cells, B: LDLR RNAi cells, C: Quantitation of LDL fluorescence in B normalized to A.

3.3.2 Functional LDL degradation RNAi screen to identify molecular motors involved in endosome motility

A functional LDL degradation RNAi screen was performed with the motor Library from Ambion with 3 independent siRNAs targeting every gene. Results from the screen were however confounding due to poor consistency in phenotypes produced by different siRNA oligos targeting the same gene indicating a general lack of silencing specificity for the target.

3.3.3 RNAi off-target detection and technology triage of commercial RNAi technologies.

siRNA oligo profiles quantitated by QMPIA (described in materials and methods) are signature phenotypes produced by individual siRNA probe targeting a specific gene, under the given assay conditions. In an ideal case, all siRNA profiles for a given gene between biological experiments should be identical, however, this is seldom the case as is shown for an exemplarily gene (Fig 19). Profile inconsistencies are attributed to several factors that include robustness of assay, measurement noise, reproducibility in parameters used to construct siRNA oligo profiles and off-targets, to name a few. Therefore, maximizing consistency in phenotype between multiple siRNAs targeting the gene of interest requires mitigating the above-mentioned sources of noise. Consistent trends in phenotype (independent of amplitude of peaks) between multiple siRNAs of

a gene or a specific siRNA of a gene between independent biological replicates are defined as "on-targets" due to phenotypic consensus and reproducibility of phenotype across multiple parameters of QMPIA. Hence, estimating the specificity or quality of a technology is in essence a methodology to estimate phenotype consistence between siRNA oligos used in the experiment.

A B

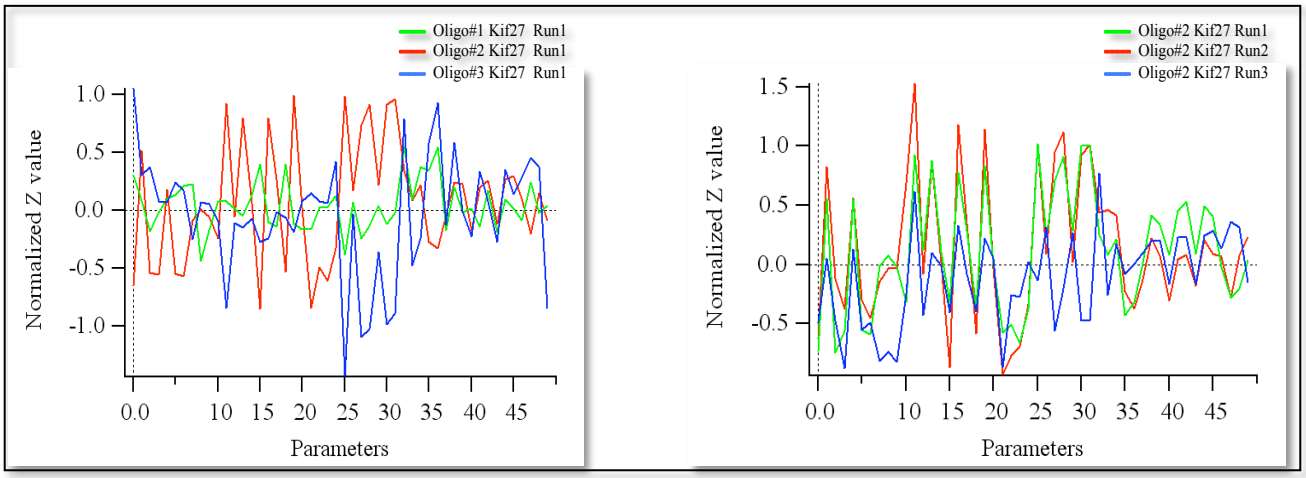

Fig 19: Phenotype profiles of siRNA targeting Kif27. A – 3 independent siRNAs from the same biological replicate. B – siRNA oligo number 2 from 3 independent biological experiments.

Given the multiplicity of factors that are potential sources of off-targets, the field of RNAi biology is challenged with the issues of detecting and identifying off-targets, and of assessing the extent of cross silencing contamination produce in RNAi screens. Irrespective of the source of off-targets, it is clear that they cannot be eliminated with the current mechanistic understanding of the pathway, instead, efforts can be made in the direction of detecting and mitigating them (Pei and Tuschl, 2006). To this end, choosing siRNA design algorithms associated with lower incidence of cross-silencing, optimizing assay conditions, honing analytical tools for detection of off targets in screens would be milestones toward comprehending results emerging from RNAi screens. Screening with sub-optimal siRNA probes and assay conditions on the contrary is counter productive due to high incidence of off-targets, misleading and obfuscating biological interpretation and their validation thereof, as was the case with the maiden motor screen. It was therefore critical to go through the following exercises before repeating the motor screen toward identifying candidate motor proteins reliably.

i. Methodology to estimate specificity of siRNA lbrary using Quantitative Multi-Parametric Image Analysis (QMPIA) using LDL degradation assay on a motor pilot screen

ii. Technology triage of commercial RNAi libraries

iii. Optimization of siRNA motor pilot screen assay to improve RNAi specificity

This section describes the methodology for detecting off-targets, estimating specificity of a siRNA library, comparative evaluation of the specificity of the following commercial siRNA technologies – Ambion, Ambion Select, Invitrogen Select, esiRNA and Dharmacon ON-TARGET Plus and guidelines for assay optimization to maximize targeting specificity in RNAi screens.

3.3.3.1 Methodology to estimate specificity of siRNA lbrary using Quantitative Multi-Parametric Image Analysis (QMPIA) using LDL degradation assay on a motor pilot screen

A medium throughput pilot screen was performed with a library of molecular motors that was assembled with indicated number of independent siRNA oligos for every gene (Table5). Methodologies developed for detecting and estimating off-targets, and determining library specificity have been described for Invitrogen Stealth technology as an example since this library was subsequently used for the motor screen. Other commercial RNAi technologies tested were Ambion, Ambion Silencer Select, Dhramacon ON-TARGET Plus and esiRNAs (endoribonuclease prepared small interfering RNA).

The pilot library was a collation of 30 genes from the motorome that includes13 Kinesin heavy chains, 1 Kinesin accessory protein, 4 Dynein heavy chains (2 axonemal, 2 cytoplasmic) 6 Dynein accessory proteins and 4 Myosin heavy chains. The genes chosen were base on two criteria – expression or its lack thereof in A431 cell line (with *a priori* knowledge form the expression profiling of molecular motors, see section on expression profiling of motorome in A431 cell line) and candidates that have been shown to be early endosomal motors and are therefore are expected to produce phenotypes (positive controls). EEA1 and LDLR were the assay controls. Motor genes in the pilot screen are listed in (Table6).

All pilot screens were performed in A431 cells using the LDL cargo degradation assay established for the motor screen. The degradation assay was performed as in Materials and Methods with a minor variation, i.e, the assay read out was 3 channels, with LDL-Alexa488 as

the degradative marker, EEA1 as early endosomal marker and DAPI and SYTO 42 to identify nuclei and cell contour, instead of the 4-channel assay in the motor screen. Images acquired on the Opera Confocal system, were processed, objects (endosome and nuclei) identified, and endosome parameters quantified through Quantitative Multi-Parametric Image Analysis (QMPIA). Pilot screens for all technologies were performed thrice as independent biological experiments.

Table5

Technologies tested	siRNA duplexes/gene
Ambion	3
Ambion Select	3
Invitrogen Silencer Select	3
Dharmacon ON-TARGET plus	4
esiRNA	2

Table6

Based on expression		Based on phenotype expected	
DCTN1	KIF1A	DCTN1	KIF1A
DCTN2	KIF1B	DCTN2	KIF1B
DYNAH8	KIF1C	DYNAH8	KIF1C
DYNAH9	KIF21B	DYNAH9	KIF21B
DYNAI2	KIF27	DYNAI2	KIF27
DYNAL4	KIF5B	DYNAL4	KIF5B
DYNALI1	KIF5C	DYNALI1	KIF5C
DYNC1H1	KIFAP3	DYNC1H1	KIFAP3
DYNC1I1	KIFC1	DYNC1I1	KIFC1
DYNCLRB1	KIFC2	DYNCLRB1	KIFC2
DYNC2H1	MYO1D	DYNC2H1	MYO1D
TCTEX1D1	MYO1F	TCTEX1D1	MYO1F
KIF11	MYO5B	KIF11	MYO5B
KIF12	MYO6	KIF12	MYO6
KIF13B	EEA1	KIF13B	EEA1
Kif16B	LDLR	Kif16B	LDLR
expressed	not expressed	Expected	unknown

Table 5: Commercial technologies tested and number of siRNA oligos used for every technology
Table 6: List of motor genes used for pilot screen

Estimating quality of a siRNA library entails estimating robustness of phenotype parameters computed through QMPIA, excluding unstable parameters, computing phenotype correlation between different siRNAs targeting the same gene and correlation between independent biological experiments. The ratio of the two correlations is the specificity score (Q) of any given siRNA technology. Each of the above-mentioned steps is described below -

3.3.3.1.1 Estimating reproducibility and stability of assay parameters ($C_{p\text{-}R}$)

An important factor contributing to phenotypic noise in assays is the reproducibility and stability of parameters used to construct siRNA oligo profiles. QMPIA was used to extract 56 morphometric and distribution parameters associated with objects in all 3 channels. All of these

parameters are not equally robust and reproducible between biological experiments. Pearson correlation for each parameter between biological experiments was calculated and presented in Table7 Parameters with correlation value less than 0.3 are considered irreproducible and excluded for further analysis (see Materials and methods for computing $C_{p\text{-}R,}$). Hence, out of 50 endosome parameters, 37 parameters were considered for estimation of Pearson Correlation between runs ($C_{p\text{-}R}$). Parameters related to nuclear channels (not shown) and endosome peer-peer distribution parameters have been excluded from analysis.

Parameter	Parameter correlation between runs	SD
Integ. Ves. Intens. (EEA1) Mask = TRUE	0.821	0.048
Mean Integ. Intens. (EEA1) Weighed=FALSE CalcType = Mode	0.396	0.194
Mean Integ. Intens. (EEA1) Weighed=TRUE WeighingFunc=GetVolume CalcType = Mean	0.738	0.083
Mean Integ. Intens. (EEA1) Weighed=TRUE WeighingFunc=GetMeanIntensity CalcType = Mean	0.732	0.036
Mean Intens. (EEA1) Weighed=FALSE CalcType = Mode	0.348	0.295
Mean Intens. (EEA1) Weighed=TRUE WeighingFunc=GetVolume CalcType = Mean	0.742	0.023
Mean Intens. (EEA1) Weighed=TRUE WeighingFunc=GetMeanIntensity CalcType = Mean	0.722	0.066
Mean Area (EEA1) Weighed=FALSE CalcType = Mode	0.434	0.112
Mean Area (EEA1) Weighed=TRUE WeighingFunc=GetVolume CalcType = Mean	0.603	0.128
Mean Area (EEA1) Weighed=TRUE WeighingFunc=GetMeanIntensity CalcType = Mean	0.610	0.070
Coloc. (EEA1/LDL488) Thresh=0.35 SubstRand=TRUE ByVolume=TRUE	0.839	0.054
Coloc. (EEA1/LDL488) Thresh=0.35 SubstRand=TRUE ByVolume=FALSE	0.790	0.063
Dist. Distr. (EEA1) Min. Distance=0.9 Max. Distance=30 Weighed=FALSE Param 0	0.215	0.051
Dist. Distr. (EEA1) Min. Distance=0.9 Max. Distance=30 Weighed=FALSE Param 1	0.809	0.026
Dist. Distr. (EEA1) Min. Distance=0.9 Max. Distance=30 Weighed=FALSE Param 2	0.531	0.090
Dist. Distr. (EEA1) Min. Distance=0.9 Max. Distance=30 Weighed=TRUE WeighingFunc=GetVolume Param 0	0.074	0.135
Dist. Distr. (EEA1) Min. Distance=0.9 Max. Distance=30 Weighed=TRUE WeighingFunc=GetVolume Param 1	0.762	0.087
Dist. Distr. (EEA1) Min. Distance=0.9 Max. Distance=30 Weighed=TRUE WeighingFunc=GetVolume Param 2	0.353	0.145
Dist. Distr. (EEA1) Min. Distance=0.9 Max. Distance=30 Weighed=TRUE WeighingFunc=GetMeanIntensity Param 0	0.188	0.048
Dist. Distr. (EEA1) Min. Distance=0.9 Max. Distance=30 Weighed=TRUE WeighingFunc=GetMeanIntensity Param 1	0.755	0.069
Dist. Distr. (EEA1) Min. Distance=0.9 Max. Distance=30 Weighed=TRUE WeighingFunc=GetMeanIntensity Param 2	0.441	0.048
Dist. to Nucl. (EEA1/Nucleus) Weighed=FALSE Per Nucleous=FALSE Normalize by Nucleous Size=TRUE CalcType = Mode	0.682	0.061
Dist. to Nucl. (EEA1/Nucleus) Weighed=TRUE WeighingFunc=GetVolume Per Nucleous=FALSE Normalize by Nucleous Size=TRUE CalcType = Mean	0.842	0.036
Dist. to Nucl. (EEA1/Nucleus) Weighed=TRUE WeighingFunc=GetMeanIntensity Per Nucleous=FALSE Normalize by Nucleous Size=TRUE CalcType = Mean	0.860	0.032
Numb. Ves. (EEA1) Mask = TRUE	0.759	0.024
Integ. Ves. Intens. (LDL488) Mask = TRUE	0.627	0.094
Mean Integ. Intens. (LDL488) Weighed=FALSE CalcType = Mode	0.567	0.061
Mean Integ. Intens. (LDL488) Weighed=TRUE WeighingFunc=GetVolume CalcType = Mean	0.545	0.136
Mean Integ. Intens. (LDL488) Weighed=TRUE WeighingFunc=GetMeanIntensity CalcType = Mean	0.538	0.151
Mean Intens. (LDL488) Weighed=FALSE CalcType = Mode	0.486	0.126
Mean Intens. (LDL488) Weighed=TRUE WeighingFunc=GetVolume CalcType = Mean	0.487	0.194
Mean Intens. (LDL488) Weighed=TRUE WeighingFunc=GetMeanIntensity CalcType = Mean	0.430	0.219
Mean Area (LDL488) Weighed=FALSE CalcType = Mode	0.722	0.054
Mean Area (LDL488) Weighed=TRUE WeighingFunc=GetVolume CalcType = Mean	0.832	0.051
Mean Area (LDL488) Weighed=TRUE WeighingFunc=GetMeanIntensity CalcType = Mean	0.826	0.064
Coloc. (LDL488/EEA1) Thresh=0.35 SubstRand=TRUE ByVolume=TRUE	0.855	0.018
Coloc. (LDL488/EEA1) Thresh=0.35 SubstRand=TRUE ByVolume=FALSE	0.711	0.030
Dist. Distr. (LDL488) Min. Distance=0.9 Max. Distance=30 Weighed=FALSE Param 0	0.089	0.013
Dist. Distr. (LDL488) Min. Distance=0.9 Max. Distance=30 Weighed=FALSE Param 1	0.518	0.158
Dist. Distr. (LDL488) Min. Distance=0.9 Max. Distance=30 Weighed=FALSE Param 2	0.519	0.104
Dist. Distr. (LDL488) Min. Distance=0.9 Max. Distance=30 Weighed=TRUE WeighingFunc=GetVolume Param 0	0.177	0.278
Dist. Distr. (LDL488) Min. Distance=0.9 Max. Distance=30 Weighed=TRUE WeighingFunc=GetVolume Param 1	0.501	0.160
Dist. Distr. (LDL488) Min. Distance=0.9 Max. Distance=30 Weighed=TRUE WeighingFunc=GetVolume Param 2	0.533	0.135
Dist. Distr. (LDL488) Min. Distance=0.9 Max. Distance=30 Weighed=TRUE WeighingFunc=GetMeanIntensity Param 0	0.127	0.126
Dist. Distr. (LDL488) Min. Distance=0.9 Max. Distance=30 Weighed=TRUE WeighingFunc=GetMeanIntensity Param 1	0.529	0.168
Dist. Distr. (LDL488) Min. Distance=0.9 Max. Distance=30 Weighed=TRUE WeighingFunc=GetMeanIntensity Param 2	0.585	0.102
Dist. to Nucl. (LDL488/Nucleus) Weighed=FALSE Per Nucleous=FALSE Normalize by Nucleous Size=TRUE CalcType = Mode	0.752	0.042
Dist. to Nucl. (LDL488/Nucleus) Weighed=TRUE WeighingFunc=GetVolume Per Nucleous=FALSE Normalize by Nucleous Size=TRUE CalcType = Mean	0.826	0.055
Dist. to Nucl. (LDL488/Nucleus) Weighed=TRUE WeighingFunc=GetMeanIntensity Per Nucleous=FALSE Normalize by Nucleous Size=TRUE CalcType = Mean	0.794	0.051
Numb. Ves. (LDL488) Mask = TRUE	0.583	0.136

Table 7: Pearson Correlation for phenotype parameters between biological triplicates. Threshold of 0.3 is used to assess stability of parameters across biological replicates. Those below 0.3 are (parameters marked in red) are considered unstable and are excluded while computing $C_{p\text{-}R}$. Therefore, from 50 parameters computed, only 37 are considered for analysis.

The Pearson correlation between runs (C_{p-R}) for the Invitrogen Stealth Library is 0.61, considering 37 reproducible parameters (Fig 3, red trace).

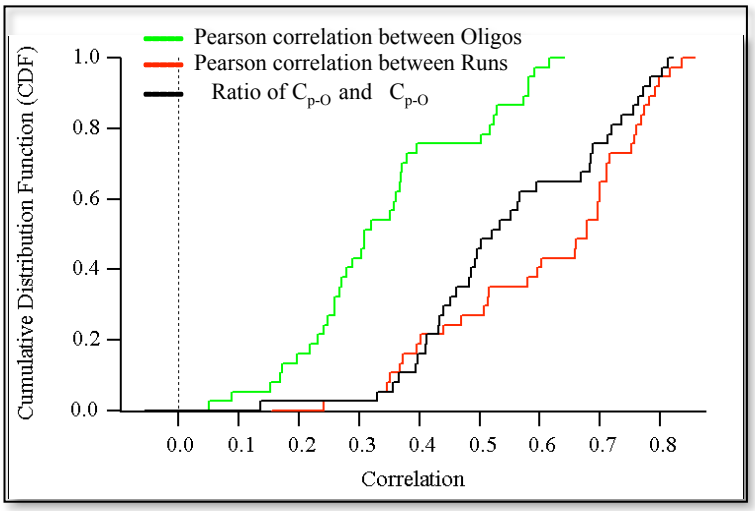

Fig 20: Cumulative distribution of Pearson correlation values for all parameters considered for phenotype scoring. Cumulative distributions for C_{p-R} and C_{p-O} and ratio of C_{p-O} to C_{p-R}. Mean of CDF for C_{p-R} is 0.61 for the LDL degradation assay.

While the Pearson correlation between biological runs reflects of the robustness and reproducibility of assay and is dependent on noise of measurements, the Pearson correlation between siRNAs is a measure of the consistency of phenotype produced between different oligos probes of the same gene and is sensitive to both the noise of measurement as well as the off-target cross silencing incidences. The correlation between siRNA oligos on its own provides very little information as it is contributed to by assay robustness (noise of measurement), on-target and off-target phenotypes. However it is invaluable for the estimation of specificity or quality of any technology. The Pearson correlation between siRNAs of a single within the same biological experiment averaged over 3 independent biological runs for the Invitrogen library was calculated to be 0.31 (Fig20).

3.3.3.1.2 Estimating Q

Q (quality or specificity of a library) is the ratio of Pearson correlation between siRNA oligos to that between runs. Q is estimated based on the fact that a phenotype produced by every single

siRNA is a composite of on-target, off-target and measurement noise components (see Materials and methods). Q for the Invitrogen Stealth library was estimated to be 0.55 (Fig 20).

3.3.3.2 *Technology triage of commercial RNAi libraries*

Having established a methodology for computing specificity (Q) of a siRNA library, an assessment of several commercial technologies was performed using the motor pilot screen with the number of siRNAs per gene as in Table5. Table 5 lists values for Correlation between runs (C_{p-R}), correlation between siRNAs (C_{p-O}) and Q.

From the analysis, Invitrogen Stealth was found to be most specific (highest Q) in terms of least off-target incidence, while that Dharmacon ON-TARGET Plus had similar Q. However, the Ambion libraries, both Silencer and Silencer Select clearly had much lower specificities. Reproducibility of assay, i.e the correlation between runs was almost the same for all technologies (as expected).

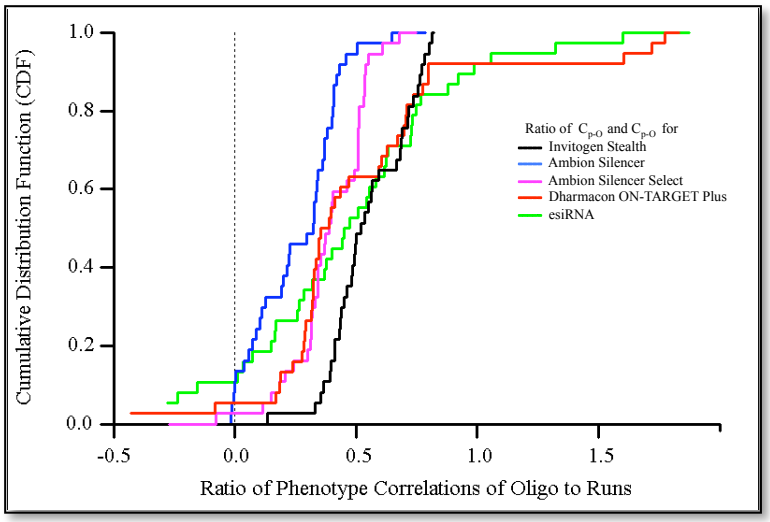

Fig21: Cumulative distribution of all technologies tested at 5nM effective concentrations and their mean values tabulate in Table 7.

Table7

5nM			
Technology	Cp-R	Cp-O	Q
Ambion Silencer	0.617 ± 0.028	0.152 ± 0.017	0.256 ± 0.028
Ambion Silencer Select	0.634 ± 0.026	0.249 ± 0.016	0.390 ± 0.025
Dharmacon ON-TARGET Plus	0.352 ± 0.026	0.163 ± 0.017	0.508 ± 0.069
Invitrogen Stealth	0.607 ± 0.027	0.340 ± 0.024	0.551 ± 0.026
esiRNA	0.447 ± 0.031	0.219 ± 0.031	0.463 ± 0.069

Assay conditions are crucial determinants of Q as is discussed in the next section. For all of the experiments discussed above, an effective siRNA concentration of 5nM was used. These experiments were performed after initially using an effective siRNA concentration of 20nM. In order to verify if Q was dependent on the concentration of siRNA used, all the pilot assays were repeated with a lower siRNA concentration of 5nM. Decreasing concentration of siRNA improved Q dramatically for all technologies tested (Table8) while assay reproducibility ($C_{p\text{-}R}$) for all libraries with the exception of The Dharmacon ON-TARGET Plus remained unaltered between the two concentrations (Fig22). This is probably attributed to the low phenotype potency and penetrance at this concentration, so much so that the phenotypes produced are closer to the noise of measurement, hence lowering phenotype stability. This technology probably performs better in terms of both ($C_{p\text{-}R}$) and Q with higher concentrations of siRNA. Ambion Silencer Select and Invitrogen Sealth perform almost twice as better (Q values) with decreasing concentrations of siRNA, validating earlier reports of cytotoxicity induced by high effective siRNA concentrations (Tschuch et al., 2008), (Persengiev et al., 2004).

Results from this section clearly show that for better target specificity of a technology assay conditions are critical. Hence the Invitrogen Stealth library was used to optimize assay conditions to maximize Q by performing a siRNA titration and time course analysis.

5nM			
Technology	Cp-R	Cp-O	Q
Ambion Silencer	0.617 ± 0.028	0.152 ± 0.017	0.256 ± 0.028
Ambion Silencer Select	0.634 ± 0.026	0.249 ± 0.016	0.390 ± 0.025
Dharmacon ON-TARGET Plus	0.352 ± 0.026	0.163 ± 0.017	0.508 ± 0.069
Invitrogen Stealth	0.607 ± 0.027	0.340 ± 0.024	0.551 ± 0.026
esiRNA	0.447 ± 0.031	0.219 ± 0.031	0.463 ± 0.069

20nM			
Technology	Cp-R	Cp-O	Q
Ambion Silencer	0.656 ± 0.019	0.116 ± 0.020	0.174 ± 0.029
Ambion Silencer Select	0.518 ± 0.029	0.108 ± 0.015	0.166 ± 0.038
Dharmacon ON-TARGET Plus	0.540 ± 0.019	0.164 ± 0.021	0.297 ± 0.037
Invitrogen Stealth	0.617 ± 0.019	0.205 ± 0.025	0.319 ± 0.038

Table8: Q estimation for all siRNA technologies assayed at 5nM and 20nM effective siRNA concentrations.

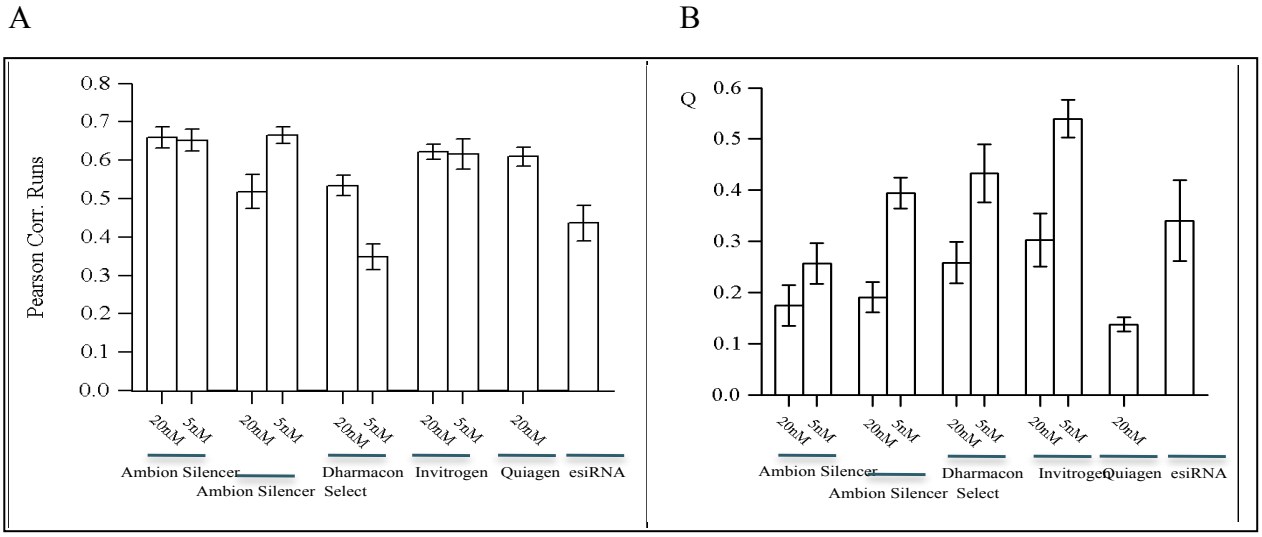

Fig22: Comparison of A: phenotype stability (C_{p-R}) and B: phenotype specificity Q for all tested technologies at 20nM and 5nM effective siRNA concentrations

3.3.3.3 *Optimization of siRNA motor pilot assay to improve RNAi specificity.*

Concentration of siRNA and assay time window are important criteria affecting Q in RNAi screens. With increasing siRNA concentrations, the incidence of off-targets as well as cytotoxicity increases while sub-critical concentrations produce weak phenotypes close to noise of measurement. The assay time window is also important as a long time window results in pleotropic and epi-phenotypes that can reduce C_{p-O}, while at early time points protein turnover is partial and insufficient for effective phenotype penetrance. Hence an optimization exercise was performed to titrate siRNA using the pilot motor library. The following concentrations of siRNA were tested – 1nM, 5nM, 20nM, and 80nM, each concentration assayed at 48hrs and 72hrs post transfection.

Increasing concentrations of siRNA, increases off-targets, this effect is more so with later time points where in pleotropic effects of cross silencing would also accumulate, producing epi-phenotypes (Fig23A, B – compare correlation between siRNAs of respective concentrations between 48 and 72hrs). Hence, the best assay conditions would either be higher siRNA concentrations with shorter incubation times, or lower siRNA concentrations with longer incubation time windows. The former strategy works well with proteins with short turn over rates, while the later is advantageous with those with

stable half-lives since longer incubation dilutes out protein with every subsequent cell cycle.

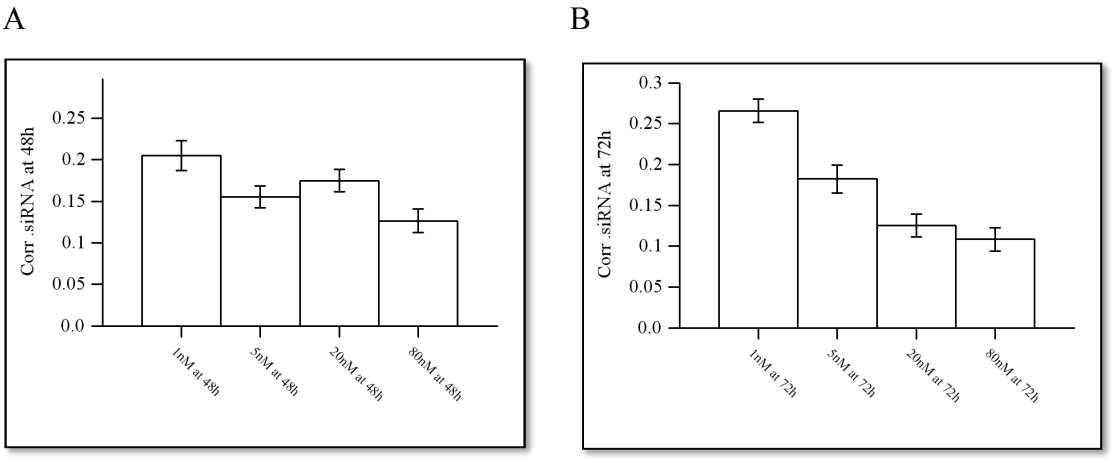

Fig23: Correlation between siRNAs as a function of their concentration. A: assayed at 48hrs, B: assayed at 72hrs post transfection of siRNA.

Of the several commercial technologies tested, Invitrogen Stealth Library had the best on-target specificity and was hence used to perform the motor screen. Results from the Invitrogen motor screen are discussed below.

In the absence of biochemical validation of candidate "hits" from the screen, potential motors involved in early endosome motility, and speculation of their role in regulating and organizing the endosomal system are presented below.

Motor candidates with a gene probability of greater or equal to 0.95 have been considered as potential "hits" involved in early endosome distribution / motility.

3.3.4 Analysis of motor candidates

The motor screen has identified several novel motor components as well as many that have been reported earlier as motors for early endosomes (Table9). Presence of reported motors such as the Dynein-Dynactin complex, Kif5B and Kif3B, validates the screening approach undertaken to identify molecular motors and also lends credibility to the methodology used for of data analysis and candidate hit list scoring. Of interest however, were novel components identified in the screen. Therefore, of novelty in the candidate hit list are

Composition of the Dynein complex

Novel Kinesins – Kif19, Kif22, STARD9, KifC2, Kif2B

Accessory Kinesin components – KLC2, KLC4 and their association with Kinesin heavy chains

Novel Myosins – Myo9B, Myo1F, MYH11, MYH9, MYH14

Phenotypes of some of the potential candidates are as shown in Fig24. The candidates are putative motors of early endosomes and await biochemical validation.

Dynein-Dynactin	Kinesin	Myosin
DCTN1	Kif19	Myo9B
DCTN2	Kif22	MYH11
DCTN3	STARD9	MYH14
DCTN4	KifC2	Myo1F
	Kif2B	MYH9
DYNC1H1	Kif5B	
DYNC1I2	Kif3B	
DYNALI1		
TCTEX1D1	KLC4	
DYNLRB1	KLC2	

Table9: Motor hit list of Dynein-Dynactin complex, Kinesins, Myosins and accessory motor components.

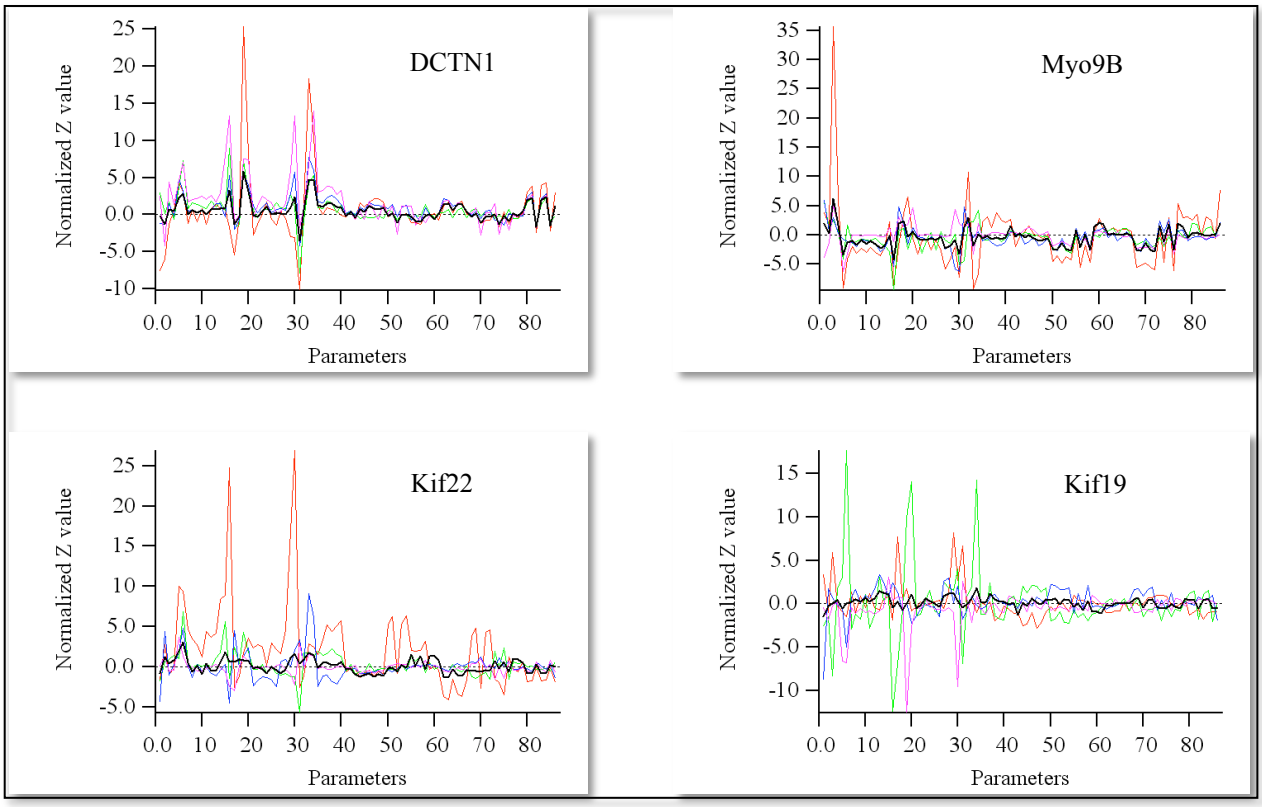

Fig24: siRNA oligo and gene profiles of potential candidates from motor screen. Thin red, green and blue and pink are traces of siRNA oligos of indicated gene, while black trace is the gene profile (mode profile of individual siRNA probes). Annotation of parameters on the X-axis can be found below.

Parameter	X-axis
Mean Integ. Intens. (EEA1) Weighted=FALSE Weighting=GetVolume CalcType = Mean	1
Mean Intens. (EEA1) Weighted=TRUE Weighting=GetVolume CalcType = Mean	2
Mean Area (EEA1) Weighted=TRUE Weighting=GetVolume CalcType = Mean	3
Dist. Distr. (EEA1) Weighted=FALSE Weighting=GetVolume Param 1	4
Dist. to Nucl. (EEA1/DAPI) Weighted=FALSE Weighting=GetVolume Per Nucleous=FALSE Normalize by Nucleous Size=TRUE CalcType = Mean	5
Dist. to Nucl. Cell Based (EEA1) Weighted=FALSE Weighting=GetVolume Normalization=Nuclei Size CalcMethod=DistToNuc CalcType = Mean	6
Coloc. (EEA1/LDL-A488) Thresh=0.35 SubstRand=TRUE ByVolume=TRUE	7
Coloc. (EEA1/LDL-A488) Thresh=0.35 SubstRand=TRUE ByVolume=FALSE	8
Coloc. (EEA1/LDL-DiD) Thresh=0.35 SubstRand=TRUE ByVolume=TRUE	9
Coloc. (EEA1/LDL-DiD) Thresh=0.35 SubstRand=TRUE ByVolume=FALSE	10
Coloc. (EEA1/(LDL-A488 & LDL-DiD)) Thresh=0.35 SubstRand=TRUE ByVolume=TRUE	11
Coloc. (EEA1/(LDL-A488 & LDL-DiD)) Thresh=0.35 SubstRand=TRUE ByVolume=FALSE	12
Numb. Ves. (LDL-A488) Mask = TRUE	13
Integ. Ves. Intens. (LDL-A488) Mask = TRUE	14
Mean Integ. Intens. (LDL-A488) Weighted=FALSE Weighting=GetSquare CalcType = Mean	15
Mean Intens. (LDL-A488) Weighted=FALSE Weighting=GetSquare CalcType = Mean	16
Mean Area (LDL-A488) Weighted=FALSE Weighting=GetVolume CalcType = Mean	17
Dist. Distr. (LDL-A488) Weighted=FALSE Weighting=GetVolume Param 1	18
Dist. to Nucl. (LDL-A488/DAPI) Weighted=FALSE Weighting=GetVolume Per Nucleous=FALSE Normalize by Nucleous Size=TRUE CalcType = Mean	19
Dist. to Nucl. Cell Based (LDL-A488) Weighted=FALSE Weighting=GetVolume Normalization=Nuclei Size CalcMethod=DistToNuc CalcType = Mean	20
Coloc. (LDL-A488/EEA1) Thresh=0.35 SubstRand=TRUE ByVolume=FALSE	21
Coloc. (LDL-A488/EEA1) Thresh=0.35 SubstRand=TRUE ByVolume=TRUE	22
Coloc. (LDL-A488/LDL-DiD) Thresh=0.35 SubstRand=TRUE ByVolume=TRUE	23
Coloc. (LDL-A488/LDL-DiD) Thresh=0.35 SubstRand=TRUE ByVolume=FALSE	24
Coloc. (LDL-A488/(EEA1 & LDL-DiD)) Thresh=0.35 SubstRand=TRUE ByVolume=TRUE	25
Coloc. (LDL-A488/(EEA1 & LDL-DiD)) Thresh=0.35 SubstRand=TRUE ByVolume=FALSE	26
Numb. Ves. (LDL-DiD) Mask = TRUE	27
Integ. Ves. Intens. (LDL-DiD) Mask = TRUE	28
Mean Integ. Intens. (LDL-DiD) Weighted=FALSE Weighting=GetVolume CalcType = Mean	29
Mean Intens. (LDL-DiD) Weighted=FALSE Weighting=GetSquare CalcType = Mean	30
Mean Area (LDL-DiD) Weighted=FALSE Weighting=GetVolume CalcType = Mean	31
Dist. Distr. (LDL-DiD) Weighted=FALSE Weighting=GetVolume Param 1	32
Dist. to Nucl. (LDL-DiD/DAPI) Weighted=FALSE Weighting=GetVolume Per Nucleous=FALSE Normalize by Nucleous Size=TRUE CalcType = Mean	33
Dist. to Nucl. Cell Based (LDL-DiD) Weighted=FALSE Weighting=GetVolume Normalization=Nuclei Size CalcMethod=DistToNuc CalcType = Mean	34
Coloc. (LDL-DiD/EEA1) Thresh=0.35 SubstRand=TRUE ByVolume=FALSE	35
Coloc. (LDL-DiD/EEA1) Thresh=0.35 SubstRand=TRUE ByVolume=TRUE	36
Coloc. (LDL-DiD/LDL-A488) Thresh=0.35 SubstRand=TRUE ByVolume=TRUE	37
Coloc. (LDL-DiD/LDL-A488) Thresh=0.35 SubstRand=TRUE ByVolume=FALSE	38
Coloc. (LDL-DiD/(EEA1 & LDL-A488)) Thresh=0.35 SubstRand=TRUE ByVolume=FALSE	39
Coloc. (LDL-DiD/(EEA1 & LDL-A488)) Thresh=0.35 SubstRand=TRUE ByVolume=TRUE	40
Dist. Distr. (EEA1) Weighted=TRUE Weighting=GetVolume Param 1"Dist. Distr. (EEA1) Weighted=FALSE Weighting=GetVolume Param 1'	41
Dist. Distr. (EEA1) Weighted=TRUE Weighting=GetMeanIntensity Param 1"Dist. Distr. (EEA1) Weighted=FALSE Weighting=GetVolume Param 1'	42
Dist. Distr. (EEA1) Weighted=TRUE Weighting=GetSquare Param 1"Dist. Distr. (EEA1) Weighted=FALSE Weighting=GetVolume Param 1'	43
Dist. to Nucl. (EEA1/DAPI) Weighted=TRUE Weighting=GetVolume Per Nucleous=FALSE Normalize by Nucleous Size=TRUE	44
Dist. to Nucl. (EEA1/DAPI) Weighted=TRUE Weighting=GetMeanIntensity Per Nucleous=FALSE Normalize by Nucleous Size=TRUE	45
Dist. to Nucl. (EEA1/DAPI) Weighted=TRUE Weighting=GetSquare Per Nucleous=FALSE Normalize by Nucleous Size=TRUE	46
Dist. to Nucl. Cell Based (EEA1) Weighted=TRUE Weighting=GetVolume Normalization=Nuclei Size CalcMethod=DistToNuc	47
Dist. to Nucl. Cell Based (EEA1) Weighted=TRUE Weighting=GetMeanIntensity Normalization=Nuclei Size CalcMethod=DistToNuc	48
Dist. to Nucl. Cell Based (EEA1) Weighted=TRUE Weighting=GetSquare Normalization=Nuclei Size CalcMethod=DistToNuc	49
Mean Integ. Intens. (LDL-A488) Weighted=TRUE Weighting=GetVolume CalcType = Mean Weighted=FALSE Weighting=GetSquare CalcType = Mean'	50
Mean Integ. Intens. (LDL-A488) Weighted=TRUE Weighting=GetMeanIntensity CalcType = Mean Weighted=FALSE Weighting=GetSquare CalcType = Mean'	51
Mean Integ. Intens. (LDL-A488) Weighted=TRUE Weighting=GetSquare CalcType = Mean Weighted=FALSE Weighting=GetSquare CalcType = Mean'	52
Mean Intens. (LDL-A488) Weighted=TRUE Weighting=GetVolume CalcType = Mean Weighted=FALSE Weighting=GetSquare CalcType = Mean'	53
Mean Intens. (LDL-A488) Weighted=TRUE Weighting=GetMeanIntensity CalcType = Mean Weighted=FALSE Weighting=GetSquare CalcType = Mean'	54
Mean Intens. (LDL-A488) Weighted=TRUE Weighting=GetSquare CalcType = Mean Weighted=FALSE Weighting=GetSquare CalcType = Mean'	55
Mean Area (LDL-A488) Weighted=TRUE Weighting=GetVolume CalcType = Mean Weighted=FALSE Weighting=GetVolume CalcType = Mean'	56

Mean Area (LDL-A488) Weighted=TRUE Weighting=GetMeanIntensity CalcType = Mean Weighted=FALSE Weighting=GetVolume CalcType = Mean'	57
Mean Area (LDL-A488) Weighted=TRUE Weighting=GetSquare CalcType = Mean Weighted=FALSE Weighting=GetVolume CalcType = Mean'	58
Dist. Distr. (LDL-A488) Weighted=TRUE Weighting=GetVolume Param 1"Dist. Distr. (LDL-A488) Weighted=FALSE Weighting=GetVolume Param 1'	59
Dist. Distr. (LDL-A488) Weighted=TRUE Weighting=GetMeanIntensity Param 1"Dist. Distr. (LDL-A488) Weighted=FALSE Weighting=GetVolume Param 1'	60
Dist. Distr. (LDL-A488) Weighted=TRUE Weighting=GetSquare Param 1"Dist. Distr. (LDL-A488) Weighted=FALSE Weighting=GetVolume Param 1'	61
Dist. to Nucl. (LDL-A488/DAPI) Weighted=TRUE Weighting=GetVolume Per Nucleous=FALSE Normalize by Nucleous Size=TRUE	62
Dist. to Nucl. (LDL-A488/DAPI) Weighted=TRUE Weighting=GetMeanIntensity Per Nucleous=FALSE Normalize by Nucleous Size=TRUE	63
Dist. to Nucl. (LDL-A488/DAPI) Weighted=TRUE Weighting=GetSquare Per Nucleous=FALSE Normalize by Nucleous Size=TRUE	64
Dist. to Nucl. Cell Based (LDL-A488) Weighted=TRUE Weighting=GetVolume Normalization=Nuclei Size CalcMethod=DistToNuc	65
Dist. to Nucl. Cell Based (LDL-A488) Weighted=TRUE Weighting=GetMeanIntensity Normalization=Nuclei Size CalcMethod=DistToNuc	66
Dist. to Nucl. Cell Based (LDL-A488) Weighted=TRUE Weighting=GetSquare Normalization=Nuclei Size CalcMethod=DistToNuc	67
Mean Integ. Intens. (LDL-DiD) Weighted=TRUE Weighting=GetVolume CalcType = Mean Weighted=FALSE Weighting=GetVolume CalcType = Mean'	68
Mean Integ. Intens. (LDL-DiD) Weighted=TRUE Weighting=GetMeanIntensity CalcType = Mean Weighted=FALSE Weighting=GetVolume CalcType = Mean'	69
Mean Integ. Intens. (LDL-DiD) Weighted=TRUE Weighting=GetSquare CalcType = Mean Weighted=FALSE Weighting=GetVolume CalcType = Mean'	70
Mean Intens. (LDL-DiD) Weighted=TRUE Weighting=GetVolume CalcType = Mean Weighted=FALSE Weighting=GetSquare CalcType = Mean'	71
Mean Intens. (LDL-DiD) Weighted=TRUE Weighting=GetMeanIntensity CalcType = Mean Weighted=FALSE Weighting=GetSquare CalcType = Mean'	72
Mean Intens. (LDL-DiD) Weighted=TRUE Weighting=GetSquare CalcType = Mean Weighted=FALSE Weighting=GetSquare CalcType = Mean'	73
Mean Area (LDL-DiD) Weighted=TRUE Weighting=GetVolume CalcType = Mean Weighted=FALSE Weighting=GetVolume CalcType = Mean'	74
Mean Area (LDL-DiD) Weighted=TRUE Weighting=GetMeanIntensity CalcType = Mean Weighted=FALSE Weighting=GetVolume CalcType = Mean'	75
Mean Area (LDL-DiD) Weighted=TRUE Weighting=GetSquare CalcType = Mean Weighted=FALSE Weighting=GetVolume CalcType = Mean'	76
Dist. Distr. (LDL-DiD) Weighted=TRUE Weighting=GetVolume Param 1"Dist. Distr. (LDL-DiD) Weighted=FALSE Weighting=GetVolume Param 1'	77
Dist. Distr. (LDL-DiD) Weighted=TRUE Weighting=GetMeanIntensity Param 1"Dist. Distr. (LDL-DiD) Weighted=FALSE Weighting=GetVolume Param 1'	78
Dist. Distr. (LDL-DiD) Weighted=TRUE Weighting=GetSquare Param 1"Dist. Distr. (LDL-DiD) Weighted=FALSE Weighting=GetVolume Param 1'	79
Dist. to Nucl. (LDL-DiD/DAPI) Weighted=TRUE Weighting=GetVolume Per Nucleous=FALSE Normalize by Nucleous Size=TRUE	80
Dist. to Nucl. (LDL-DiD/DAPI) Weighted=TRUE Weighting=GetMeanIntensity Per Nucleous=FALSE Normalize by Nucleous Size=TRUE	81
Dist. to Nucl. (LDL-DiD/DAPI) Weighted=TRUE Weighting=GetSquare Per Nucleous=FALSE Normalize by Nucleous Size=TRUE	82
Dist. to Nucl. Cell Based (LDL-DiD) Weighted=TRUE Weighting=GetVolume Normalization=Nuclei Size CalcMethod=DistToNuc	83
Dist. to Nucl. Cell Based (LDL-DiD) Weighted=TRUE Weighting=GetMeanIntensity Normalization=Nuclei Size CalcMethod=DistToNuc	84
Dist. to Nucl. Cell Based (LDL-DiD) Weighted=TRUE Weighting=GetSquare Normalization=Nuclei Size CalcMethod=DistToNuc	85
Total Intens. (LDL-A488) Mask = TRUE' / 'Total Intens. (LDL-DiD) Mask = TRUE'	86

The aim of this screen aside from identifying molecular motors of early endosomes was to understand how various motors are organized and their activities coordinated to move endosomes *in vivo*. Towards this end, the phenotype profiles (gene profiles) of candidate motors in the hit list were cross-correlated to identify phenocopies of candidates in the hit list. Such phenocopies could either potentially implicate components in molecular protein complexes or identify those involved in common regulatory mechanisms. Correlation analysis of gene profiles may be considered as quasi-"clustering" analysis. Correlations above 0.3 (3SDs) are considered significant phenocopies of profiles. Candidates from the hit list are therefore discussed in terms of potential molecular complex below.

3.3.4.1 Kinesins and potential complexes

Four putative novel kinesins (Kif22, Kif19, STARD9 and KifC2) and two that have been reported (Kif5B and Kif3B) to be involved in early endosomes motility were identified in the motor screen. Domain organizations of novel Kinesins are indicated in Fig25. Kif22, Kif19 and STARD9 are N-terminal Kinesins while KifC2 is a C-terminus kinesin. Kif22 and Kif19 are

mitotic kinesins and have been shown to be localized predominantly in the nucleus (see discussion). However, this does not exclude their role in endosome transport in interphase. Kif22 harbors a weak helix-hairpin-helix motif at its C-terminus, which could possibly bind DNA regulatory elements to drive transcription of target genes following endocytosis of signaling cargo. STARD9, another novel kinesin with the StAR sterol-sensing domain is probably involved in LDL metabolism and cholesterol sensing. STARD9 is an interesting candidate since there are very few cases of molecular motors known in regulatory processes of cellular metabolism and this kinesin may be a regulatory cholesterol sensor in cells. KifC2 is an interesting candidate since it is a C-terminal kinesin that transports cargo centripetally and can therefore function in conjunction with Dynein. If validated, it would be the first minus end kinesin involved in the motility of Rab5 endosomes.

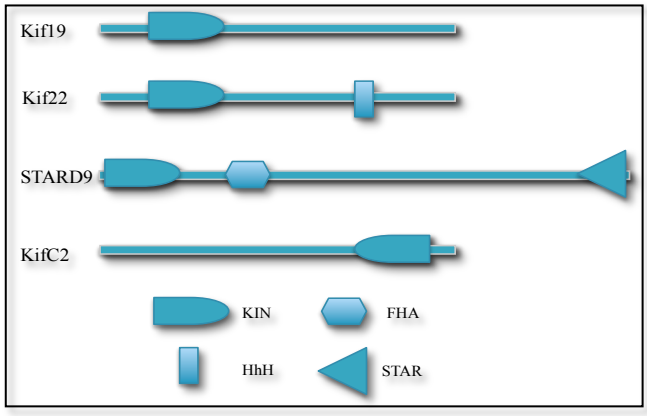

Fig25: Domain organization of putative novel Kinesins identified in the motor screen

Several classes of Kinesin motor proteins associate with accessory components such as Kinesin Accessory Proteins (KAPs) or Kinesin Light Chains (KLCs) to form holo-motor complexes. Analysis of phentotypic profiles of novel Kinesins and accessory components show strong correlation between STARD9 and KLC2, and Kif22 and KLC4 (Fig26) implying that they could form functional complexes.

A

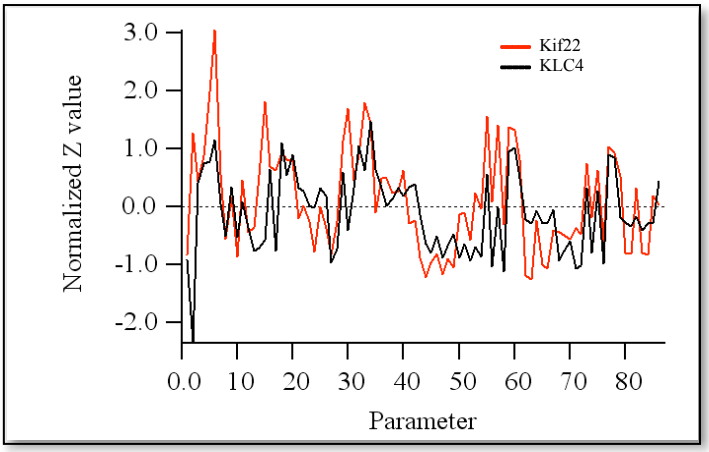

B

Potential Kinesin complexes		
KLC2	STARD9	0.614
KLC4	KIF22	0.515

Fig26: Phenotypic correlation between Kif22 and KLC4 A: Gene profiles of Kif22 and KLC4, B: Correlation scores between phenotypes produced by KLCs and Kinesin motor proteins

3.3.4.2 *Dynein-Dynactin complex*

Minus end directed microtubule dependent cytoplasmic Dynein heavy chain 1 scores in the screen as expected, however of interest are the accessory components that associate with the motor chain to form a holo-complex. The accessory components that also scored in the screen are DYNC1H1, DYNC1I2, DYNALI1, TCTEX1D1 and DYNLRB1, which include DIC, DLIC and 2 DLCs (Table10). Consistent with their function, knock down of all of Dynein components produce dispersion of endosomes (Fig27C, D) due to loss of minus end motor activity. Of interest in the putative Dynein complex are

1. Incorporation of axonemal Light Intermediate Chain in a cytoplasmic Dynein complex,
2. Use of Light chain TCTEX1D1 that has not been reported to be part of the Dynein or any motor complex.

The Dynactin complex components that score are also interesting in that, DCTN1, DCTN2, DCTN3 and DCTN4 show similar phenotypes (Fig27A, B), while DCTN5 and DCTN6 do not. One explanation may be that the phenotypes produced are subtle since they are non-essential components (Schroer, 2004). However, the lack of phenotype is consistent with the fact that these two components are not expressed in A431 cells from the expression profiling data. If the latter is the case, then the Dynactin complex used by A431 cells is akin to yeast complex than to the mammals, which might have regulatory implications. The Dynactin complex however is

functional, since knock down of core components phenocopy that of the Dynein complex (Fig27E).

DNCH-DCTN components	Type
DYNC1H1	HC
DYNC1I2	IC
DYNALI1	LIC
TCTEX1D1	LC
DYNLRB1	LC
DCTN1	Dynactin
DCTN2	Dynactin
DCTN3	Dynactin
DCTN4	Dynactin

Table10: Dynein-Dynactin components that score in the screen

A

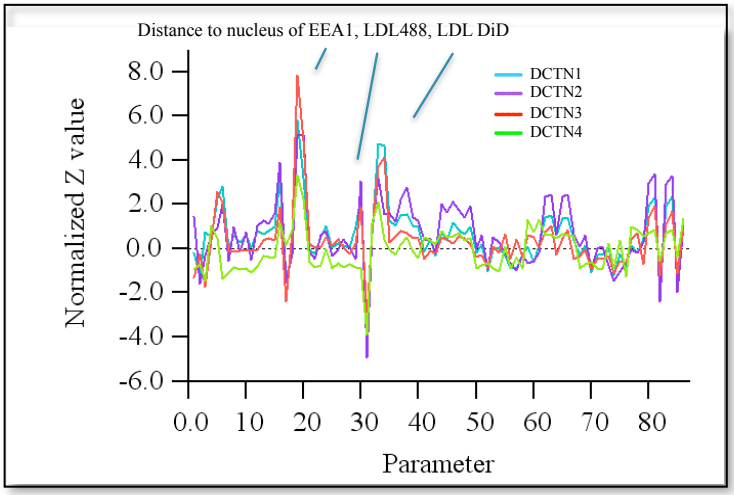

B

Dynein-Dynactin Complex components		
DCTN1	DCTN2	0.897
DCTN1	DCTN3	0.885
DCTN1	DCTN4	0.546

C

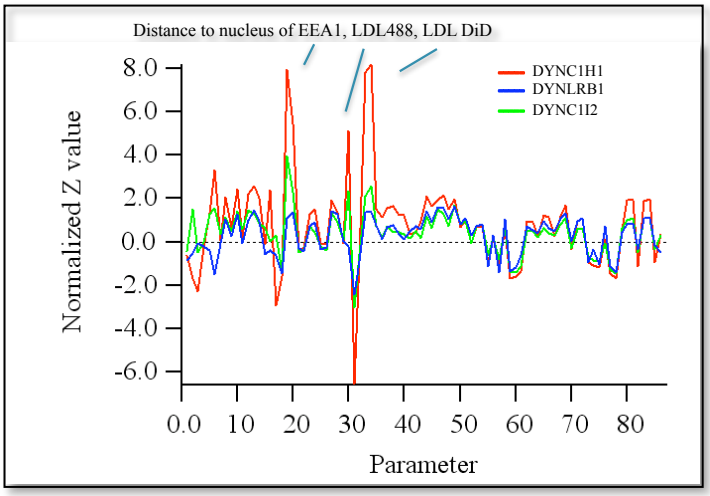

D

Dynein-Dynactin Complex components		
DNCH1	DNCI2	0.894
DNCH1	DYNLRB1	0.700

E

Dynein-Dynactin Complex components		
DCTN1	DCTN2	0.897
DCTN1	DCTN3	0.885
DCTN1	DYNC1H1	0.871
DCTN1	DYNC1I2	0.745
DCTN1	DCTN4	0.546
DCTN1	DYNLRB1	0.461
DCTN1	DYNALI1	0.318

Fig27: Phenotype produced by Dynein-Dynactin components. A: Phenotype profiles of Dynactin components, B: Correlation scores between phenotype profiles of Dynactin components, C: Phenotype profiles of Dynein components, D: Correlation scores between phenotype profiles of Dynein components, E: Correlation scores between phenotype profiles of Dynein and Dynactin components.

3.3.4.3 Novel endosomal Myosins

Several actin based motors scored in the motor screen (Table9). On a molecular level, all of these myosins are novel and interesting since none of them are characterized in terms of vesicular transport. MYH9, MYH11 and MYH14 are ClassII Myosins, while Myo1F and Myo9B belong to classI and IX respectively. Identified Myosins may either be used for actin-based transport of early endosomes, in vesicle fission or as molecular tethers. The latter two functions may more likely be the case since microtubule dependent transport is the predominant mode of intracellular transport in mammalian cells.

3.3.4.4 Potential molecular complexes

Another potentially interesting phenotype correlation is that between DYNC1H1, Kif19 and MYH9 (Fig28). Kif19 is a plus end Kinesin, however, it phenocopies a minus end motor Dynein. This could mean that Kif19 is a minus end motor with a N-terminus Kinesin motor domain, or that it transports Dynein and localizes it to the periphery in cells, where cargo is loaded and transported centripetally. The latter is an interesting hypothesis since the mechanism of localization of Dynein in mammalian cells is not known.

MYH9, a non-skeletal classII Myosin also phenocopies DYNC1H1.Whether the two motors interact to regulate track switching during transport or localize each other is a question that needs to be tested.

A

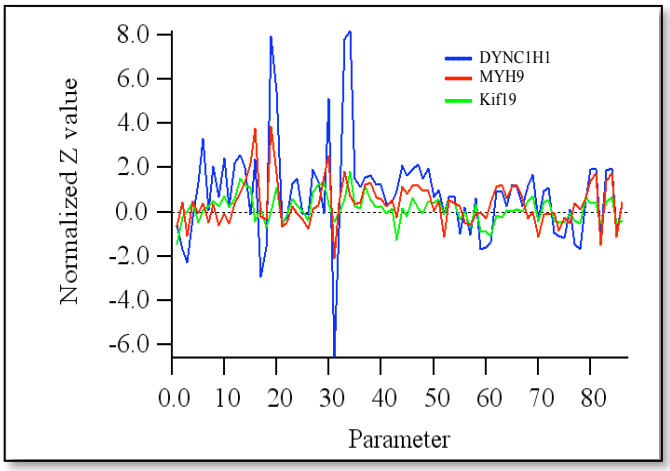

B

Dynein HC phenocopies		
DYNC1H1	MYH9	0.698
DYNC1H1	Kif19	0.568

Fig28: Phenotype of DYNC1H1, Kif19 and MYH9. A: Gene profiles of DYNC1H1, Kif19 and MYH9, B: Correlation scores between phenotype profiles of DYNC1H1, Kif19 and MYH9.

3.3.4.5 *Differential utilization of Dynein functions by sub-populations of early endosomes*

Loss of function of Dynein by RNAi knock down results in peripheral cortical accumulation of a subpopulation of Rab5 structures that immunostain for APPL and not EEA1. EEA1 vesicles on the contrary are dispersed in the cell with a phenotype akin to that resulting from nocodazole treatment. This could imply that Dynein is involved in actively transporting APPL endosomes, while tethering EEA1 positive Rab5 endosomes in the juxtanuclear region (Fig29).

A Zoomed image C Zoomed image

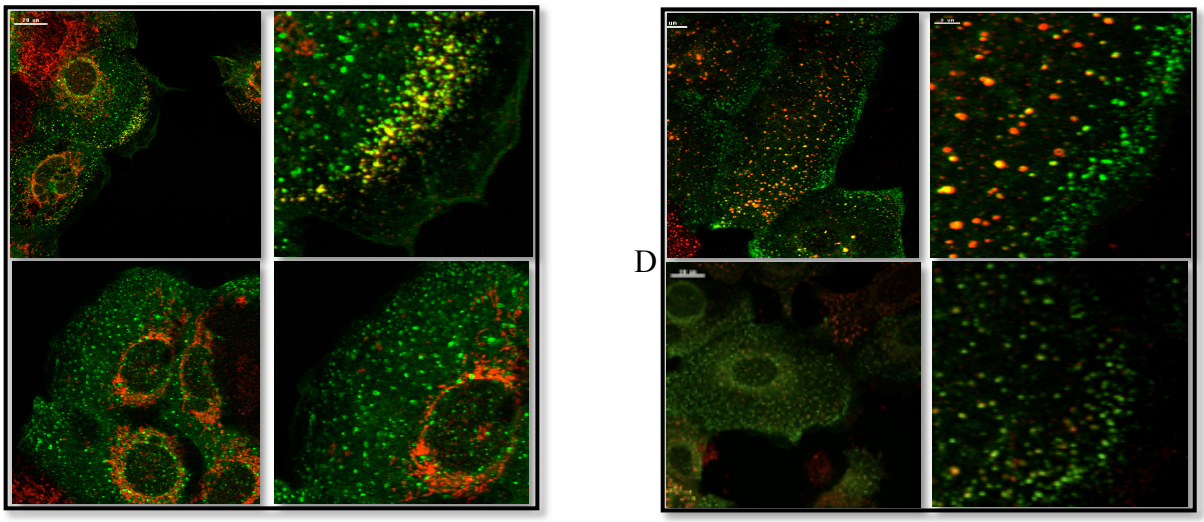

B D

Fig29: DYNC1H1 knock down in A431 GFP-Rab5 cells. Green – Rab5 endosomes, Red – immunostained for APPL1 or EEA1. A: Immunostained for APPL1, B: APPL1+ DYNC1H1 double knock down, immunostained for APPL1, C: Immunostained for EEA1, D: EEA1+ DYNC1H1 double knock down, immunostained for EEA1. Scalebar-20μm.

3.4 Expression profiling of molecular motors in A431 cell line.

Semi-quantitative RT-PCR analysis to detect mRNA transcripts in A431 cells was performed after extraction of total RNA and reverse transcribing it to cDNA using oligodT primers. Gene expression was detected using two independent exon-spanning primers to ubiquitously expressed isoform by standard Taq PCR. Examples of positive and negative expression are as shown in Fig30A with two sets of primers for DCTN1 and MYH7 genes. Table11 is an overview of the all the genes tested, green - expression was detected, red – expression not detected.

Of 124 genes tested, transcripts for 101 genes were detected in A431 cells for at least one primer probe used corresponding to 81% of the motorome (Fig30B). For the other 23 genes, no transcript was detected in the cDNA preparation from A431 cells for either primer pairs. PCRs were repeated to confirm the results. HT (Human Transcriptome - pool of human cDNA from 32 human tissues and 34 human cancer lines) was used as the positive control to confirm efficiency of primer in detecting gene transcripts.

Of interest from the expression profile of motor genes in A431 cell line is the expression of axonemal heavy chain and accessory components in addition to the cytoplasmic Dynein heavy chains and associated cytoplasmic Dynein components. A431 cells are non-ciliated and are no expected to express axonemal components and yet they do. Among the Kinesins, the most striking dichotomy is the lack of expression of a fairly ubiquitous Kinesin complex, Kif3A/Kif3C and the accessory protein KifKAP3. A431 cells also show an abundant expression of muscle specific Conventional Myosins, the functional significance of which is intriguing.

Segregated by motor class, A431 cell line expresses 7/11 Axonemal Dynein, 36/44 Kinesin and 34/39 Myosin heavy chains. Given the proteomic complexity of molecular motors and nature of motors expressed, it was of interest to identify the molecular motors involved in the transport of endosomes through an RNAi screen targeting the motor complement of the human genome.

A

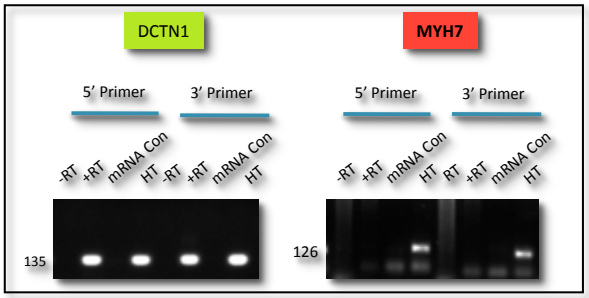

Table 4

DCTN1	DYNAH17	DYNC2LI1	KIF19	Kif3A	MYH13	MYO1B
DCTN2	DYNAH2	DYNLL1	KIF1A	Kif3B	MYH14	MYO1C
DCTN3	DYNAH3	DYNLL2	KIF1B	KIF3C	MYH15	MYO1D
DCTN4	DYNAH5	DYNLT3	KIF1C	KIF4A	MYH2	MYO1E
DCTN5	DYNAH6	KIF9	KIF2	KIF4B	MYH3	MYO1F
DCTN6	DYNAH7	KifSTARD9	KIF20A	KIF5A	MYH4	MYO1G
DNAH10	DYNAH8	KIF10	Kif20B	Kif5B	MYH6	MYO3A
TCTE3	DYNAH9	Kif11	KIF21A	KIF5C	MYH7	MYO3B
DYNLT1	DYNAI1	KIF12	KIF21B	KIF6	MYH7B	MYO5A
TCTEX1D1	DYNAI2	KIF13A	KIF22	Kif7	MYH8	MYO5B
DYN1LRB1	DYNAL4	KIF13B	KIF23	KIFAP3	MYH9	MYO5C
DYN1LRB2	DYNALI1	KIF14	Kif24	KIFC1	MYO10	MYO6
TCTEX1D2	DYNC1H1	KIF15	KIF25	KIFC2	MYO15A	MYO7A
DYNAH1	DYNC1I1	Kif16	Kif26A	KIFC3	MYO15B	MYO7B
DYNAH11	DYNC1I2	Kif16B	KIF26B	MYOHD1	MYO16	MYO9A
DYNAH11	DYNC1LI1	KIF17	KIF27	MYH1	MYO18A	MYO9B
DYNAH14	DYNC1LI2	KIF18A	KIF2B	MYH10	MYO18B	
DYNAH14	DYNC2H1	Kif18B	KIF2C	MYH11	MYO1A	

B

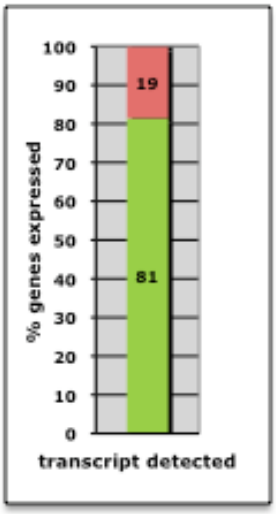

Fig30: Transcriptional profiling of molecular motors in A431 cell line. A: Representative examples of genes probed with 2 primer pairs that were expressed (green) or not (red) in A431 cells. RT – Reverse transcriptase enzyme, mRNA con(trol) – reaction cocktail with water instead of mRNA, HT-Human transcriptome mix (positive control). B: Percent motors expressed out of 124 genes tested in A431 cells.
Table11: Overview of expression profile of motor genes in A431 cells. Green-expressed, Red-not expressed,

4 Discussion

4.1 Systems analysis of early endosome motility

Intracellular motility is a fundamental process that allows trafficking of molecules between various cellular compartments, maintaining identity of intracellular organelles and cellular homeostasis. Molecular motors of the Dynein, Kinesin and Myosin families have evolved to cater to the function of intracellular transport in eukaryotes. The aim of this study was to understand the regulation of motility of early endosomes and its implication in the functional organization of the endosomal system.

The complex motility behavior of early endosomes is a consequence of the consorted activities of molecular motors, cellular cytoskeleton and other regulators such as microtubule and actin associated proteins, and components of the Rab5 machinery. This study focuses on identifying potential molecular motors that are involved in early endosome motility and candidates involved in saltatory Rab5 endosome motility.

4.1.1 Regulation of Rab5 machinery by motility

Cargo that is internalized by cells into early endosomes moves centripetally with time and congregate close to the nucleus before they mature into (Stoorvogel et al., 1991), (Rink et al., 2005) or fuse with (Herman and Albertini, 1984) late endosomes/lysosomes. During the process of centripetal translocation, they undergo several events of homotypic fusion, grow in size and Rab5 content, and concentrate cargo with concomitant fission to extricate membrane devoid of Rab5. These events serve to sort recycling cargo whilst committing the rest for degradation. Critical for degradation is the movement of early Rab5 endosomes to the centre of the cell. It has been shown that impairment of this migration using nocodazole a microtubule depolymerization agent that disperses early endosomes delays the degradation kinetics of LDL (Rink et al., 2005). Hence motility of endosomes by molecular motors is important not just to move early endosomes toward the cells's nucleus, but also in determining the frequency of fusion and fission. Also, the endosomal network is regulated in terms of the number, size and spatial positioning in the cell. It has been shown that more the number of endosomes, smaller their size and the farther they are from the nucleus (Collinet et al., 2010), i.e, as they move centripetally, they tend to undergo homotypic fusion, grow in size, increase Rab5 content by extracting Rab5 negative membrane

through fission. At regions proximal to the nucleus, the Rab5 vesicles then convert to Rab7 late endosomes (Rink et al., 2005), triggered through a toggle switch sensitive to Rab5 concentration on vesicles (Del Conte-Zerial et al., 2008).

Previous studies by Rink *et al* and Collinet *et al* have demonstrated a correlation between spatial positioning of Rab5 endosomes, endosome size and Rab5 content, not distinguishing causality and consequence. Studies with kinetic live cell experiments and motor screen performed here suggest motility in regulating Rab5 machinery and function. Candidates from the motor screen where function of molecular motors are abrogated lead to changes in morphometric properties and content of EEA1 (Rab5 by extension) on early endosomes demonstrating that perturbation of motility cause of perturbation of Rab5 dynamics. Similar phenotypes are mimicked in kinetic live cell imaging screen of Kinesin candidates. Hence motility or molecular motors can potentially regulate the endosomal system through frequency of encounter (fusion). They may also act as sensors in detecting Rab5 concentration on vesicles since increase in Rab5 density on vesicles and Rab5 size lead to a decrease speed of endosomes (from correlation analysis).

Rab5 has been shown to regulate motility, in that, increasing Rab5 concentration on endosomes increases the number of minus end motility events (Nielsen et al., 1999). Hence coupling motility to Rab5 status may involve feedback regulation, whereby one endosomal property regulates the other. Although motility and fusion of early endosomes may are not directly linked (Nielsen et al., 1999), density of Rab5 may modulate recruitment of motors, thereby processivity (increasing copy numbers) or regulators of motors that modulate speed of endosomes.

Impaired transport in aged monkey neuroblastoma cells (model system for neurodegenerative diseases) due to mislocalization of Dynein and Kinesin heavy chain (Kimura et al., 2007) leads to upregulation of Rab5, 7 and 11, and enlargement of early endosomes that are mislocalized (Kimura et al., 2009). Hence activity of molecular motors and motility can alter dynamics of Rab5 on early endosomes.

Saltatory motility or territories is a regime of motility where endosomes are involved in short range movements that are motor driven. It is qualitatively similar to that executed by several other organelles. This regime of motility “captures” endosomes in a spatial confined area that serves to potentially regulate endosome fusion and fission. Hence saltatory motility is thought to facilitate molecular sorting of cargo through regulation of fusion/fission rates, however, the hypothesis needs to be tested with candidates that abolish this mode of motility. Hence saltatory

behavior in conjunction with long range endosomal motility and bi-directional motility possibly coordinate molecular sorting of cargo through regulation speed of endosome movement, fusion and fission.

Several mechanistic hypotheses were considered to explain saltatory motility. Among them were the cytoskeletal cage, actin tether and endosome tether models (see schematic below). In the cytoskeletal cage model, cytoskeletal "cages" or confines are thought to restrict long range movement of early endosomes; the nature of cages being either microtubules or actin. Hence cytoskeletal perturbation experiments were performed to clarify the hypothesis. In the actin-tether model, actin nucleators such as annexin2 on early endosomes are thought to nucleate actin on endosome and tether them through actin cables to possibly microtubule tracks thereby spatially confining motility of endosomes. Hence, annexin2 was knocked down to evaluate saltatory motility. However, neither actin, nor annexin2 were found to alter this mode of motility. In the endosome tether model endosomes through their pleomorphic extensions are posited to be tethered by multiple motors on several of their tubular extensions simultaneously, resulting in confined motility. Several Rab5 effectors were tested in a search for molecular candidates involved in any of these speculative hypotheses. EHD proteins were also tested since they have been shown to regulate transferrin recycling and therefore molecular sorting of cargo. Hook proteins were also tested as they are MAPs that could potentially forge links between microtubules and endosomes to tether the latter wthin spatial confines. Rho proteins (RhoD and RhoB) have been shown to localize on early endosomes and regulate endosome motility. In that, overexpression of Rhos lead to early endosomes stall on actin filaments, akin qualitatively to increased saltatory behavior. However, none of the mentioned candidate genes tested showed a altered saturation of MSD plots, except for perturbation of microtubules with sub-nanomolar doses of nocodazole. Low doses of nocodazole have been shown to inhibit dynamic instability of microtubules, suggesting potential regulation of saltatory motility by microtubule dynamics. Functional cargo sorting under conditions of inhibition of saltatory behavior is yet to be evaluated.

Actin tethering model

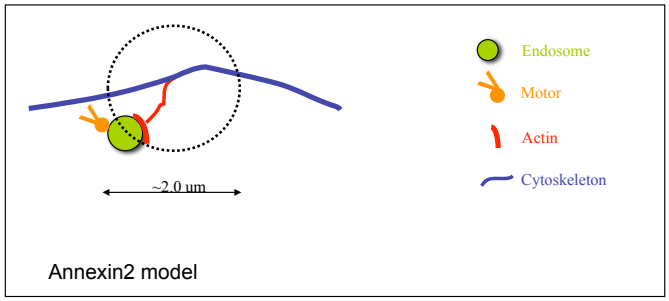

Cytoskeletal cage model

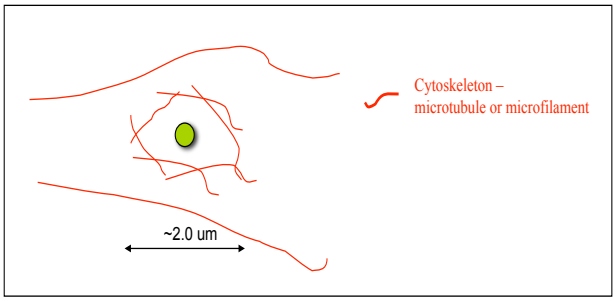

Endosome tether model

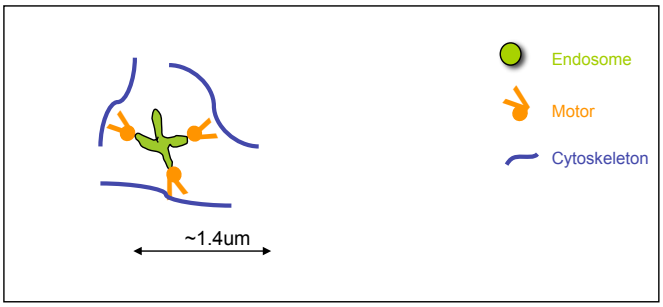

Models for saltatory motility of early endosomes. Actin tethering model – wherein actin nucleators on early endosomes such as annexin2 nucleate actin cables that tether endosomes and restrict long range movement. Cytoskeletal cage model – cellular cytoskeleton, MT or MF form spatio-temporal caged barriers during their remodeling confining endosome motility. Endosome tether model – pleomorphic tubular structures of endosomes bound to several motor proteins simultaneously are confined spatially.

4.2 RNAi screen for molecular motors involved in endosome motility

4.2.1 LDL cargo degradation kinetics and assay

Cells deal with cargo internalized in into early endosomes in either of the two ways - they are sorted for either recycling through iterative fission events or routed to for degradation. LDL is an archetypal degradative cargo that on its binding to its receptor at the cell surface is internalized into Rab5 early endosomes. Within this environment, owing to decrease in pH, the ligand dissociates form the receptor, the former routed for degradation, while the receptor is recycled back to the plasma membrane. LDL uptake and metabolism provides the cells with cholesterol, and the amino acids released enter the anabolic pathway. Uptake, transport through the endocytic

network and degradation of LDL are fairly well established and was used in the motor screen as a canonical degradative cargo marker.

In the motor screen, LDL conjugated with two different fluorophores was used. The differential persistence of fluorophores in cells inherent in their chemistry was exploited in the assay of the screen and formed the basis of the functional read out. Succinimidyl ester derivatized Alexa488 is conjugated to the ApoB protein moiety of LDL though its linkage with primary amine of Lysine, while DiD, a lipophilic fluorophore incorporates in the lipidic component of LDL. Upon internalization and metabolism of LDL-flourophore conjugates, the Alexa488-tyrosyl moiety of ApoB is presumably secreted by cells out into the extracellular medium, akin to metabolized radiolabelled-mono-iodotyrosine from radiolabelled-iodo-LDL metabolism (Brown and Goldstein, 1975). Hence, the fluorescence associated with the cargo (and cells) decreases with time as it traffics from the early endosomal compartment to late degradative compartments making it a useful read-out for optimal transport from early to late compartment and subsequent degradation. A decrease in intracellular LDL-Alexa488 fluorescence could however mean either efficient cargo processing, or inefficient internalization. To distinguish between the scenarios, an additional cargo marker LDL-DiD was included in the assay. Unlike LDL-Alexa488 whose fluorescence decreases with chase time, that of LDL-DiD persists in cells for as long as 48hrs. DiD being lipophillic presumably integrates into the delimiting membrane of the late compartments and cannot be excluded from endomembrane of cells. Interestingly, the fluorescence of DiD in fact increases linearly with time of chase. This might possibly reflect dynamic de-quenching effect of the fluorophore as it is sterically relieved from the LDL core (Loyter et al., 1988) (where the local dense environment causes auto-quenching as the DiD molecules) and disassembled during catabolism.

In conclusion, LDL-Alexa488 is the primary functional marker, while LDL-DiD was used as the reference marker to follow the degradation efficiency of LDL-Alexa488. Also, in the time frame used in the assay, LDL-DID is distributed between the early and late endosomal compartments. Non-colocalized LDL-DiD represents post early compartments and not pre early compartments since the kinetics of cargo exit for both the species of LDL is similar. Also, the cargoes are pulsed and chased after removing pulse medium. Given the chase time frame, it is highly unlikely that LDL-DiD is selectively retained in the pre-early compartments. In conclusion, the

motor screen identified molecular motors involved in early endosome distribution and by extension, motility along the degradative arm of the endocytic system.

4.2.2 Motor screen – what has been identified and what may been missed

The LDL degradation assay was designed to identify endosomal motors whose loss of function should result in altered kinetics of cargo degradation. The chase interval was standardized based on the fact that with 10min pulse and 60min chase of co-pulsed cargo, about half of the internalized degradative marker would be lost, allowing for a broad dynamic range in detection of both degradation defective and acceleration phenotypes. An important caveat of the screen is however that it might not be able to identify motors that produce subtle defects, especially given that intracellular transport is never an all or none phenomenon due to the presence of redundant or partially redundant motors. For such motors, the kinetics of cargo processing may be altered, but not devoid. Kif16B, a plus end early endosomal Kinesin that has been shown to regulate cargo recycling and degradation kinetics (Hoepfner et al., 2005) does not score in the screen as it produces weak phenotype that is partially compensated for by other redundant motors. In such cases, the live cell kinetic Kinesin screen would probably identify motors with weak phenotypes that would be missed in the degradation screen. Nevertheless, the degradation screen did identify several putative motors and more importantly molecular complexes and putative transporters of motors, which are entirely novel atleast in the mammalian system. The motor screen identified the following –

Composition of cytoplasmic Dynein complex, which is unconventioanl in its incorporation of axonemal components.

Composition of the Dynactin complex which if validated is unexpected and may impose regulatory and/or recruitment of cargo.

Novel Kinesins that have not so far been implicated in endosome motility.

Novel Myosins in endosome function.

4.2.3 Potential molecular motors of early endosomes

Some of the motors identified in the screen have been implicated in functions unrelated to organelle transport such as mitotic Kineins Kif22, Kif19, while Myosins from the screen have not been characterized in terms of its transport functions. Some of the motors identified in the

screen with interesting functional implications are discussed below.

4.2.3.1 Kinesins

4.2.3.1.1 Kif19

Kif19 is a Family 8 Kinesin known to affect the microtubule dynamics (Du et al., 2010), (Varga et al., 2009). Kif19, a Kinesin with its motor domain at the N-terminus shows an endosome distribution phenotype akin to a minus end motor and phenocopies the Dynein-Dynactin complex. This could mean either that Kif19 is a minus end Kinesin with N-terminus motor domain, or that it transports and localizes Dynein at the peripheral regions in the cell from where the later can bind cargo and transport it retrogradely. All plus end Kinesins harbor their motor domain at the N-terminus. Kif19 being a N-terminus kinesin intuitively would be expected to be a plus end Kinesin. However, given that the determinants of directionality of Kinesins are not within the Kinesin motor domain (Henningsen and Schliwa, 1997), (Vale and Fletterick, 1997) but rather regions outside the motor domain and given the phenotype produced by Kif19 in the screen, this Kinesin may be an exception to the rule.

Kif19 as an anterograde transporter of Dynein - The mechanism of localization of Dynein has been an open question in vertebrates. In *Aspergillus nidulans* (Zhang et al., 2003) and *Ustilago maydis* (Lenz et al., 2006) targeting of Dynein-Dynatin complex at the hyphal tip is dependent on Kinesin. Hence, the distal end of he hyphal tip has a reservoir of inactive Dynein and Dynactin where retrograde cargo is loaded and transported by activation of Dynein by Lis1. In mammalian cells, CLIP170 that colocalizes with transferrin vesicles (Pierre et al., 1992) bind p150-Glued of the Dynactin complex and localizes to the Plus end of growing microtubules (Vaughan et al., 1999). Hence a plausible mechanism of localizing and loading Dynein with cargo a the cell periphery is through its interaction with p150Glued which binds CLIP170 at the plus ends of microtubules and endosmes, However, it was also shown that the binding of P-150Glued subunit of Dynactin to plus ends of microtubules did not require CLIP150 (Vaughan et al., 2002), (Lenz et al., 2006). Hence it is unclear how Dynein is localized at the cell periphery. Yeast Hybrid and immunoprecipitation studies with rat brain homogenate have shown that Dynein IC can directly interact with Kinesin Light Chains (Ligon et al., 2004) and hence might be actively transported to the periphery of cells. However, the mechanism of localization of Dynein at the cell periphery has not been demonstrated *in vivo*. The phenotype of Kif19 suggests

this motor as a putative plus end transporter of the Dynein complex that needs to be tested.

4.2.3.1.2 Kif22

Kif22 also known as Kid (**Ki**nesin Like DNA-binding) was identified as a transcription factor that binds the promoter of c-erbB-2 in MDA-MB453 breast cancer cells over-expressing c-erbB-2. The N-terminus of this protein has the kinesin motor domain, while the C-terminal region has a heix-haipin-helix motif that binds DNA (Tokai et al., 1996). This protein is predominantly localized in the nucleus in interphase, although some cytoplasmic speckles are also observed (Levesque and Compton, 2001), (Tokai et al., 1996). Kif22 has been shown to be important for chromosomes segregation during mitosis (Levesque and Compton, 2001). Kif22 is a plus end directed Kinesin with speeds of 0.15um/sec (Yajima et al., 2003), monomeric, and has a second microtubule binding site outside the motor domain hat enhances its affinity for microtubules (Shiroguchi et al., 2003). In the motor screen, it phenocopies the plus end directed Kinesins, Kif5B and putative plus end motor STARD9. Kif22 is an interesting motor as its knockdown in live time-lapse microscopy produces kinetic phenotype that closely phenocopies that of APPL1 knock-down. APPL1, an effector of Rab5 has been shown to translocate into the nucleus and interact with the NuRD/MeCP complex (Miaczynska et al., 2004). Hence Kif22 may be involved in regulation of kinetics of APPL1 endosome and/or of its nuclear translocation. Conversely, it might tanslocate along with or without APPL1 into the nucleus where it can drive transcription of target genes as has been shown for Kif17 (Macho, science, 2002) following endocytosis of cargo.

4.2.3.1.3 STARD9

STARD9 is a novel Kinesin with a FHA and StAR domain. This Kinesin harbors its motor domain at the N-terminus and is likely to be a plus end directed motor consistent with the phenotype produced in the screen. The StAR (Steroidogenic Acute Regulatory) domain is found in proteins involved in steroidogeneis in the gonads and adrenal cortex (Kallen et al., 1998), (Stocco, 2000). This domain is involved in sterol transfer and may therefore be a regulatory component of LDL metabolism. STARD9 is interesting from the point of view of a Kinesin involved in potential feedback regulation of cholesterol metabolism.

4.2.3.1.4 KifC2

Among the Kinesins identified in the screen, KifC2 is particularly interesting for the following three reasons – Firstly, KifC2 is a C-terminus Kinesin. It transports cargo retrogradely in cells. There are no minus end motors other than Dynein, known so far in Rab5 endosome motility. KifC2 could therefore be the first minus end Kinesin that functions together with Dynein in centripetal transport of cargo. Second, in terms of regulation of motility, it would be very interesting to investigate how the activities of Dynein and KifC2 are coordinated in minus end transport of early endosomes. Third, *in vitro* motility assay show that Dynein is not involved in transport of early endosomes since anti-Dynein function blocking antibodies do not inhibit minus end motility of these organelles. However, anti-Kinesin function blocking antibodies inhibit minus end directed motility of early endosomes, suggesting the involvement of a Kinesin rather than Dynein in centripetal motility of early endosomes (Nielsen et al., 1999). This might also suggest a tethering or regulatory role for Dynein rather than transport while KifC2 might function in transport of early endosomes.

4.2.3.1.5 Dynein-Dynactin Complex in Rab5 endosome motility/distribution

Functional Dynein *in vivo* is a complex of several polypeptides that associate with the motor heavy chain. Since the Dynein motor components are notorious for their expanded genetic inventory and isoform diversity, combinatorial assembly of this complex has been proposed to generate holo-motor complexes that generate cargo specificity and kinetic specificities (Kini and Collins, 2001). In the screen performed in A431 cells, the composition of Dynein complex that emerges is DYNC1H1 (Heavy Chain-HC), DYNC1I2 (Intermediate Chain-IC) DYNALI1 (Light Intermediate Chain-LIC), TCTEX1D1 (Light Chain-LC) and DYNLRB1 (Light Chain-LC). The presence of DYNC1H1 and DYNC1I2 is not surprising and has been shown to be involved in transporting several cargoes (Susalka and Pfister, 2000), (Palmer et al., 2009). The LIC that scores in screen is interesting, in that, of the 2 cytoplasmic LICs, DYNCLI1 is not expressed in A431 cells and DYNCLI2 does not score in the screen. The only LIC with a phenotype which phenocopies the Dynactin subunits (DCTN1, DCTN2 and DCTN4) is DYNALI1. DYNALI1 is an axonemal component and may promiscuously be incorporated in a complex that transports non-axonemal cargoes. Amongst the LCs that score, DYNLRB1 which phenocopies DYNC1H1 and DYNC1I2 has been found to be a fairly ubiquitous component of the Dynein complex

(Palmer et al., 2009). TCTEX1D1, a LC is novel component that has not been shown to be a part of the Dynein complex. The composition of Dynein complex if bona fide is a novel complex as it is doped with axonemal subunits.

A recent study identified composition of Dynein complexes involved in transport of several organelles in COS cells. The difference in Dynein composition between the motor complex involved in the transport of Golgi vesicles and transferring vesicles (early/recycling endosomes) lies in the LIC, the former using DYNL1C1 while the later DYNLIC2 (Palmer et al., 2009) (see table below). This study is consistent with the notion that the LCs may not be cargo specifiers or linkers in the complex as was believed earlier, but may confer stability to the ICs instead (Williams et al., 2007) and the cargo defining components may be IC (Steffen et al., 1997) and /or LICs (Tynan et al., 2000).

Composition of Dynein complex involved in transport of Golgi and EE/RE in Cos and A431 cells

	Golgi/COS	EE,REi/COS	EE/A431
HC	DYNC1H1	DYNC1H1	DYNC1H1
IC	DYNC1I2	DYNC1I2	DYNC1I2
LIC	DYNLIC1	DYNLIC2	DYNALI1
LC	DYNLT1	DYNLT1	TCTEX1D1
LC	DYNLRB1	DYNLRB1	DYNLRB1
LC	DYNLL1	DYNLL1	

The requirement of Dynein for transport of Rab5 early endosomes has not been shown unequivocally. Dynein has been shown to be required for cargo sorting from early endosome (Driskell et al., 2007), requirement for late endosome motility via RILP, ECV, and for recycling endosomes, but not for motility of early endosomes. In fact, in vitro motility assays show that function-blocking antibodies cannot inhibit minus end motility (Nielsen et al., 1999). Dynein complex can be used for two mutually independent purposes - transport and anchor (Gupta et al., 2008), (Delanoue and Davis, 2005).

DYNC1H1 knock down in A431 cells shows an interesting phenotype, in that, it produces a peripheral cortical band of endosomes which stain positive for APPL1, but not EEA1 or clathrin heavy chain. This cortical band of APPL1 endosomes is not as dramatic in control or mock treated cells as it is under DYNC1H1 knock down conditions. EEA1 positive vesicles are

however randomly dispersed in the cytoplasm with loss of juxtanuclear localization. Hence, DYN1CH1 may be a retrograde motor for a sub-population of Rab5 endosomes (APPL1 endosomes), while a tether for EEA1 endosomes.

4.2.3.1.6 Myosins in Rab5 endosome motility/distribution

The predominant mode of intracellular traffic in mammalian cells is microtubule dependent, mediated by Kinesins and Dynein. Hence, few actin-based motors have been reported to be involved in early endosome motility. Myo6 is the only Myosin implicated during early stages on endocytosis, such as transport of nascent endosomes through the cortical actin mesh (Aschenbrenner et al., 2004), its association with Dab2, an adaptor for LDLR (Morris et al., 2002) and clathrin coated vesicles (Buss et al., 2001), however, several Myosins have been identified as regulators of the recycling pathway, such as Myo5 (Yan et al., 2005) and Myo6 (Chibalina et al., 2007). Hence, all of the Myosins that have been identified in the screen are novel. Myo6 did not score in the screen perhaps since adaptors other than Dab2 (with which Myo6 associates to internalize LDLR) compensate (Maurer and Cooper, 2006) for internalization of LDLR. Myosins have also been implicated in vesicle fission, in stabilizing and exerting tension on actin cables during membrane fission in yeasts. Myo5p, the orthologue of Myo1F identified in the screen was shown to localize at sites of internalization and function as actin nucleation promoting factor (Sun et al., 2006). It was also shown to mediate vesicle fission (Jonsdottir and Li, 2004). Whether Myo1F in mammalian cells perform similar roles is an open question. MYH9 an MYH14 are non-muscle classII Myosins (Conti and Adelstein, 2008). MYH9 has been shown to mediate crosstalk between actin and microtubules by stabilization of the latter through acetylation (Even-Ram et al., 2007). Functional contribution of Myosins identified in the screen in early endosome motility or traction-mediated fission needs to be tested.

4.2.3.2 Molecular protein complexes

Several molecular motors function as complexes, often associating with other motor proteins and/or accessory non-motor components. Exemplarily are the Dynein complexes (King et al., 2002), conventional kinesin (DeBoer et al., 2008), Kinesin2 complex (Kif3A/Kif3B/KifAP3) and several classes of Kinesin motors (Verhey and Hammond, 2009). An interesting approach to

analyzing potential candidates forming complexes from the screen is through "clustering analysis" based on co-relations between the gene profiles. Candidates with high phenotype co-relations potentially implicate them in molecular complex or as regulators of each other with a common regulatory denominator. The motor screen has revealed several such potential molecular complex candidates that need to be tested and validated. Phenocopies of Kif22 and KLC4 or STARD9 and KLC2 probably imply functional molecular complex, while phenocopies of DYNC1H1, MYH9 and DYNC1H1, Kif19 may imply regulatory or localization functions of motors.

4.3 Expression profiling of molecular motors in A431 cell line.

Intracellular transport is complex given multitude of transport routes and destinations, diversity of cargoes transported, regulation of transport (Susalka and Pfister, 2000) and the expansion of the motor complement in eukaryotes (Vale, 2003) that presumably caters to the former. Hence, it was of interest to identify the number and nature of motors expressed in A431 that might potentially contribute to early endosome motility.

Motor genes annotated in the human genome (NCBI RsfSeq 28) along with accessory components required to form functional holo-motor complex (Pfister et al., 2006), (Rahman et al., 1999), (Yamazaki et al., 1996) and proteins with domains that may potentially be complex components such as (TCTEX domain containing proteins) (Lader et al., 1989) were all compiled, dubbed the "motorome" and was probed for expression at the level of messenger RNA in A431 cells.

Interesting in the expression profile of A431 cells is that of Axonamal Dynein components, both heavy an accessory, despite the lack of axonemes. This might reflect anomalous expression of genes given A431 cell line is of carcinoma origin (Herr et al., 2005) or the promiscuous use of axonemal components in intracellular transport (Vaisberg et al., 1996), alternatively, a case of regulation of transport of specific cargoes. A431 do not express the DYNC1I1 gene, which is known to be neuron specific (Nurminsky et al., 1998) and also DYNLT1 and DYNC1LI1, which were shown to be components of the Dynein complex involved in the transport of Golgi vesicles (Palmer et al., 2009). A431 cells also express DYN1LRB2 and DYNLL2 that are not expressed by several other cell lines such as Hela, HepG2, (human telomerase immortalized retinal pigment epithelial cells [hTERT-RPE1] and human dermal fibroblasts (Palmer et al., 2009), indicating

that the composition of molecular motors put together to transport cargoes may be tissue specific catering perhaps to the kinetic requisite at the site of expression.

Expression profiling of only the core components of the Dynactin complex that includes DCTN1-6 was performed. Arp1 and Arp11 were not included. Of the Dynactin components tested, DCTN1, DCTN2, DCTN3, DCTN4 are transcriptionally active while DCTN5 and DCTN6 are not expressed in A431 cells. This is very interesting since in mammals, the purified dynactin complex has been shown to composed of all 8 components, some incorporated in more than one copy number, however, the requirement for all components for a functional complex has been a matter of debate since the yeast genome is devoid of DCTN4, DCTN5 and DCTN6 indicating that in Yeasts at least, the Dynactin complex is functional as a smaller complex (Schroer, 2004). Expression analyses of Dynactin components in A431 cells indicate that the functional complex might be akin to that of yeasts.

A431 cells show an interesting expression pattern of Kinesins, in that, they do not express Kif3A, Kif3C and KifAP3. Kif3A, Kif3B and KifKAP3 are known to form a heterotrimeric functional complex (Yamazaki et al., 1995) that is involved in the transport of late endsomes (Brown et al., 2005) and golgi vesicles (Stauber et al., 2006). Also Kif3A/Kif3C have been shown to form functional motor complexes that associate with membrane bound vesicles in neurons (Muresan et al., 1998). Absence of transcripts Kif3A, Kif3C and KifAP3 indicates the use of alternative motors for the transport of these organelles. In addition, it has also been shown that Kif3B can produce motive force in the absence of Kif3A, which is an interesting possibility in vivo in A431 cells in the absence of all other associated proteins.

In addition to Dynein and Kinesins, A431 cells express a substantial number of Myosins, both conventional and unconventional. The former are muscle specific and it would be interesting to know if these are functional in endosome transport in a non-muscle cell line such as A431.

It should be noted that the multitude and nature of motors expressed in A431 cells represents a conservative figure and that the candidates tested negative for their expression may either be expressed in low messenger RNA copy numbers that is below the detection limit of semi-quantitative RT-PCR technique used, and/or that the genes may be alternatively spliced as is known for Dynein and Dynactin components (Nurminsky et al., 1998) and are not detected with primer probes used. Nevertheless, since A431 express 81% of the genome's motor complement, these cells presents an ideal model system to study both the motor repertoire that specifically

contribute to endosome motility and combinatorial protein inventories for functional holo-motor complexes.

4.4 RNAi screening

RNAi has become a powerful tool in exploring gene functions and in therapeutics, however, prevalent cross silencing and off targets set limitations in its use. Gene off-targets and cross silencing have become a major challenge in the field of RNAi biology. It is clear that with current mechanistic understanding of the process, off-targets cannot be eliminated. Therefore, it becomes critical to assess the extent of off-target contamination associated for interpretation of results emerging from RNAi exercises.

An important caveat with siRNA knock down studies is in having to define "on-target" phenotypes. Microarray analysis remains the existing method of detecting and estimating off-targets (Birmingham et al., 2006; van Dongen et al., 2008). However, arrays are rate limiting in terms of the scale of analysis. Also, distinguishing an off-target from on-target phenotype from microarray analysis is impossible. RNAi screens performed often use single siRNA probes (Kulkarni et al., 2006) and/or mono-parametric readouts, which are thwart by ambiguity in defining "on-target phenotypes".

This study was therefore performed to develop several concepts, all tending toward defining on-target phenotypes, assessing level of contamination by off-target effects and attempts toward maximizing specificity of gene silencing. Therefore, firstly, QIMPA was used to extract quantitative parameters from image-based screens and multi-parametric analysis was used to construct siRNA profiles. Second, use of multiple siRNAs for every target gene together with cross-correlation multi-parametric analysis of siRNA oligo profiles were used to define "on-target phenotypes" as those with consistent trends in deviation of phenotype from normalized mode profiles of the data set. Third, a methodology to specificity of RNAi knock down libraries was developed. Further, a technology triage of commercial RNAi technologies was performed. The Stealth technology from Invitrogen produced least off-targets. The choice of RNAi technology together with the use of multiple siRNAs (atleast 3) was shown to be a reasonable choice for screening exercises. The number of siRNAs required however depends on the number of genes contributing to the process under investigation and screening conditions. For technologies with specificities, increasing the number of siRNAs screened could potentially

offset high incidence of off-targets. Off-targets can increase if screening assay is sub-optimal, in terms of the concentration of siRNA used for transfection or assay time window.

Higher the concentration of siRNA (within the linear range), shorter the time required for development of phenotype. The results from the image based pilot screens have also been corroborated by Western blotting analysis of several candidate proteins where protein levels are inversely correlated with assay time (Collinet, unpublished results). However, for proteins with longer half-lives and stability, this approach is counter productive since longer the incubation time with reduced concentrations of siRNA allows for dilution of protein under conditions of transcription arrest.

Assay time window is dependent on the nature of proteins investigated. Some motor components such as Eg5, a mitotic kinesin was shown to have half-lives in the range of 12hrs (Liu et al., 2008) while DCTN1, Arp1 have been shown to have short half life with protein levels reduced to ~35% after 24hrs of siRNA transfection (Brown et al., 2005). Others such as cardiac myosin heavy chain are extremely stable with protein turn over rates of several days (Martin et al., 1977). In addition, association of accessory components may also enhance stability of motor proteins as is proposed for cardiac Myosin heavy chain (Martin et al., 1977). Knock down of DYNC1H1 was shown to lead to the degradation of DYNC1I2 and reduction to 50% protein of the DYNLIC chains (Palmer et al., 2009), due to reduced stability of motor complex. Given varying half-lives of proteins, for a given functional class of proteins, pilot screens serve as guidelines in establishing average protein turnover and assay time window.

Chemical modification of siRNA probes has been an important milestone in quelling gene cross silencing. 2'-O-methyl ribosyl substitution at position 2 of the guide strand decreased off-target cross silencing by 66% (Jackson et al., 2006) and also in mitigating IFN response (Hornung et al., 2005). All technologies tested here except for esiRNAs bear chemical modifications, yet their knock down specificities vary considerably, indicating that this factor alone is insufficient in limiting cross silencing. esiRNAs, despite their lack of chemical modifications have fairly good knock down specificities. esRNAs are pools of 19-22mers obtained by the enzymatic cleavage of target amplicons of ~400bps. The reduced incidence of off targets is presumably due to reduced specific concentration of and individual siRNA oligo within the pool that contributes toward off-targets (Kittler et al., 2007).

To conclude, from the above exercise, it is clear that the Invitrogen Stealth library offers an

advantage of reduced off-targets. However, given that off-targets is an inevitable problem of any RNAi technology, increasing the number of siRNA probes used and optimization of assay conditions in screening procedures would off set off-target contamination and increase confidence of phenotype identified.

5 Conclusions and future directions

This work has provided several interesting mechanistic insights into the distribution, organization and function of the early endocytic network. Analyzes of the motor screen has resulted in a preliminary list of molecular candidates involved in early endsosome transport. Correlation analyses of the phenotypes produced in the screen have indicated toward several potential multi-protein complexes of molecular motors that could regulate early endosome motility. Aside form the motor screen, several molecular candidates regulating saltatory dynamics have also been identified. The goal would be to integrate kinetic data with results from the motor screen to get a global view of the regulation of endosome motility *in vivo*.

The results presented in this thesis are preliminary, in that, the screen has provided a list of interesting molecular candidates and hypothesis. Therefore, the immediate objective would be in testing and validating the molecular candidates from the motor screen to confirm that they are bona fide motors of early endosomes. Validation of assembly of molecular motors into multi-protein complexes is also an impending objective since it would provide considerable insights into the regulatory aspect of early endosome motility in cells.

Identification of several motors for a single organelle evinces the complexity of intracellular transport and its regulation *in vivo*. It remains to be seen if all of the candidates that score in the motor screen are indeed involved in motility of early endosomes per se or if they perform mutually independent functions such as organelle tethering, vesicle scission, saltatory dynamics and other regulatory aspects of early endosome motility. Hence, the functional convergence of activities of several molecular motors would result in transport of early endosomes, coordinated with its function *in vivo*.

6 Materials and Methods

6.1 Compilation of Human motorome gene library

The genetic complement of molecular motors annotated in human genome which includes Dyneins (both Axonemal and cytoplasmic), Kinesins, Myosins, the Dynactin complex and accessory proteins that have been demonstrated to be part of some of the holo-motor complexes were dubbed the "motorome" and compiled in three steps -

First, a representative motor domain of each family of molecular motors i.e, Kinesin, Dynein and Myosin was blasted (BLASTP, e-value cut off 1e-4) against the human proteome database (NCBI nr database). Next, the output was compared with the domain database profiles (Pfam) through HMMer searches (HMMER 2.3.2) to verify the presence of a conserved motor domain. Finally, the resulting sequences were cross-compared with the Reference Sequences (NCBI RefSeq Release 28) to eliminate redundant candidates or those without supporting evidence for their expression or annotation in the database.

The motorome consisting of a non-redundant ensemble of 128 motor genes, which included 11 DYNAH, 2 DYNCH, 44 Kinesin and 39 Myosin motor proteins along with accessory sub-units of the Dynein complex (5 Axonemal and 16 Cytoplasmic), 6 Dynactin components and 5 Kinesin Related Proteins (KRPs) was assembled.

6.2 Cell Culture and cell line maintenance

A431 cells were cultured in DMEM high Glucose (4.5g/l) (PAA Laboratories, GmbH), supplemented with10% FCS (Gibco) and antibiotics 100units/ml Pen, 100µg/ml Strep-Pen Sterp, Gibco) at 37°C with 5%CO_2. A431GFP-Rab5 cells were cultured under similar conditions as A431lines, however, they were additionally supplemented with G418 (0.6mg/ml).

6.3 Semi-quantitative RT-PCR

Semi-quantitative RT-PCR was performed for genes in the motorome library. A431 cells cultured in 3.5cm dish were seeded at cell numbers corresponding to that used in the motor screen. 48hrs post seeding, the cells were serum starve for 24hrs and processed. cells were lysed,

and total RNA prepared as per protocol provided with RNeasy Kit (Qiagen). 1ug of total RNA (measured using the nanodrop spectrophotometer) was used per reaction to reverse transcribe into cDNA (SuperScript III First Strand Synthesis System for RT-PCR, Invitrogen). PCR reactions were performed with Taq polymerase in 96 well format plates with 2 exon- primers specific per gene. Positive control for primer efficiency was the MegaMan™ Human Transcriptome Library from Stratagene. Negative control was the reaction without the RT enzyme and assay control was the reaction with nuclease free water instead of RNA.

RT-PCR primers were designed with the Autoprime program (© Gunnar Wrobel & Felix Kokocinski, DKFZ , 2003 – 2009) to amplify amplicons of 100-200bps, to be specifically exon – spanning and to the most ubiquitous transcript isoform represented in the search output of the program. List of primers used can be found in the Appendix.

Touch-down PCR was performed to detect amplicons. Conditions for cycling are follows –

Initial Denaturing - 94°C – 5mins, subsequent denaturing - 94°C for 30secs, Tm - 68°C-55°C for 30secs with 2°C decrease in Tm per cycle, Elongation - 72°C for 30secs. Tm for amplification - 60°C for 30secs, Final extension - 72°C for 10mins. Amplification was done for 30 cycles.

6.4 Human LDL isolation from serum

LDL was isolated from human plasma according to protocol from (Vieira et al., 1996). Briefly, frozen human plasma (Red Cross blood bank) was thawed at 37°C. 0.22 g of KBr/ml of serum was dissolved in the serum, transferred to a Ti45 ultra-centrifuge tube, over-layered with de-gassed LDL-PBS (25 mM Na-phosphate buffer, pH 7.4, 110mM NaCl, 1 mM EDTA), filling the tubes completely and centrifuged at 40 000 rpm for 5 h at 15°C. LDL resolved as a light-scattering band about 1 cm above the yellow bottom fraction and was aspirated and dialyzed in 10,000MW CO dialysis cassette (Pierce) for 12hrs against PBS containing 1X antioxidant cocktail (88mg Ascorbic acid + 0.1MEDTA, pH8.0 +0.4M NaOH), exchange buffer and dialyze for an additional 12hrs. LDL was collected, supplemented with 5 mM ascorbic acid and 10% (W/V) sucrose, aliquoted and snap-frozen in liquid nitrogen. Aliquots were stored at -80°C.

6.5 LDL degradation assay

A431 cells (transfected with siRNA or not) were cultured for 48hrs in complete medium, serum starved for 24hrs in starvation medium (DMEM+antibiotics+0.3% FCS). Serum starved cells were pulsed/co-pulsed with LDL conjugated to fluorophore (Alexa488 or DiD) in starvation medium for 10mins. Both LDL-fluorophore species were used at dilutions of 1 in 50. Cargo containing medium was aspirated at the end of pulse and chased in fresh cargo free starvation medium for 60' (for the motor screen) or indicated time intervals (for kinetic experiments). All pulse and chase incubations were performed at 37°C. Cells were fixed with 4% PFA (Electron Microscopy Sciences) at the end of the assay and immunostained for EEA1. Fuorophore containing cell medium was filtered through 0.22 μm PVDF filter (MILLEX-GV) to remove aggregates to LDL conjugates prior to pulsing cells.

6.6 siRNA transfection

Pilots and motor screen were performed in 96 well plates (Greiner®). Reverse transfection protocol was to transfect siRNA. 5nM of siRNA (Invitrogen motor screen), or 15ng/well of esiRNA was incubated with 0.6ul INTERFERin (PolyPLUS) in 50μl of Opi-MEM (Invitrogen) for 10mins. A431 cells trypsinized, and seeded at density of 2000cells/well in 125μl of culture medium. Cells were overlaid with transfection mix and incubated for 48hrs under culture conditions. Cells were serum starved in culture medium containing 0.3%FCS for 24hrs before LDL degradation assay was performed.

6.7 EEA1 and Lamp1 Immunostaining for motor screen and LDL kinetics

Cells fixed in PFA were permeabilized with permeabilization buffer for 5mins, and incubated with EEA1antibody (rabbit polyclonal lab antibody, clone 077F, 5th bleed, 1:500 dilution) or Lamp1 antibody (mouse monoclonal, BD Parmingen, 1:500 dilution), in dilution buffer for 30mins. Cells were washed with PBS for 5mins, thrice and incubated with fluorophore conjugated secondary antibody (1:500) diluted in dilution buffer along with DAPI (500ng/ml) for 30mins. Cells were washed in PBS for 5mins thrice, rinsed with water and incubated for 30mins with 1μM SYTO 42 (Invitrogen Molecular Probes), following which the plates were stored in water containing 0.03% Sodium Azide until imaged.

Permeabilization buffer - 0.2%V/V saponin + 5%W/V BSA in PBS

Dilution buffer – 0.01%V/V saponin + 5%W/V BSA in PBS

Primary and secondary antibodies were filtered through 0.22 μm PVDF filter (MILLEX-GV) to remove aggregates prior to incubation with cells.

All secondary antibodies used were from Invitrogen Molecular probes.

6.8 Live-cell Kinesin screen

Live – cell Kinesin screen and all other Live cell experiments were performed in A431GFP-Rab5 cell line seeded in 3.5mm non-coated MatTek Glass bottom dishes (*Mat Tek* Corporation). Cells were imaged on the single photon Zeiss LSM 510 confocal microscope with a 40X, 1.3NA, scanning area of 500×200 pixels, single section of 3.0μm thickness at scan speeds of 13, delivering a frame rate of 10.4frs/sec. Movies were streamed using bi-directional scanning as 12bit movies. The pixel resolution under these conditions was 0.12μm. The objective was heated to 37°C using a n objective color and cells were imaged in CO_2 independent medium (Gibco) containing 10%FCS in Bachhoffer chamber heated to 37°C.

6.9 Particle Tracking

The track assignment algorithm was developed as generalization of the Hungarian algorithm, essentially overcoming the use greedy algorithm for score calculation. Four consecutive image frames were assigned in our case and track breaks were also incorporated as assignment possibility to account for the dynamic appearance and disappearance of particles in the image sequences. Track assignments were made on basis of the weighted sum of scores for position, speed, cross-sectional area, maximum intensity, and total particle fluorescence and termination penalty. The score was calculated by

$$S = 1 - \frac{2\sqrt{V_1 - V_2}}{V_1 - V_2}$$

according to (Verestoy et al., 1999). The score value of the termination penalty and the relative weights of other scores were chosen *ad hoc* by comparing the results of automated and manual tracking.

6.10 Image acquisition for motor screen

Images were acquired as 4-colored high resolution (0.151 pixel size) confocal sections of 0.3. Critical to the screen were colocalization and intensity parameters of markers used in the assay. However, the microscope used suffered from chromatic offsets between imaging channels owing to skews in detection system (cameras) and uneven laser illumination in the view field. Chromatic offset artifacts were corrected for using multicolored beads of 2.5um immobilized in the Opera Adjustment Plate provided by Evotech. 10 fields with approximately 50 beads were acquired. B-spline non-linear chromatic corrections performed to align the beads was saved as correction files and applied to images acquired. Uneven illumination was corrected for with fluorescent dyes imaged and the intensity across the filed made uniform using non-linear B spline corrections. Images were then processed by QMPIA.

6.11 Quantitative Multi-Parametric Image Analysis (QMPIA)

QMPIA was implemented to extract quantitative parameters associated with objects identified in images using MotionTracking software. It involves object search and identification, followed by extracting quantitative parameters, both morphometric and distribution associated with objects found.

Object search was performed to identify fluorescently labeled structures in acquired images by fitting their intensity to a sum of powered Lorenzian functions, the coefficients of which describe morphometric properties of individual endosomes (Rink et al., 2005). Fitting single vesicles by the sum of base functions (i.e. point spread function of the microscope and its approximation by computationally tractable formulae) overcomes limits of "sub-resolution" object size and allows for the description of "pleomorphic" objects. Given that images were acquired as 4 channels, vesicle search would have been computationally rate limiting in data processing. To circumvent this limitation, a Pluk-based automated task distribution system[i] was used to share calculation in the heterogeneous computer environment, which includes Windows based PCs (31 CPUs), Linux-based in-house cluster (60 CPUs) and PC-Farm computer of High Performance Computing department of Technical University of Dresden (2500 CPUs) (Kalaidzidis Y. 19970). This scaled up the performance of task distribution almost linearly up to 1000 CPUs allowing image processing to be at par with acquisition.

For objects identified (endosomes), distributions of the parameters were drawn and mean values of these distributions were extracted. Since most distributions were non-Gaussian by nature, mean values were often insufficient to define phenotypes, hence, weighting of distributions were introduced - two additional mean values were considered: one weighted by the total fluorescence (integral intensity) of the endosomes and the other weighted by their density (mean intensity). Mean values were considered for all distributions to consider tails of distributions and outlier phenotypes.

The number and size of cells in imaging field influence parameters such as the number of endosomes and total fluorescence associated with endosomes. Hence, these parameters were normalized to the image area (cell mask) stained by cytosolic marker SYTO 42 to reveal cell contours. Cell mask is proportional to both number and size of the cells. Further, parameters measuring distance between endosomes and nucleus were normalized to nuclear radius and by extension, cell size.

Endosome clustering was assessed using three parameters (Fig 1) calculated from endosome peer-to-peer distance distribution, a distribution of the probability of finding another endosome in the unit area for a given distance from a given endosome. From this distribution 3 parameters were calculated:

1) Position of the maximum (corresponding to the most probable distance between endosomes in a cluster; indicated as Param.0

2) Integral of the part of the distribution above the uniform probability distribution level (proportional to the number of endosomes being part of the cluster, indicated as Param.1and

3) Peer-to-peer distance where the distribution crosses the uniform distribution level, corresponding to the size of cluster, Param.2

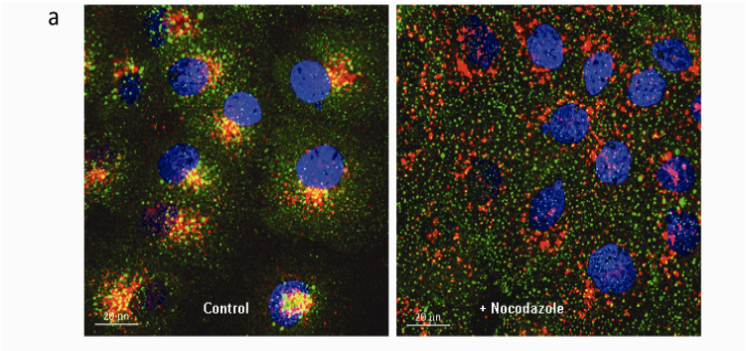

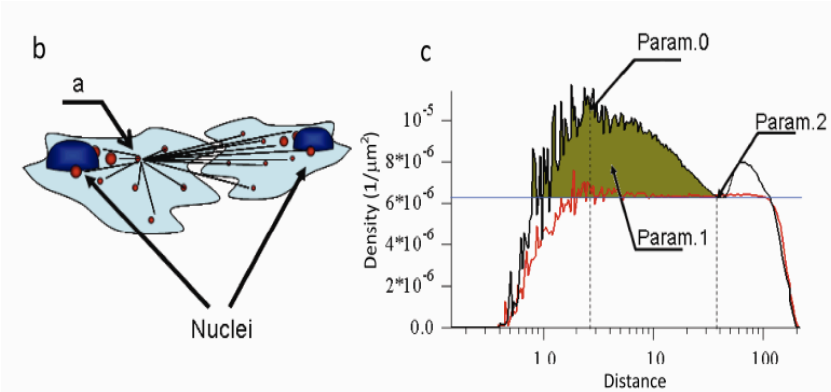

Fig 1: Endosome peer-to-peer distribution.
*Distribution of relative endosome density as a function of the distance of any given endosome from all others averaged over all endosomes. (**a**) Endosome subcellular distribution in A431 cells. Nuclei are stained with DAPI (blue), EEA1 (green), LDL pulsed for 10mins, chased for 40mins (red). (**b**) Illustration of the peer-to-peer distance distribution for a marked endosome "a". The total distribution is the average over all endosome distributions. (**c**) Peer-to-peer distribution in control condition (black); peer-to-peer distribution after treatment of the cells with nocodazole, a microtubule depolymerising agent that redistributes endosomes randomly, (red) and theoretical uniform distribution (blue). Param. 0 is the distribution peak position, Param. 1 the integral of the area above the uniform distribution (area in brown), Param. 2 is the distance to the point where the distribution crosses the uniform distribution level. The second (right) peak corresponds to endosomes, which belong to different cells. peer-to-peer distance distribution of the nocodazole treatment shows uniform distribution, demonstrating accuracy of measuring endosomes clustering.*

Colocalization between endocytic markers is the simultaneous presence of the two markers in a given pixel and in the case of this assay reflects the endocytic compartment that LDL is transiting

Colocalization is the fraction of total amount of each cargo resident in given structure. Calculated colocalization can result by chance as well. This apparent colocalization is corrected by randomly permutating objects maintaining the local density distribution and computing colocalization. The process is iterated 5 times, averaged, and the resulting colocalization value is subtracted from that calculated for acquired images.

$$C_{corrected} = \frac{C_{measured} - C_{random}}{1 - C_{random}}$$

6.12 Image processing

After QMPIA, image processing was performed to exclude empty files, images with less than 5 and more than 65 cells (nuclei) and out of focus images (using calculated nuclei contrast parameter). For all endosome related parameters, two rounds of normalizations were performed. The first round of normalization eliminates plate-to-plate variability by normalizing to "mock" (i.e. treated with the transfection reagent but no siRNA/esiRNAs) included in each plate Z-scores were calculated for each parameter relative to the MOCK control condition as follows -

$$z_i = \frac{p_i - \langle p_{MOCK} \rangle}{SD_{MOCK}}$$

where P_i is a parameter i, *P MOCK* is the mean of each parameter in MOCK-treated wells and *SD MOCK* the standard deviation for each parameter in MOCK-treated wells calculated per plate.

The second round of normalization was performed to score genes based on deviations from base-line. The latter is however ambiguous in the data-set in the absence of a "true" negative control since every condition, untransfected, mock or any scrambled control gives a phenotype. Hence, the base-line is set by normalizing over the entire data set as follows –

$$\tilde{z}_i = \frac{z_i - \mathrm{mode}(\{z_i\})}{mean(SD_{z_i:equal\_condition})}$$

Where *(SD equal _ condition)* is the mean of SD of each parameter *i* (averaged over all wells), i.e. the SD of the noise of the experimental measurements. Hence, the mode is set to 0 with variance equal to unity. Phenotype amplitudes of ±2 (2SDs) are significant. With all normalized parameters, Pearson correlation (assay reproducibility) was computed and those over 0.3 were considered stable and used to construct phenotypic profile of every image, which were 86 parameters. Phenotypic profiles of images belonging to the same biological conditions (i.e. the same si/esiRNA) were combined by distribution-mode searching procedures (Sivia D.S., 1996) for siRNA oligo profiles.

6.13 Estimating reproducibility and stability of parameters and assay robustness ($C_{p\text{-}R}$)

The Pearson correlation coefficient between runs ($C_{P\text{-}R}$) is calculated as follows -

Let the measured phenotype $\chi_{i,j}$ of each parameter (i) for given RNAi in the *j*-th run consist of two components such that $\chi_{i,j} = \eta_i + \varepsilon_{i,j}$, where η_i - phenotype response produced by given siRNA, $\varepsilon_{i.j}$ - noise of measurement and biological variability of assay in the *j*-th run. Then Pearson correlation between two runs for each parameter i is:

To compute the Pearson correlation between runs, the measured phenotype $\chi_{i,j}$ of each parameter (i) of assay in the *j*-th biological replicate for given RNAi consists of two components such that $\chi_{i,j} = \eta_i + \varepsilon_{i,j}$ where η_i - phenotype response on given RNAi, $\varepsilon_{i.j}$ - noise of measurement and biological variability of assay in the *j*-th run. Then Pearson correlation between two runs for each parameter i is

$$c_i = \frac{\langle \chi_{i,1} \cdot \chi_{i,2} \rangle}{\sqrt{\langle \chi_{i,1}^2 \rangle \langle \chi_{i,2}^2 \rangle}}$$

where, 1 or 2 are biological replicates.

Given that noise is independent between biological replicates, mean of noise value is $E(\varepsilon) = 0$ and variance of noise is, $D(\varepsilon_i) = \sigma_i^2$ then

$$c_i = \frac{\langle \eta_i^2 \rangle}{\langle \eta_i^2 \rangle + \sigma_i^2} = \frac{SNR_i^2}{SNR_i^2 + 1}$$

where $SNR_i = \sqrt{\frac{\langle \eta_i^2 \rangle}{\sigma_i^2}}$ is the "signal-to-noise" ratio for parameter *i*.

Pearson correlation coefficient between runs therefore is a measure of the robustness of assay to noise in measurement.

6.14 Estimating Q

Q (quality or specificity of a library) is the ratio of Pearson correlation between siRNA oligo to that between runs. Q is estimated based on the fact that a phenotype produced by every single oligo is a composite of on-target, off-target and measurement noise components. Hence, every measured oligo phenotype χ_i can be expressed as $\chi_i = t_i + \xi_i + \varepsilon_i$, where t_i - "on-target" phenotype, ξ_i - off-target silencing and ε_i - noise of measurement and biological variability of assay. Assuming that off-target phenotypes are random and independent between different siRNA/esiRNA targeting the same gene,

Correlation between Oligos ($C_{p\text{-}O}$) is $C_{p-O} = \frac{\langle t_i^2 \rangle}{\langle t_i^2 \rangle + \langle \xi_i^2 \rangle + \langle \varepsilon_i^2 \rangle}$ and

Correlation between Runs ($C_{p\text{-}R}$) is

$$C_{p-R} = \frac{\langle t_i^2 \rangle + \langle \varepsilon_i^2 \rangle}{\langle t_i^2 \rangle + \langle \xi_i^2 \rangle + \langle \varepsilon_i^2 \rangle}$$

where $\langle t \rangle$ is the amplitude of on-target phenotype, $\langle \xi \rangle$ is the amplitude of off-target phenotype and $\langle \varepsilon_i \rangle$ is the amplitude of noise in measurement. ($C_{p\text{-}R}$) is dependent on measurement noise and assay robustness, ($C_{p\text{-}O}$) depends on both the measurement noise and off-target component. The ratio Q of the two, is

$$Q = \left\langle \frac{C_{p\_o}}{C_{r\_o}} \right\rangle = \frac{\langle t^2 \rangle}{\langle t^2 \rangle + \langle \xi^2 \rangle} \quad \text{or}$$

$$\frac{\langle t^2 \rangle}{\langle \xi^2 \rangle} = \frac{Q}{1-Q}$$

7 Publication during thesis work

Lissanu Deribe, Y., Wild, P., **Chandrashaker, A**., Curak, J., Schmidt, M.H.H., Kalaidzidis, Y., Milutinovic, N., Kratchmarova, I., Buerkle, L., Fetchko, M.J., *et al.* (2009). Regulation of Epidermal Growth Factor Receptor Trafficking by Lysine Deacetylase HDAC6. Science Signaling *2*, ra84-ra84.

8 References

Albrecht-Buehler, G. (1977). Daughter 3T3 cells. Are they mirror images of each other? J Cell Biol *72*, 595-603.

Alexopoulou, L., Holt, A.C., Medzhitov, R., and Flavell, R.A. (2001). Recognition of double-stranded RNA and activation of NF-kappaB by Toll-like receptor 3. Nature *413*, 732-738.

Ally, S., Larson, A.G., Barlan, K., Rice, S.E., and Gelfand, V.I. (2009). Opposite-polarity motors activate one another to trigger cargo transport in live cells. The Journal of Cell Biology *187*, 1071-1082.

Aschenbrenner, L., Naccache, S.N., and Hasson, T. (2004). Uncoated endocytic vesicles require the unconventional myosin, Myo6, for rapid transport through actin barriers. Mol Biol Cell *15*, 2253-2263.

Atkinson, S.J., Doberstein, S.K., and Pollard, T.D. (1992). Moving off the beaten track. Curr Biol *2*, 326-328.

Bananis, E., Murray, J.W., Stockert, R.J., Satir, P., and Wolkoff, A.W. (2003). Regulation of early endocytic vesicle motility and fission in a reconstituted system. J Cell Sci *116*, 2749-2761.

Bartel, D.P. (2004). MicroRNAs: genomics, biogenesis, mechanism, and function. Cell *116*, 281-297.

Behnia, R., and Munro, S. (2005). Organelle identity and the signposts for membrane traffic. Nature *438*, 597-604.

Berezuk, M.A., and Schroer, T.A. (2007). Dynactin Enhances the Processivity of Kinesin-2. Traffic *8*, 124-129.

Berg, J.S., Powell, B.C., and Cheney, R.E. (2001). A millennial myosin census. Mol Biol Cell *12*, 780-794.

Birmingham, A., Anderson, E.M., Reynolds, A., Ilsley-Tyree, D., Leake, D., Fedorov, Y., Baskerville, S., Maksimova, E., Robinson, K., Karpilow, J.*, et al.* (2006). 3' UTR seed matches, but not overall identity, are associated with RNAi off-targets. Nature Publishing Group *3*, 199-204.

Blangy, A., Arnaud, L., and Nigg, E.A. (1997). Phosphorylation by p34cdc2 protein kinase regulates binding of the kinesin-related motor HsEg5 to the dynactin subunit p150. J Biol Chem *272*, 19418-19424.

Block, M.R., Glick, B.S., Wilcox, C.A., Wieland, F.T., and Rothman, J.E. (1988). Purification of an N-ethylmaleimide-sensitive protein catalyzing vesicular transport. Proc Natl Acad Sci USA *85*, 7852-7856.

Bonnet, C., Boucher, D., Lazereg, S., Pedrotti, B., Islam, K., Denoulet, P., and Larcher, J.C. (2001). Differential binding regulation of microtubule-associated proteins MAP1A, MAP1B, and MAP2 by tubulin polyglutamylation. J Biol Chem *276*, 12839-12848.

Brady, S.T., Pfister, K.K., and Bloom, G.S. (1990). A monoclonal antibody against kinesin inhibits both anterograde and retrograde fast axonal transport in squid axoplasm. Proc Natl Acad Sci USA *87*, 1061-1065.

Bretscher, M.S. (1982). Surface uptake by fibroblasts and its consequences. Cold Spring Harb Symp Quant Biol *46 Pt 2*, 707-712.

Bright, N.A., Gratian, M.J., and Luzio, J.P. (2005). Endocytic delivery to lysosomes mediated by concurrent fusion and kissing events in living cells. Curr Biol *15*, 360-365.

Broadie, K., Prokop, A., Bellen, H.J., O'Kane, C.J., Schulze, K.L., and Sweeney, S.T. (1995). Syntaxin and synaptobrevin function downstream of vesicle docking in Drosophila. Neuron *15*, 663-673.

Brown, C.L., Maier, K.C., Stauber, T., Ginkel, L.M., Wordeman, L., Vernos, I., and Schroer, T.A. (2005). Kinesin-2 is a Motor for Late Endosomes and Lysosomes. Traffic *6*, 1114-1124.

Brown, M.S., and Goldstein, J.L. (1975). Regulation of the activity of the low density lipoprotein receptor in human fibroblasts. Cell *6*, 307-316.

Buss, F., Arden, S.D., Lindsay, M., Luzio, J.P., and Kendrick-Jones, J. (2001). Myosin VI isoform localized to clathrin-coated vesicles with a role in clathrin-mediated endocytosis. The EMBO Journal *20*, 3676-3684.

Cai, D., McEwen, D.P., Martens, J.R., Meyhofer, E., and Verhey, K.J. (2009). Single molecule imaging reveals differences in microtubule track selection between Kinesin motors. PLoS Biol *7*, e1000216.

Cai, H., Reinisch, K., and Ferro-Novick, S. (2007). Coats, tethers, Rabs, and SNAREs work together to mediate the intracellular destination of a transport vesicle. Developmental Cell *12*, 671-682.

Carlton, J.G., and Cullen, P.J. (2005). Coincidence detection in phosphoinositide signaling. Trends Cell Biol *15*, 540-547.

Casey, J.R., Grinstein, S., and Orlowski, J. (2010). Sensors and regulators of intracellular pH. Nat Rev Mol Cell Biol *11*, 50-61.

Chavrier, P., Parton, R.G., Hauri, H.P., Simons, K., and Zerial, M. (1990). Localization of low molecular weight GTP binding proteins to exocytic and endocytic compartments. Cell *62*, 317-329.

Chibalina, M.V., Seaman, M.N.J., Miller, C.C., Kendrick-Jones, J., and Buss, F. (2007). Myosin VI and its interacting protein LMTK2 regulate tubule formation and transport to the endocytic recycling compartment. J Cell Sci *120*, 4278-4288.

Christoforidis, S., McBride, H.M., Burgoyne, R.D., and Zerial, M. (1999a). The Rab5 effector EEA1 is a core component of endosome docking. Nature *397*, 621-625.

Christoforidis, S., Miaczynska, M., Ashman, K., Wilm, M., Zhao, L., Yip, S.C., Waterfield, M.D., Backer, J.M., and Zerial, M. (1999b). Phosphatidylinositol-3-OH kinases are Rab5 effectors. Nat Cell Biol *1*, 249-252.

Christoforidis, S., and Zerial, M. (2000). Purification and identification of novel Rab effectors using affinity chromatography. Methods *20*, 403-410.

Collinet, C., Stöter, M., Bradshaw, C.R., Samusik, N., Rink, J.C., Kenski, D., Habermann, B., Buchholz, F., Henschel, R., Mueller, M.S.*, et al.* (2010). Systems survey of endocytosis by multiparametric image analysis. Nature, 1-8.

Conti, M.A., and Adelstein, R.S. (2008). Nonmuscle myosin II moves in new directions. J Cell Sci *121*, 11-18.

Coy, D.L., Hancock, W.O., Wagenbach, M., and Howard, J. (1999). Kinesin's tail domain is an inhibitory regulator of the motor domain. Nat Cell Biol *1*, 288-292.

de Renzis, S., Sönnichsen, B., and Zerial, M. (2002). Divalent Rab effectors regulate the sub-compartmental organization and sorting of early endosomes. Nat Cell Biol *4*, 124-133.

Deacon, S.W., Serpinskaya, A.S., Vaughan, P.S., Lopez Fanarraga, M., Vernos, I., Vaughan, K.T., and Gelfand, V.I. (2003). Dynactin is required for bidirectional organelle transport. The Journal of Cell Biology *160*, 297-301.

DeBoer, S.R., You, Y., Szodorai, A., Kaminska, A., Pigino, G., Nwabuisi, E., Wang, B., Estrada-Hernandez, T., Kins, S., Brady, S.T.*, et al.* (2008). Conventional kinesin holoenzymes are composed of heavy and light chain homodimers. Biochemistry *47*, 4535-4543.

Del Conte-Zerial, P., Brusch, L., Rink, J.C., Collinet, C., Kalaidzidis, Y., Zerial, M., and Deutsch, A. (2008). Membrane identity and GTPase cascades regulated by toggle and cut-out switches. Mol Syst Biol *4*, 206.

Delanoue, R., and Davis, I. (2005). Dynein anchors its mRNA cargo after apical transport in the Drosophila blastoderm embryo. Cell *122*, 97-106.

Dixit, R., Ross, J.L., Goldman, Y.E., and Holzbaur, E.L.F. (2008). Differential regulation of dynein and kinesin motor proteins by tau. Science *319*, 1086-1089.

Doherty, G.J., and McMahon, H.T. (2009). Mechanisms of endocytosis. Annu Rev Biochem *78*, 857-902.

Driskell, O.J., Mironov, A., Allan, V.J., and Woodman, P.G. (2007). Dynein is required for receptor sorting and the morphogenesis of early endosomes. Nat Cell Biol *9*, 113-120.

Du, Y., English, C.A., and Ohi, R. (2010). The Kinesin-8 Kif18A Dampens Microtubule Plus-End Dynamics. Current Biology *20*, 374-380.

Dunn, K.W., McGraw, T.E., and Maxfield, F.R. (1989). Iterative fractionation of recycling receptors from lysosomally destined ligands in an early sorting endosome. The Journal of Cell Biology *109*, 3303-3314.

Dunn, S., Morrison, E.E., Liverpool, T.B., Molina-Paris, C., Cross, R.A., Alonso, M.C., and Peckham, M. (2008). Differential trafficking of Kif5c on tyrosinated and detyrosinated microtubules in live cells. J Cell Sci *121*, 1085-1095.

Durrbach, A., Louvard, D., and Coudrier, E. (1996). Actin filaments facilitate two steps of endocytosis. J Cell Sci *109 (Pt 2)*, 457-465.

Echard, A., Jollivet, F., Martinez, O., Lacapère, J.J., Rousselet, A., Janoueix-Lerosey, I., and Goud, B. (1998). Interaction of a Golgi-associated kinesin-like protein with Rab6. Science *279*, 580-585.

Echeverri, C.J., Paschal, B.M., Vaughan, K.T., and Vallee, R.B. (1996). Molecular characterization of the 50-kD subunit of dynactin reveals function for the complex in chromosome alignment and spindle organization during mitosis. The Journal of Cell Biology *132*, 617-633.

Ecker, J.R., and Davis, R.W. (1986). Inhibition of gene expression in plant cells by expression of antisense RNA. Proc Natl Acad Sci USA *83*, 5372-5376.

Elbashir, S.M., Harborth, J., Lendeckel, W., Yalcin, A., Weber, K., and Tuschl, T. (2001). Duplexes of 21-nucleotide RNAs mediate RNA interference in cultured mammalian cells. Nature *411*, 494-498.

Even-Ram, S., Doyle, A.D., Conti, M.A., Matsumoto, K., Adelstein, R.S., and Yamada, K.M. (2007). Myosin IIA regulates cell motility and actomyosin-microtubule crosstalk. Nat Cell Biol *9*, 299-309.

Fasshauer, D., Antonin, W., Subramaniam, V., and Jahn, R. (2002). SNARE assembly and disassembly exhibit a pronounced hysteresis. Nat Struct Biol *9*, 144-151.

Fedorov, Y., King, A., Anderson, E., Karpilow, J., Ilsley, D., Marshall, W., and Khvorova, A. (2005). Different delivery methods-different expression profiles. Nature Publishing Group *2*, 241.

Fire, A., Xu, S., Montgomery, M.K., Kostas, S.A., Driver, S.E., and Mello, C.C. (1998). Potent and specific genetic interference by double-stranded RNA in Caenorhabditis elegans. Nature *391*, 806-811.

Garzon, R., Calin, G.A., and Croce, C.M. (2009). MicroRNAs in Cancer. Annu Rev Med *60*, 167-179.

Gasman, S., Kalaidzidis, Y., and Zerial, M. (2003). RhoD regulates endosome dynamics through Diaphanous-related Formin and Src tyrosine kinase. Nat Cell Biol *5*, 195-204.

Gill, S.R., Schroer, T.A., Szilak, I., Steuer, E.R., Sheetz, M.P., and Cleveland, D.W. (1991). Dynactin, a conserved, ubiquitously expressed component of an activator of vesicle motility mediated by cytoplasmic dynein. The Journal of Cell Biology *115*, 1639-1650.

Gould, G.W., and Lippincott-Schwartz, J. (2009). New roles for endosomes: from vesicular carriers to multi-purpose platforms. Nat Rev Mol Cell Biol *10*, 287-292.

Grimm, D., Streetz, K.L., Jopling, C.L., Storm, T.A., Pandey, K., Davis, C.R., Marion, P., Salazar, F., and Kay, M.A. (2006). Fatality in mice due to oversaturation of cellular microRNA/short hairpin RNA pathways. Nature *441*, 537-541.

Gross, S.P. (2004). Hither and yon: a review of bi-directional microtubule-based transport. Phys Biol *1*, R1-11.

Gruenberg, J. (2001). The endocytic pathway: a mosaic of domains. Nat Rev Mol Cell Biol *2*, 721-730.

Gruenberg, J. (2009). Viruses and endosome membrane dynamics. Current Opinion in Cell Biology *21*, 582-588.

Gruenberg, J., Griffiths, G., and Howell, K.E. (1989). Characterization of the early endosome and putative endocytic carrier vesicles in vivo and with an assay of vesicle fusion in vitro. The Journal of Cell Biology *108*, 1301-1316.

Gupta, V., Palmer, K.J., Spence, P., Hudson, A., and Stephens, D.J. (2008). Kinesin-1 (uKHC/KIF5B) is Required for Bidirectional Motility of ER Exit Sites and Efficient ER-to-Golgi Transport. Traffic *9*, 1850-1866.

Habermann, A., Schroer, T.A., Griffiths, G., and Burkhardt, J.K. (2001). Immunolocalization of cytoplasmic dynein and dynactin subunits in cultured macrophages: enrichment on early endocytic organelles. J Cell Sci *114*, 229-240.

Hammond, J.W., Cai, D., Blasius, T.L., Li, Z., Jiang, Y., Jih, G.T., Meyhofer, E., and Verhey, K.J. (2009). Mammalian Kinesin-3 motors are dimeric in vivo and move by processive motility upon release of autoinhibition. PLoS Biol *7*, e72.

Harada, A., Takei, Y., Kanai, Y., Tanaka, Y., Nonaka, S., and Hirokawa, N. (1998). Golgi vesiculation and lysosome dispersion in cells lacking cytoplasmic dynein. The Journal of Cell Biology *141*, 51-59.

Hawryluk, M.J., Keyel, P.A., Mishra, S.K., Watkins, S.C., Heuser, J.E., and Traub, L.M. (2006). Epsin 1 is a Polyubiquitin-Selective Clathrin-Associated Sorting Protein. Traffic *7*, 262-281.

Henningsen, U., and Schliwa, M. (1997). Reversal in the direction of movement of a molecular motor. Nature *389*, 93-96.

Herman, B., and Albertini, D.F. (1984). A time-lapse video image intensification analysis of cytoplasmic organelle movements during endosome translocation. The Journal of Cell Biology *98*, 565-576.

Herr, A., Grützmann, R., Matthaei, A., Artelt, J., Schröck, E., Rump, A., and Pilarsky, C. (2005). High-resolution analysis of chromosomal imbalances using the Affymetrix 10K SNP genotyping chip. Genomics *85*, 392-400.

Heuser, J. (1989). Changes in lysosome shape and distribution correlated with changes in cytoplasmic pH. The Journal of Cell Biology *108*, 855-864.

Hirokawa, N., Noda, Y., Tanaka, Y., and Niwa, S. (2009). Cytoskeletal motors: Kinesin superfamily motor proteins and intracellular transport. Nat Rev Mol Cell Biol *10*, 682-696.

Hoepfner, S., Severin, F., Cabezas, A., Habermann, B., Runge, A., Gillooly, D., Stenmark, H., and Zerial, M. (2005). Modulation of receptor recycling and degradation by the endosomal kinesin KIF16B. Cell *121*, 437-450.

Holleran, E.A., Ligon, L.A., Tokito, M., Stankewich, M.C., Morrow, J.S., and Holzbaur, E.L. (2001). beta III spectrin binds to the Arp1 subunit of dynactin. J Biol Chem *276*, 36598-36605.

Hornung, V., Guenthner-Biller, M., Bourquin, C., Ablasser, A., Schlee, M., Uematsu, S., Noronha, A., Manoharan, M., Akira, S., de Fougerolles, A.*, et al.* (2005). Sequence-specific potent induction of IFN-alpha by short interfering RNA in plasmacytoid dendritic cells through TLR7. Nat Med *11*, 263-270.

Howard, J., Hudspeth, A.J., and Vale, R.D. (1989). Movement of microtubules by single kinesin molecules. Nature *342*, 154-158.

Huang, J.D., Brady, S.T., Richards, B.W., Stenolen, D., Resau, J.H., Copeland, N.G., and Jenkins, N.A. (1999). Direct interaction of microtubule- and actin-based transport motors. Nature *397*, 267-270.

Jackson, A.L., Bartz, S.R., Schelter, J., Kobayashi, S.V., Burchard, J., Mao, M., Li, B., Cavet, G., and Linsley, P.S. (2003). Expression profiling reveals off-target gene regulation by RNAi. Nat Biotechnol *21*, 635-637.

Jackson, A.L., Burchard, J., Leake, D., Reynolds, A., Schelter, J., Guo, J., Johnson, J.M., Lim, L., Karpilow, J., Nichols, K.*, et al.* (2006). Position-specific chemical modification of siRNAs reduces "off-target" transcript silencing. RNA *12*, 1197-1205.

Jinek, M., and Doudna, J.A. (2009). A three-dimensional view of the molecular machinery of RNA interference. Nature *457*, 405-412.

Johnson, C.S., Buster, D., and Scholey, J.M. (1990). Light chains of sea urchin kinesin identified by immunoadsorption. Cell Motil Cytoskeleton *16*, 204-213.

Jonsdottir, G.A., and Li, R. (2004). Dynamics of yeast Myosin I: evidence for a possible role in scission of endocytic vesicles. Curr Biol *14*, 1604-1609.

Jordens, I., Fernandez-Borja, M., Marsman, M., Dusseljee, S., Janssen, L., Calafat, J., Janssen, H., Wubbolts, R., and Neefjes, J. (2001). The Rab7 effector protein RILP controls lysosomal transport by inducing the recruitment of dynein-dynactin motors. Curr Biol *11*, 1680-1685.

Kallen, C.B., Billheimer, J.T., Summers, S.A., Stayrook, S.E., Lewis, M., and Strauss, J.F. (1998). Steroidogenic acute regulatory protein (StAR) is a sterol transfer protein. J Biol Chem *273*, 26285-26288.

Kardon, J.R., Reck-Peterson, S.L., and Vale, R.D. (2009). Regulation of the processivity and intracellular localization of Saccharomyces cerevisiae dynein by dynactin. Proc Natl Acad Sci USA *106*, 5669-5674.

Karki, S., LaMonte, B., and Holzbaur, E.L. (1998). Characterization of the p22 subunit of dynactin reveals the localization of cytoplasmic dynein and dynactin to the midbody of dividing cells. The Journal of Cell Biology *142*, 1023-1034.

Keen, J.H., Willingham, M.C., and Pastan, I.H. (1979). Clathrin-coated vesicles: isolation, dissociation and factor-dependent reassociation of clathrin baskets. Cell *16*, 303-312.

Kharchenko, M.V., Aksyonov, A.A., Melikova, M.M., and Kornilova, E.S. (2007). Epidermal growth factor (EGF) receptor endocytosis is accompanied by reorganization of microtubule system in HeLa cells. Cell Biol Int *31*, 349-359.

Khvorova, A., Reynolds, A., and Jayasena, S.D. (2003). Functional siRNAs and miRNAs exhibit strand bias. Cell *115*, 209-216.

Kimura, N., Imamura, O., Ono, F., and Terao, K. (2007). Aging attenuates dynactin-dynein interaction: down-regulation of dynein causes accumulation of endogenous tau and amyloid precursor protein in human neuroblastoma cells. J Neurosci Res *85*, 2909-2916.

Kimura, N., Inoue, M., Okabayashi, S., Ono, F., and Negishi, T. (2009). Dynein Dysfunction Induces Endocytic Pathology Accompanied by an Increase in Rab GTPases: A POTENTIAL MECHANISM UNDERLYING AGE-DEPENDENT ENDOCYTIC DYSFUNCTION. Journal of Biological Chemistry *284*, 31291-31302.

King, S.J., Bonilla, M., Rodgers, M.E., and Schroer, T.A. (2002). Subunit organization in cytoplasmic dynein subcomplexes. Protein Sci *11*, 1239-1250.

King, S.J., and Schroer, T.A. (2000). Dynactin increases the processivity of the cytoplasmic dynein motor. Nat Cell Biol *2*, 20-24.

Kini, A.R., and Collins, C.A. (2001). Modulation of cytoplasmic dynein ATPase activity by the accessory subunits. Cell Motil Cytoskeleton *48*, 52-60.

Kittler, R., Surendranath, V., Heninger, A.-K., Slabicki, M., Theis, M., Putz, G., Franke, K., Caldarelli, A., Grabner, H., Kozak, K., *et al.* (2007). Genome-wide resources of endoribonuclease-prepared short interfering RNAs for specific loss-of-function studies. Nature Publishing Group *4*, 337-344.

Kloepper, T.H., Kienle, C.N., and Fasshauer, D. (2007). An elaborate classification of SNARE proteins sheds light on the conservation of the eukaryotic endomembrane system. Mol Biol Cell *18*, 3463-3471.

Klopfenstein, D.R., Tomishige, M., Stuurman, N., and Vale, R.D. (2002). Role of phosphatidylinositol(4,5)bisphosphate organization in membrane transport by the Unc104 kinesin motor. Cell *109*, 347-358.

Kobayashi, T., Gu, F., and Gruenberg, J. (1998). Lipids, lipid domains and lipid-protein interactions in endocytic membrane traffic. Seminars in Cell and Developmental Biology *9*, 517-526.

Kojima, H., Muto, E., Higuchi, H., and Yanagida, T. (1997). Mechanics of single kinesin molecules measured by optical trapping nanometry. Biophysical Journal *73*, 2012-2022.

Konishi, Y., and Setou, M. (2009). Tubulin tyrosination navigates the kinesin-1 motor domain to axons. Nat Neurosci *12*, 559-567.

Korn, E.D. (2000). Coevolution of head, neck, and tail domains of myosin heavy chains. Proc Natl Acad Sci USA *97*, 12559-12564.

Kornfeld, S., and Mellman, I. (1989). The biogenesis of lysosomes. Annu Rev Cell Biol *5*, 483-525.

Krendel, M., Osterweil, E.K., and Mooseker, M.S. (2007). Myosin 1E interacts with synaptojanin-1 and dynamin and is involved in endocytosis. FEBS Letters *581*, 644-650.

Kulkarni, M.M., Booker, M., Silver, S.J., Friedman, A., Hong, P., Perrimon, N., and Mathey-Prevot, B. (2006). Evidence of off-target effects associated with long dsRNAs in Drosophila melanogaster cell-based assays. Nature Publishing Group *3*, 833-838.

Kull, F.J., Vale, R.D., and Fletterick, R.J. (1998). The case for a common ancestor: kinesin and myosin motor proteins and G proteins. J Muscle Res Cell Motil *19*, 877-886.

Lader, E., Ha, H.S., O'Neill, M., Artzt, K., and Bennett, D. (1989). tctex-1: a candidate gene family for a mouse t complex sterility locus. Cell *58*, 969-979.

Langford, G.M. (1995). Actin- and microtubule-dependent organelle motors: interrelationships between the two motility systems. Current Opinion in Cell Biology *7*, 82-88.

Lantz, V.A., and Miller, K.G. (1998). A class VI unconventional myosin is associated with a homologue of a microtubule-binding protein, cytoplasmic linker protein-170, in neurons and at the posterior pole of Drosophila embryos. The Journal of Cell Biology *140*, 897-910.

Lenz, J.H., Schuchardt, I., Straube, A., and Steinberg, G. (2006). A dynein loading zone for retrograde endosome motility at microtubule plus-ends. The EMBO Journal *25*, 2275-2286.

Levesque, A.A., and Compton, D.A. (2001). The chromokinesin Kid is necessary for chromosome arm orientation and oscillation, but not congression, on mitotic spindles. The Journal of Cell Biology *154*, 1135-1146.

Lewis, B.P., Shih, I.-h., Jones-Rhoades, M.W., Bartel, D.P., and Burge, C.B. (2003). Prediction of mammalian microRNA targets. Cell *115*, 787-798.

Lewis, T.L., Mao, T., Svoboda, K., and Arnold, D.B. (2009). Myosin-dependent targeting of transmembrane proteins to neuronal dendrites. Nat Neurosci *12*, 568-576.

Ligon, L.A., Tokito, M., Finklestein, J.M., Grossman, F.E., and Holzbaur, E.L.F. (2004). A direct interaction between cytoplasmic dynein and kinesin I may coordinate motor activity. J Biol Chem *279*, 19201-19208.

Lin, S.X., Gundersen, G.G., and Maxfield, F.R. (2002). Export from pericentriolar endocytic recycling compartment to cell surface depends on stable, detyrosinated (glu) microtubules and kinesin. Mol Biol Cell *13*, 96-109.

Lissanu Deribe, Y., Wild, P., Chandrashaker, A., Curak, J., Schmidt, M.H.H., Kalaidzidis, Y., Milutinovic, N., Kratchmarova, I., Buerkle, L., Fetchko, M.J., *et al.* (2009). Regulation of Epidermal Growth Factor Receptor Trafficking by Lysine Deacetylase HDAC6. Science Signaling *2*, ra84-ra84.

Liu, M., Aneja, R., Sun, X., Xie, S., Wang, H., Wu, X., Dong, J.-T., Li, M., Joshi, H.C., and Zhou, J. (2008). Parkin Regulates Eg5 Expression by Hsp70 Ubiquitination-dependent Inactivation of c-Jun NH2-terminal Kinase. Journal of Biological Chemistry *283*, 35783-35788.

Loubéry, S., Wilhelm, C., Hurbain, I., Neveu, S., Louvard, D., and Coudrier, E. (2008). Different microtubule motors move early and late endocytic compartments. Traffic *9*, 492-509.

Loyter, A., Citovsky, V., and Blumenthal, R. (1988). The use of fluorescence dequenching measurements to follow viral membrane fusion events. Methods Biochem Anal *33*, 129-164.

Mallik, R., Petrov, D., Lex, S.A., King, S.J., and Gross, S.P. (2005). Building complexity: an in vitro study of cytoplasmic dynein with in vivo implications. Curr Biol *15*, 2075-2085.

Malsam, J., Kreye, S., and Söllner, T.H. (2008). Membrane fusion: SNAREs and regulation. Cell Mol Life Sci *65*, 2814-2832.

Manna, T., Honnappa, S., Steinmetz, M.O., and Wilson, L. (2008). Suppression of microtubule dynamic instability by the +TIP protein EB1 and its modulation by the CAP-Gly domain of p150glued. Biochemistry *47*, 779-786.

Martin, A.F., Rabinowitz, M., Blough, R., Prior, G., and Zak, R. (1977). Measurements of half-life of rat cardiac myosin heavy chain with leucyl-tRNA used as precursor pool. J Biol Chem *252*, 3422-3429.

Maurer, M.E., and Cooper, J.A. (2006). The adaptor protein Dab2 sorts LDL receptors into coated pits independently of AP-2 and ARH. Journal of Cell Science *119*, 4235-4246.

Maxfield, F.R., and McGraw, T.E. (2004). Endocytic recycling. Nat Rev Mol Cell Biol *5*, 121-132.

Mayor, S., Presley, J.F., and Maxfield, F.R. (1993). Sorting of membrane components from endosomes and subsequent recycling to the cell surface occurs by a bulk flow process. The Journal of Cell Biology *121*, 1257-1269.

McMahon, H.T., and Gallop, J.L. (2005). Membrane curvature and mechanisms of dynamic cell membrane remodelling. Nature *438*, 590-596.

Melkonian, K.A., Maier, K.C., Godfrey, J.E., Rodgers, M., and Schroer, T.A. (2007). Mechanism of Dynamitin-mediated Disruption of Dynactin. Journal of Biological Chemistry *282*, 19355-19364.

Merrifield, C.J., Feldman, M.E., Wan, L., and Almers, W. (2002). Imaging actin and dynamin recruitment during invagination of single clathrin-coated pits. Nat Cell Biol *4*, 691-698.

Merrifield, C.J., Perrais, D., and Zenisek, D. (2005). Coupling between clathrin-coated-pit invagination, cortactin recruitment, and membrane scission observed in live cells. Cell *121*, 593-606.

Mettlen, M., Pucadyil, T., Ramachandran, R., and Schmid, S.L. (2009). Dissecting dynamin's role in clathrin-mediated endocytosis. Biochem Soc Trans *37*, 1022-1026.

Miaczynska, M., Christoforidis, S., Giner, A., Shevchenko, A., Uttenweiler-Joseph, S., Habermann, B., Wilm, M., Parton, R.G., and Zerial, M. (2004). APPL proteins link Rab5 to nuclear signal transduction via an endosomal compartment. Cell *116*, 445-456.

Morfini, G., Szebenyi, G., Elluru, R., Ratner, N., and Brady, S.T. (2002). Glycogen synthase kinase 3 phosphorylates kinesin light chains and negatively regulates kinesin-based motility. The EMBO Journal *21*, 281-293.

Morris, S.M., Arden, S.D., Roberts, R.C., Kendrick-Jones, J., Cooper, J.A., Luzio, J.P., and Buss, F. (2002). Myosin VI binds to and localises with Dab2, potentially linking receptor-mediated endocytosis and the actin cytoskeleton. Traffic *3*, 331-341.

Mullock, B.M., Bright, N.A., Fearon, C.W., Gray, S.R., and Luzio, J.P. (1998). Fusion of lysosomes with late endosomes produces a hybrid organelle of intermediate density and is NSF dependent. The Journal of Cell Biology *140*, 591-601.

Muresan, V., Abramson, T., Lyass, A., Winter, D., Porro, E., Hong, F., Chamberlin, N.L., and Schnapp, B.J. (1998). KIF3C and KIF3A form a novel neuronal heteromeric kinesin that associates with membrane vesicles. Mol Biol Cell *9*, 637-652.

Murray, J.W., and Wolkoff, A.W. (2003). Roles of the cytoskeleton and motor proteins in endocytic sorting. Adv Drug Deliv Rev *55*, 1385-1403.

Nakata, T., and Hirokawa, N. (1995). Point mutation of adenosine triphosphate-binding motif generated rigor kinesin that selectively blocks anterograde lysosome membrane transport. The Journal of Cell Biology *131*, 1039-1053.

Nath, S., Bananis, E., Sarkar, S., Stockert, R.J., Sperry, A.O., Murray, J.W., and Wolkoff, A.W. (2007). Kif5B and Kifc1 interact and are required for motility and fission of early endocytic vesicles in mouse liver. Mol Biol Cell *18*, 1839-1849.

Nielsen, E., Severin, F., Backer, J.M., Hyman, A.A., and Zerial, M. (1999). Rab5 regulates motility of early endosomes on microtubules. Nat Cell Biol *1*, 376-382.

Niwa, S., Tanaka, Y., and Hirokawa, N. (2008). KIF1Bbeta- and KIF1A-mediated axonal transport of presynaptic regulator Rab3 occurs in a GTP-dependent manner through DENN/MADD. Nat Cell Biol *10*, 1269-1279.

Nurminsky, D.I., Nurminskaya, M.V., Benevolenskaya, E.V., Shevelyov, Y.Y., Hartl, D.L., and Gvozdev, V.A. (1998). Cytoplasmic dynein intermediate-chain isoforms with different targeting properties created by tissue-specific alternative splicing. Mol Cell Biol *18*, 6816-6825.

O'Connell, C.B., Tyska, M.J., and Mooseker, M.S. (2007). Myosin at work: motor adaptations for a variety of cellular functions. Biochim Biophys Acta *1773*, 615-630.

Ohno, H., Stewart, J., Fournier, M.C., Bosshart, H., Rhee, I., Miyatake, S., Saito, T., Gallusser, A., Kirchhausen, T., and Bonifacino, J.S. (1995). Interaction of tyrosine-based sorting signals with clathrin-associated proteins. Science *269*, 1872-1875.

Ohya, T., Miaczynska, M., Coskun, U., Lommer, B., Runge, A., Drechsel, D., Kalaidzidis, Y., and Zerial, M. (2009). Reconstitution of Rab- and SNARE-dependent membrane fusion by synthetic endosomes. Nature *459*, 1091-1097.

Pal, A., Severin, F., Lommer, B., Shevchenko, A., and Zerial, M. (2006). Huntingtin-HAP40 complex is a novel Rab5 effector that regulates early endosome motility and is up-regulated in Huntington's disease. The Journal of Cell Biology *172*, 605-618.

Palmer, K.J., Hughes, H., and Stephens, D.J. (2009). Specificity of cytoplasmic dynein subunits in discrete membrane-trafficking steps. Mol Biol Cell *20*, 2885-2899.

Pangarkar, C., Dinh, A., and Mitragotri, S. (2005). Dynamics and Spatial Organization of Endosomes in Mammalian Cells. Phys Rev Lett *95*, 158101.

Pei, Y., and Tuschl, T. (2006). On the art of identifying effective and specific siRNAs. Nature Publishing Group *3*, 670-676.

Peris, L., Thery, M., Fauré, J., Saoudi, Y., Lafanechère, L., Chilton, J.K., Gordon-Weeks, P., Galjart, N., Bornens, M., Wordeman, L*., et al.* (2006). Tubulin tyrosination is a major factor affecting the recruitment of CAP-Gly proteins at microtubule plus ends. The Journal of Cell Biology *174*, 839-849.

Perrimon, N., and Mathey-Prevot, B. (2007). Applications of high-throughput RNA interference screens to problems in cell and developmental biology. Genetics *175*, 7-16.

Persengiev, S.P., Zhu, X., and Green, M.R. (2004). Nonspecific, concentration-dependent stimulation and repression of mammalian gene expression by small interfering RNAs (siRNAs). RNA *10*, 12-18.

Pfister, K.K., Shah, P.R., Hummerich, H., Russ, A., Cotton, J., Annuar, A.A., King, S.M., and Fisher, E.M.C. (2006). Genetic analysis of the cytoplasmic dynein subunit families. PLoS Genet *2*, e1.

Pierre, P., Scheel, J., Rickard, J.E., and Kreis, T.E. (1992). CLIP-170 links endocytic vesicles to microtubules. Cell *70*, 887-900.

Provance, D.W., Addison, E.J., Wood, P.R., Chen, D.Z., Silan, C.M., and Mercer, J.A. (2008). Myosin-Vb functions as a dynamic tether for peripheral endocytic compartments during transferrin trafficking. BMC Cell Biol *9*, 44.

Pucadyil, T.J., and Schmid, S.L. (2009). Conserved Functions of Membrane Active GTPases in Coated Vesicle Formation. Science *325*, 1217-1220.

Rahman, A., Kamal, A., Roberts, E.A., and Goldstein, L.S. (1999). Defective kinesin heavy chain behavior in mouse kinesin light chain mutants. The Journal of Cell Biology *146*, 1277-1288.

Reed, N.A., Cai, D., Blasius, T.L., Jih, G.T., Meyhofer, E., Gaertig, J., and Verhey, K.J. (2006). Microtubule acetylation promotes kinesin-1 binding and transport. Curr Biol *16*, 2166-2172.

Rink, J., Ghigo, E., Kalaidzidis, Y., and Zerial, M. (2005). Rab conversion as a mechanism of progression from early to late endosomes. Cell *122*, 735-749.

Rodionov, V.I., Hope, A.J., Svitkina, T.M., and Borisy, G.G. (1998). Functional coordination of microtubule-based and actin-based motility in melanophores. Curr Biol *8*, 165-168.

Romberg, L., and Vale, R.D. (1993). Chemomechanical cycle of kinesin differs from that of myosin. Nature *361*, 168-170.

Sakamoto, T., Wang, F., Schmitz, S., Xu, Y., Xu, Q., Molloy, J.E., Veigel, C., and Sellers, J.R. (2003). Neck length and processivity of myosin V. J Biol Chem *278*, 29201-29207.

Salisbury, J.L., Condeelis, J.S., and Satir, P. (1980). Role of coated vesicles, microfilaments, and calmodulin in receptor-mediated endocytosis by cultured B lymphoblastoid cells. The Journal of Cell Biology *87*, 132-141.

Sato-Yoshitake, R., Yorifuji, H., Inagaki, M., and Hirokawa, N. (1992). The phosphorylation of kinesin regulates its binding to synaptic vesicles. J Biol Chem *267*, 23930-23936.

Schafer, D.A., Gill, S.R., Cooper, J.A., Heuser, J.E., and Schroer, T.A. (1994). Ultrastructural analysis of the dynactin complex: an actin-related protein is a component of a filament that resembles F-actin. The Journal of Cell Biology *126*, 403-412.

Schenck, A., Goto-Silva, L., Collinet, C., Rhinn, M., Giner, A., Habermann, B., Brand, M., and Zerial, M. (2008). The endosomal protein Appl1 mediates Akt substrate specificity and cell survival in vertebrate development. Cell *133*, 486-497.

Schmid, E.M., Ford, M.G.J., Burtey, A., Praefcke, G.J.K., Peak-Chew, S.-Y., Mills, I.G., Benmerah, A., and McMahon, H.T. (2006). Role of the AP2 beta-appendage hub in recruiting partners for clathrin-coated vesicle assembly. PLoS Biol *4*, e262.

Schmid, S.L. (1997). Clathrin-coated vesicle formation and protein sorting: an integrated process. Annu Rev Biochem *66*, 511-548.

Schnitzer, M.J., Visscher, K., and Block, S.M. (2000). Force production by single kinesin motors. Nat Cell Biol *2*, 718-723.

Schroer, T.A. (2004). Dynactin. Annu Rev Cell Dev Biol *20*, 759-779.

Schroer, T.A., and Sheetz, M.P. (1991). Two activators of microtubule-based vesicle transport. The Journal of Cell Biology *115*, 1309-1318.

Schulze, E., and Kirschner, M. (1986). Microtubule dynamics in interphase cells. The Journal of Cell Biology *102*, 1020-1031.

Scita, G., and Di Fiore, P.P. (2010). The endocytic matrix. Nature *463*, 464-473.

Shiroguchi, K., Ohsugi, M., Edamatsu, M., Yamamoto, T., and Toyoshima, Y.Y. (2003). The second microtubule-binding site of monomeric kid enhances the microtubule affinity. J Biol Chem *278*, 22460-22465.

Short, B., Preisinger, C., Schaletzky, J., Kopajtich, R., and Barr, F.A. (2002). The Rab6 GTPase regulates recruitment of the dynactin complex to Golgi membranes. Curr Biol *12*, 1792-1795.

Söllner, T., Whiteheart, S.W., Brunner, M., Erdjument-Bromage, H., Geromanos, S., Tempst, P., and Rothman, J.E. (1993). SNAP receptors implicated in vesicle targeting and fusion. Nature *362*, 318-324.

Sönnichsen, B., De Renzis, S., Nielsen, E., Rietdorf, J., and Zerial, M. (2000). Distinct membrane domains on endosomes in the recycling pathway visualized by multicolor imaging of Rab4, Rab5, and Rab11. The Journal of Cell Biology *149*, 901-914.

Soppina, V., Rai, A.K., Ramaiya, A.J., Barak, P., and Mallik, R. (2009). Tug-of-war between dissimilar teams of microtubule motors regulates transport and fission of endosomes. Proc Natl Acad Sci USA *106*, 19381-19386.

Sorkin, A., and Von Zastrow, M. (2009). Endocytosis and signalling: intertwining molecular networks. Nat Rev Mol Cell Biol *10*, 609-622.

Spudich, G., Chibalina, M.V., Au, J.S.-Y., Arden, S.D., Buss, F., and Kendrick-Jones, J. (2007). Myosin VI targeting to clathrin-coated structures and dimerization is mediated by binding to Disabled-2 and PtdIns(4,5)P2. Nat Cell Biol *9*, 176-183.

Stagi, M., Gorlovoy, P., Larionov, S., Takahashi, K., and Neumann, H. (2006). Unloading kinesin transported cargoes from the tubulin track via the inflammatory c-Jun N-terminal kinase pathway. FASEB J *20*, 2573-2575.

Stauber, T., Simpson, J.C., Pepperkok, R., and Vernos, I. (2006). A role for kinesin-2 in COPI-dependent recycling between the ER and the Golgi complex. Curr Biol *16*, 2245-2251.

Steffen, W., Karki, S., Vaughan, K.T., Vallee, R.B., Holzbaur, E.L., Weiss, D.G., and Kuznetsov, S.A. (1997). The involvement of the intermediate chain of cytoplasmic dynein in binding the motor complex to membranous organelles of Xenopus oocytes. Mol Biol Cell *8*, 2077-2088.

Stenmark, H. (2009). Rab GTPases as coordinators of vesicle traffic. Nature Publishing Group *10*, 513-525.

Stocco, D.M. (2000). StARTing to understand cholesterol transfer. Nat Struct Biol *7*, 445-447.

Stoorvogel, W., Strous, G.J., Geuze, H.J., Oorschot, V., and Schwartz, A.L. (1991). Late endosomes derive from early endosomes by maturation. Cell *65*, 417-427.

Stowell, M.H., Marks, B., Wigge, P., and McMahon, H.T. (1999). Nucleotide-dependent conformational changes in dynamin: evidence for a mechanochemical molecular spring. Nat Cell Biol *1*, 27-32.

Sun, Y., Martin, A.C., and Drubin, D.G. (2006). Endocytic internalization in budding yeast requires coordinated actin nucleation and myosin motor activity. Developmental Cell *11*, 33-46.

Susalka, S.J., and Pfister, K.K. (2000). Cytoplasmic dynein subunit heterogeneity: implications for axonal transport. J Neurocytol *29*, 819-829.

Sztul, E., and Lupashin, V. (2006). Role of tethering factors in secretory membrane traffic. Am J Physiol, Cell Physiol *290*, C11-26.

Takamori, S., Holt, M., Stenius, K., Lemke, E.A., Grønborg, M., Riedel, D., Urlaub, H., Schenck, S., Brügger, B., Ringler, P.*, et al.* (2006). Molecular anatomy of a trafficking organelle. Cell *127*, 831-846.

Thorn, K.S., Ubersax, J.A., and Vale, R.D. (2000). Engineering the processive run length of the kinesin motor. The Journal of Cell Biology *151*, 1093-1100.

Tokai, N., Fujimoto-Nishiyama, A., Toyoshima, Y., Yonemura, S., Tsukita, S., Inoue, J., and Yamamota, T. (1996). Kid, a novel kinesin-like DNA binding protein, is localized to chromosomes and the mitotic spindle. The EMBO Journal *15*, 457-467.

Tschuch, C., Schulz, A., Pscherer, A., Werft, W., Benner, A., Hotz-Wagenblatt, A., Barrionuevo, L., Lichter, P., and Mertens, D. (2008). Off-target effects of siRNA specific for GFP. BMC Mol Biol *9*, 60.

Tsui, M.M., and Banfield, D.K. (2000). Yeast Golgi SNARE interactions are promiscuous. J Cell Sci *113 (Pt 1)*, 145-152.

Tynan, S.H., Purohit, A., Doxsey, S.J., and Vallee, R.B. (2000). Light intermediate chain 1 defines a functional subfraction of cytoplasmic dynein which binds to pericentrin. J Biol Chem *275*, 32763-32768.

Uchida, A., Alami, N.H., and Brown, A. (2009). Tight functional coupling of kinesin-1A and dynein motors in the bidirectional transport of neurofilaments. Mol Biol Cell *20*, 4997-5006.

Ullrich, O., Reinsch, S., Urbé, S., Zerial, M., and Parton, R.G. (1996). Rab11 regulates recycling through the pericentriolar recycling endosome. The Journal of Cell Biology *135*, 913-924.

Ungewickell, E.J., and Hinrichsen, L. (2007). Endocytosis: clathrin-mediated membrane budding. Current Opinion in Cell Biology *19*, 417-425.

Vaisberg, E.A., Grissom, P.M., and McIntosh, J.R. (1996). Mammalian cells express three distinct dynein heavy chains that are localized to different cytoplasmic organelles. The Journal of Cell Biology *133*, 831-842.

Vale, R.D. (2003). The molecular motor toolbox for intracellular transport. Cell *112*, 467-480.

Vale, R.D., and Fletterick, R.J. (1997). The design plan of kinesin motors. Annu Rev Cell Dev Biol *13*, 745-777.

Vale, R.D., Reese, T.S., and Sheetz, M.P. (1985). Identification of a novel force-generating protein, kinesin, involved in microtubule-based motility. Cell *42*, 39-50.

Valetti, C., Wetzel, D.M., Schrader, M., Hasbani, M.J., Gill, S.R., Kreis, T.E., and Schroer, T.A. (1999). Role of dynactin in endocytic traffic: effects of dynamitin overexpression and colocalization with CLIP-170. Mol Biol Cell *10*, 4107-4120.

Vallee, R.B., Williams, J.C., Varma, D., and Barnhart, L.E. (2004). Dynein: An ancient motor protein involved in multiple modes of transport. J Neurobiol *58*, 189-200.

van Dongen, S., Abreu-Goodger, C., and Enright, A.J. (2008). Detecting microRNA binding and siRNA off-target effects from expression data. Nat Methods *5*, 1023-1025.

Varga, V., Leduc, C., Bormuth, V., Diez, S., and Howard, J. (2009). Kinesin-8 motors act cooperatively to mediate length-dependent microtubule depolymerization. Cell *138*, 1174-1183.

Vasquez, R.J., Howell, B., Yvon, A.M., Wadsworth, P., and Cassimeris, L. (1997). Nanomolar concentrations of nocodazole alter microtubule dynamic instability in vivo and in vitro. Mol Biol Cell *8*, 973-985.

Vaughan, K.T., Tynan, S.H., Faulkner, N.E., Echeverri, C.J., and Vallee, R.B. (1999). Colocalization of cytoplasmic dynein with dynactin and CLIP-170 at microtubule distal ends. J Cell Sci *112 (Pt 10)*, 1437-1447.

Vaughan, K.T., and Vallee, R.B. (1995). Cytoplasmic dynein binds dynactin through a direct interaction between the intermediate chains and p150Glued. The Journal of Cell Biology *131*, 1507-1516.

Vaughan, P.S., Miura, P., Henderson, M., Byrne, B., and Vaughan, K.T. (2002). A role for regulated binding of p150(Glued) to microtubule plus ends in organelle transport. The Journal of Cell Biology *158*, 305-319.

Verhey, K.J., and Gaertig, J. (2007). The tubulin code. Cell Cycle *6*, 2152-2160.

Verhey, K.J., and Hammond, J.W. (2009). Cytoskeletal motors: Traffic control: regulation of kinesin motors. Nat Rev Mol Cell Biol *10*, 765-777.

Verhey, K.J., Lizotte, D.L., Abramson, T., Barenboim, L., Schnapp, B.J., and Rapoport, T.A. (1998). Light chain-dependent regulation of Kinesin's interaction with microtubules. The Journal of Cell Biology *143*, 1053-1066.

Westermann, S., and Weber, K. (2003). Post-translational modifications regulate microtubule function. Nat Rev Mol Cell Biol *4*, 938-947.

Williams, J.C., Roulhac, P.L., Roy, A.G., Vallee, R.B., Fitzgerald, M.C., and Hendrickson, W.A. (2007). Structural and thermodynamic characterization of a cytoplasmic dynein light chain-intermediate chain complex. Proc Natl Acad Sci USA *104*, 10028-10033.

Woolner, S., and Bement, W.M. (2009). Unconventional myosins acting unconventionally. Trends Cell Biol *19*, 245-252.

Woźniak, M.J., and Allan, V.J. (2006). Cargo selection by specific kinesin light chain 1 isoforms. The EMBO Journal *25*, 5457-5468.

Yajima, J., Edamatsu, M., Watai-Nishii, J., Tokai-Nishizumi, N., Yamamoto, T., and Toyoshima, Y.Y. (2003). The human chromokinesin Kid is a plus end-directed microtubule-based motor. The EMBO Journal *22*, 1067-1074.

Yamazaki, H., Nakata, T., Okada, Y., and Hirokawa, N. (1995). KIF3A/B: a heterodimeric kinesin superfamily protein that works as a microtubule plus end-directed motor for membrane organelle transport. The Journal of Cell Biology *130*, 1387-1399.

Yamazaki, H., Nakata, T., Okada, Y., and Hirokawa, N. (1996). Cloning and characterization of KAP3: a novel kinesin superfamily-associated protein of KIF3A/3B. Proc Natl Acad Sci USA *93*, 8443-8448.

Yan, Q., Sun, W., Kujala, P., Lotfi, Y., Vida, T.A., and Bean, A.J. (2005). CART: an Hrs/actinin-4/BERP/myosin V protein complex required for efficient receptor recycling. Mol Biol Cell *16*, 2470-2482.

Yarar, D., Waterman-Storer, C.M., and Schmid, S.L. (2005). A dynamic actin cytoskeleton functions at multiple stages of clathrin-mediated endocytosis. Mol Biol Cell *16*, 964-975.

Zerial, M., and McBride, H. (2001). Rab proteins as membrane organizers. Nat Rev Mol Cell Biol *2*, 107-117.

Zhang, J., Li, S., Fischer, R., and Xiang, X. (2003). Accumulation of cytoplasmic dynein and dynactin at microtubule plus ends in Aspergillus nidulans is kinesin dependent. Mol Biol Cell *14*, 1479-1488.

Zhapparova, O.N., Bryantseva, S.A., Dergunova, L.V., Raevskaya, N.M., Burakov, A.V., Bantysh, O.B., Shanina, N.A., and Nadezhdina, E.S. (2009). Dynactin subunit p150Glued isoforms notable for differential interaction with microtubules. Traffic *10*, 1635-1646.

9 Abbreviations

ApoB – Apolipoprotein B
APPL1 - Adaptor Protein containing PH doamin, PTB domain an Leucine zipper motif
cDNA – Complementary DNA
DAPI - 4',6-diamidino-2-phenylindole
DHC (HC) - Dynein Heavy Chain
DIC (IC) - Dynein Intermediate Chain
DiD – 1,1'-dioctadecyl-3,3,3',3'-tetramethylindodicarbocyanine, 4-chlorobenzenesulfonate
DLC (LC) - Dynein Light Chain
DLIC (LIC) - Dynein Light Intermediate Chain
DMEM - Dulbecco's modified Eagle's medium
DYNAH - Dynein Axonemal Heavy
DYNAI - Dynein Axonemal Intermediate
DYNAL - Dynein Axonemal Light
DYNALI - Dynein Axonemal Light Intermediate
DYNCH – Dynein Cytoplasmic Heavy
DYNCI - Dynein Cytoplasmic Intermediate
DYNCL - Dynein Cytoplasmic Light
DYNCLI - Dynein Cytoplasmic Light Intermediate
EEA1 – Early Endosome Antigen1
esiRNA - endoribonuclease-digested short interfering RNA
FCS – Fetal Calf Serum
GAP - GTPase activating protein
GDP: Guanine-nucleotide-diphosphate
GEF - Guanine nucleotide Exchange factor
GFP - Green Fluorescent Protein
GTP: Guanine-nucleotide-triphosphate
HT – Human Transcriptome
KAP – Kinesin Associated Protein
Kif – Kinesin
KRP – Kinesin Related Protein
LAMP1 - Lysosomal Associated Membrane Protein1
LDL – Low Density Lipoprotein
LDLR – Low Density Lipoprotein Receptor
Motorome – Motors in genome (motor complement of genome)
mRNA – messenger RNA
MF - Microfilaments
MSD – Mean Square Displacement
MTOC – Microtubule Organizing Centre
MT - Microtubules
MYH – Myosin Heavy chain
Myo – Myosin
Myr – Myosin from Rat
NSF: N-ethylmaleimide-sensitive factor
PtdInsP: Phosphatidyl-Inositol Phosphate

QMPIA - Quantitative Multi-Parametric Image Analysis
RNAi – RNA interference
RT-PCR – Reverse Transcriptase – Polymerase Chain Reaction
siRNA – short interfering RNA
SNAP - Soluble NSF-attachment protein
SNARE: Soluble NSF-attachment factor receptor